FUNCTIONAL AND STRUCTURAL MODIFICATIONS ASSOCIATED

WITH HYPERTENSION, OBESITY AND DIABETES IN THE RESISTANCE

VASCULATURE

A Dissertation

presented to

the Faculty of the Graduate School

at the University of Missouri-Columbia

In Partial Fulfillment

of the Requirements for the Degree

Doctor of Philosophy

By

JORGE A. CASTORENA-GONZALEZ

Dr. Luis A. Martinez-Lemus, Dissertation Supervisor

DECEMBER 2014

The undersigned, appointed by the dean of the Graduate School, have examined the dissertation entitled

FUNCTIONAL AND STRUCTURAL MODIFICATIONS ASSOCIATED WITH HYPERTENSION, OBESITY AND DIABETES IN THE RESISTANCE VASCULATURE

presented by Jorge A. Castorena-Gonzalez,

a candidate for the degree of Doctor of Philosophy,

and hereby certify that, in their opinion, it is worthy of acceptance.

_____
Professor Luis A. Martinez-Lemus
(Advisor/Committee Chair)

_____
Professor Luis Polo-Parada
(Co-Advisor/Outside Member)

_____
Professor Sheila Grant
(Committee Member)

_____
Professor Shramik Sengupta
(Committee Member)

_____
Professor Li-Qun Gu
(Committee Member)

"Science is not only a disciple of reason but, also, one of romance and passion."
Stephen Hawking

Thanks to all of those who I crossed paths with, those who have had an impact on my formation, those whose knowledge and example made me a better person and a better scientist, all those who, although I may have forgotten, made this journey possible.

To my parents, Lucy and Jorge, who have supported me in every step of my education and in every part of my life. It has been a long journey, full of achievements, happiness, tears and sacrifice. Thank you Mom and Dad for your love and example, for working incredibly hard to give me and my brother the opportunity to have a better future, and for helping me be a better man everyday. To my brother, Emmanuel, who although is younger than me, his hard work and determination have been an excellent and invaluable example. Thank you Mom, Dad, Emmanuel, Mariana, Dante, Daria and Flubby for your support, your love and for missing me as much as I have missed you while I have been away from home. I love you with all my heart.

To my lovely Lauren, who has supported me and loved me day after day. Thank you for being the amazing person you are, for being with me in tough times and also for letting me enjoy beautiful moments with you. Completing my doctorate has not been easy, but having you by my side has definitely made it easier. I love you and I cannot wait to spend the rest of my days with you.

To the Mattson Family for all your support, for everything you all have done for me and all you have given me, but even more important for always making me feel loved and welcomed.

Thank you Francisco, David and all my friends for all those great moments we have shared. We may follow different paths, but I sure hope there are a lot more experiences to come. I cannot wait to see what is next.

ACKNOWLEDGEMENTS

TABLE OF CONTENTS

ABSTRACT

Cardiovascular diseases are considered the leading cause of death nowadays. Hypertension, obesity and type-2 diabetes are deemed major risk factors for the development of cardiovascular diseases. In essential hypertension, one of the most important structural changes is the inward remodeling of the resistance arteries. I found that the mechanical properties of inwardly remodeled cremasteric-arterioles from rats are affected. Furthermore, it is the F-actin components of the cytoskeleton the ones that are strongly modified. In old spontaneously hypertensive rats, my results showed that, resistance arteries undergo hypertrophic inward remodeling; and, adrenergic-vasoconstriction and vasodilation pathways are impaired. In diet-induced-obesity, mice-mesenteric arterioles were observed to undergo remodeling of the extracellular matrix components. Obesity and type-2 diabetes have been associated with insulin resistance, endothelial dysfunction and arterial stiffening. Jejunal-submucosal arterioles from diabetic obese patients had a reduced vasorelaxation to insulin in comparison to obese non-diabetics, while acetylcholine-vasodilation was similar in both groups. Reduced amounts of the subunit-alpha of the insulin receptor and MMP-9 were found in diabetics as well. This suggests that, in type-2 diabetes, the presence of a blunted insulin-vasodilation response is a form of endothelial dysfunction that is not correlated with the body-to-mass index, but whose mechanism may be related with the activity of MMPs.

CHAPTER 1

INTRODUCTION

In the most recent report published by the *National Vital Statistics Reports* in December of 2013 (74), the top 10 leading causes of death in the United States for 2010, which account for 75% of the total number of deaths, and their corresponding percentage of deaths are: Diseases of the heart (24.2%), Malign neoplasms (Cancer) (23.3%), Chronic lower respiratory diseases (5.6%), Cerebrovascular diseases (5.2%), Accidents (4.9%), Alzheimer's disease (3.4%), Diabetes mellitus (2.8%), Nephritis, nephritic syndrome and nephrosis (2.0%), Influenza and pneumonia (2.0%), and Intentional self-harm (suicide) (1.6%). From all these, heart diseases, cerebrovascular diseases and diabetes can be classified as cardiovascular and/or cardiovascular-related diseases, and they accounted for 32.2% of all deaths in the United States, becoming the major life threatening health condition.

Hypertension is a chronic medical condition characterized by presence of elevated arterial blood pressure. It is considered an asymptomatic condition, in other words, it does not have any specific associated symptoms, which makes it even more difficult to

detect and to treat. Hypertension is deemed a major risk factor for various heart and cerebrovascular diseases. This is the reason why it is very important to study and understand hypertension, from its early stages of development until the advanced stages where the vasculature undergoes functional and structural changes.

Another major health problem with a dramatically increased prevalence worldwide in the last decade is obesity. In the years 2011-2012, it was reported that 34.9% of the adults (>20 years old) in the United States were obese. Obesity has been associated with hypertension, and it is known to increase the risk for the development of cardiovascular diseases, type 2 diabetes, some respiratory diseases, and even cancer among others.

The information contained in this dissertation focuses on the study, characterization and understanding of the main functional and structural modifications in the resistance vasculature that are associated with hypertension, type 2 diabetes and obesity.

Chapters 2 and 3 will center in studying and understanding one of the main structural changes that is associated with essential hypertension known as inward remodeling of the resistance blood vessels. In Chapter 4, I will present and discuss the main results obtained from experimentation using the most commonly used animal model for hypertension, the spontaneously hypertensive rat. These three chapters are intended to give a thorough description of essential hypertension and the vascular functional and

structural changes associated with it, based on the results obtained during my doctoral research and the available literature.

Chapter 5 covers the results obtained from an animal (mouse) model that was used to study the effects of a diet high in fats and carbohydrates on the vasculature and in the overall health of mice. These studies represent a good model for obesity in young and adult individuals, and allowed us to study the vascular dysfunctions and vascular remodeling and stiffening associated with obesity.

Finally, in Chapter 6, I present and discuss some novel data obtained in a study conducted on human jejunal and mesenteric arteries. In that study we looked at the effects of obesity on the vasculature of adult humans undergoing bariatric surgery. Furthermore, we focused on understanding the connection between obesity and type 2 diabetes. Previously, insulin resistance and endothelium dysfunction had been associated with obesity; however, whether there is a connection between these two, or not, had not been established.

CHAPTER 2

MECHANISMS OF THE INWARD REMODELING PROCESS IN RESISTANCE VESSELS: IS THE ACTIN CYTOSKELETON INVOLVED?[†]

2.1 Introduction

Cardiovascular diseases are the most important life-threatening health conditions today, with hypertension and cerebrovascular disease being two of the most predominant ones, and projected to rapidly increase in the next few years (121). The majority of cases of hypertension are considered essential, as no apparent cause can be established for the elevated arterial pressure. Given the importance and the impact that hypertension has in human lives, a detailed study and better understanding of its pathophysiology is warranted, especially on the role that the structure and function of resistance vessels play

in it, because recent studies indicate that remodeling of resistance arteries is one of the earliest detectable parameters that predict subsequent life threatening cardiovascular events (123, 156). In this article, we present a review of some of the main results from several studies that focused on the characterization of the most prominent structural changes that occur in the resistance vasculature in hypertension, i.e., the inward eutrophic remodeling of arterioles (11, 12, 120, 179, 194). We will present evidence that the inward eutrophic remodeling of arterioles is closely associated with augmented active tone induced via prolonged agonist-induced vasoconstriction, which stimulates structural modifications in the arteriolar wall, leading to changes in the elastic and mechanical properties of the vascular wall. Evidence indicates that during the initial stages of the remodeling process these changes occur mainly at the level of the actin cytoskeleton and are associated with the repositioning of vascular smooth muscle cells, actin polymerization pathways, and the accumulation of fibrillar (F)-actin. As results indicate that blockade of Rho and Rac-1 associated pathways prevent prolonged vasoconstriction from inducing inward eutrophic remodeling, we end with a hypothetical model of how these small GTPases may contribute to the remodeling process.

2.2 Structure and elastic properties of resistance arteries

The structure and composition of arterioles, and blood vessels in general, has been widely studied and described (114, 152, 153). However, much remains to be understood about the mechanics and interactions of the different components in the vessel wall. Resistance arteries play a preponderant role in the regulation of blood flow and

modulation of blood pressure in the cardiovascular system. For this reason, any structural change that occurs in the resistance vasculature, e.g., the narrowing of blood vessels, the thickening of vessel walls, increased/decreased stiffness, etc., can impact the mechanics of the arteriolar wall, the control of the cardiovascular system and the development of cardiovascular diseases (38). To characterize the mechanical properties of the blood vessel wall, the most common parameters studied are the stress, strain, and elastic modulus of vessels placed under passive condition.

2.2.1 Circumferential stress

The stress profile characterizes the internal forces exerted in between the individual components of a continuous material, for example, the forces in between adjacent smooth muscle cells in the vessel wall, due to an external force (e.g., intraluminal pressure). The stress represents an average force per unit-area. In the study of blood vessels associated with hypertension, the circumferential stress is more often examined as it contains information on the dimensions of the vascular luminal diameter and wall thickness at a given pressure, which are dimensions commonly affected by changes in blood pressure. In the microcirculation, circumferential stress is commonly expressed in dynes/cm^2, and can be written as $\sigma_{\theta,i} = (P_i \cdot r_i)/\tau_i = (P_i \cdot D_i)/2\tau_i$, where $\sigma_{\theta,i}$ is the circumferential stress at the ith level of intraluminal pressure with its respective vascular diameter and wall thickness, P_i is the intraluminal pressure, and D_i and τ_i are the internal diameter and the wall thickness at a given pressure, respectively. When studying resistance arteries, it is commonly assumed that the arteriolar wall volume remains constant under changes in pressure, at a fixed vessel length, this would result in a

CSA (cross-sectional area) that remains constant. (18-20) In this case, the wall thickness could be calculated and expressed in terms of the CSA and the internal diameter as follows $\tau = \sqrt{(CSA/\pi)+(D_i^2/4)} - (D_i/2)$.

2.2.2 Strain

Strain is a normalized measure of the displacement between the components of a continuous material. In the case of blood vessels, the strain (circumferential strain) represents a measure of the change in internal diameter due to a change in intraluminal pressure normalized by a reference diameter, which normally is the diameter measurable at the lowest possible pressure (because vessels pressurized at 0 mmHg would collapse, pressures between 5-10 mmHg are commonly used as reference). Being a normalized measure, the strain has no-units, and it can be written as $\varepsilon_i = (D_i - D_0)/D_0$, where D_i is the diameter at a given pressure and D_0 is the reference diameter.

2.2.3 Modulus of elasticity

The modulus of elasticity, also known as tangential elastic modulus, is a parameter that measures the stiffness of an elastic continuous material. Mathematically it represents the point-by-point slope in a strain vs. stress curve. At every single point in this curve, the elastic modulus can be calculated as $E_{T,i} = \sigma_{\theta,i}/\varepsilon_i$.

Traditionally the extracellular matrix components of the vascular wall are considered the major contributors to the elastic properties of arterioles under passive conditions (85, 86, 193). Due to their relative amount and elastic properties, collagen and

7

elastin are the extracellular matrix components with major influence in vascular wall mechanics (193). However, to the best of our knowledge there are no systematic studies that have experimentally established the proportion by which different cellular and extracellular components of arterioles contribute to the elastic properties of the vascular wall. This is particularly important to establish in arterioles where smooth muscle is the major component of the vascular wall.

Anatomically, the arteriolar wall is traditionally segmented from the lumen out into three different parts: *The initma* is composed of endothelial cells and a basement membrane. Endothelial cells are major contributors to the control of vascular tone. Evidence indicates that endothelial cells modify their intracellular (i.e., cytoskeletal) structure based on the shear stress they are exposed to as blood flows in the vascular lumen. It has also been shown that a number of mechanical and physiological mechanisms, and intracellular/cell-cell interactions are shear-stress mediated (e.g., production of nitric oxide and other vasodilator compounds, expression of nitric oxide synthase, presence and activity of adhesions between adjacent endothelial cells, cell membrane stability, cytoskeletal remodeling, etc.) (110, 112, 170, 182, 183, 190). The direct contribution of endothelial cells themselves to the elastic properties of the vascular under passive conditions, however, is likely to be minimal as indicated by experiments in which the vascular intima of arterioles has been denuded (50).

The media, which in arterioles consists mostly of one or two layers of smooth muscle cells, is in charge of controlling the functional vascular diameter via mechanisms

of cellular contraction and relaxation. Recent results from our laboratory also suggest that in the early stages of the inward eutrophic remodeling process they provide a significant contribution to the passive diameter of arterioles (179). An additional component of the media in arterioles is the internal elastic lamina. The elastic laminas are constituted primarily of elastin fibers, which provide blood vessels with recoiling properties that allow them to expand and recover to their original diameter when external forces are applied and withdrawn. In inwardly remodeled arteries it has been shown that the fenestra (holes) present in the internal elastic lamina are reduced in size (27, 28), suggesting that remodeling of elastin may contribute to the reduction in passive diameter observed in inwardly remodeled vessels. In arterioles, the media is the thickest layer in the vascular wall. It contributes in a very important way to wall mechanics under active vasoconstriction. The contractile level of smooth muscle cells, the interactions in between multiple cells, the intracellular structure of the cell (e.g., actin cytoskeleton), and their interactions with the extracellular matrix including elastin molecules in the elastic laminas, will determine one of the major components of the elastic properties of the actively contracted arteriolar wall. The contribution of the media to the circumferential elastic properties of the arteriolar wall under passive conditions, however, appears to be minimal in "normal" arterioles obtained from normotensive rats, as actin cytoskeletal disruption or elastin degradation have no impact on maximal arteriolar passive diameter (40, 179).

The adventitia, the outermost segment of blood vessels, is mainly composed of collagen and fibroblasts, which are embedded within the collagen. This layer is

9

considered to give support and structure to the arteriolar wall. It is considered to be a major contributor to vascular stiffness and elasticity, as collagen disruption severely affects vascular mechanics and is commonly used to dissociate the cellular elements of the wall.

2.3 The inward remodeling of resistance arteries

In essential hypertension, inward remodeling is the most commonly observed change in arteriolar structure. It is characterized by a reduced luminal diameter under passive conditions, and further categorized as eutrophic when the cross-sectional area of the vascular wall remains without significant changes (Fig. 2.1-A,B). It has been postulated that inward eutrophic remodeling occurs when resistance vessels exposed to high blood pressure are able to normalize circumferential stress via the repositioning of vascular smooth muscle cells around a smaller luminal diameter, a process that preserves wall cross-sectional area (70, 71, 117). If this process is insufficient, wall hypertrophy occurs to normalize the circumferential stress of the vascular wall.

A reduced luminal diameter with a cross-sectional area that remains constant would cause the wall to lumen ratio to be increased, in other words, it would cause materials in the arteriolar wall to rearrange, leading to thickening of the arteriolar wall. An increased media to lumen ratio is an arteriolar feature commonly observed in essential hypertension, and based on the available evidence, is mainly due to rearrangement of the existent normal-sized cells around a smaller luminal diameter (11, 69). That is, there is no

cell hypertrophy or hyperplasia. It is important to consider that any structural modifications in the arteriolar wall would induce changes in the viscoelastic properties and mechanics of the vessel. However, the overall change in vascular mechanics would depend on the viscoelastic characteristics of the materials being modified and the relative amount of these materials in the arteriolar wall.

As an example, let us consider the curves shown in Figure 2.1, where the elastic characteristics of a control (non-remodeled) and an inwardly eutrophic remodeled arteriole are compared. From the equations for stress, strain and elastic modulus presented in the previous section, we know that the stress is directly proportional to the inner diameter and inversely proportional to wall thickness. In Figure 2.1-B, the inner passive diameter in the remodeled vessels is smaller than the control at all intravascular pressures. The resulting strain-stress relationship of these two vessels is represented in Figure 2.1-C. Notice that the point-by-point circumferential stress at a given level of strain is greater in the remodeled arteriole. However the greatest level of stress achieved at the highest intraluminal pressure is slightly reduced after remodeling because the remodeled vessel is less pliable and distended less at the highest pressure. In the remodeled vessel, the strain has been substantially reduced (i.e., is less distensible) due to the stiffening (increased modulus of elasticity) of the arteriolar wall (Figure 2.1-C, D).

The mechanisms that control inward eutrophic remodeling have not been completely elucidated, in particular those associated with the initial stages of the process. Overall, substantial evidence indicates prolonged vasoconstriction is a primary condition

that induces inward remodeling (12, 71, 115, 120). Whether all stimuli capable of inducing prolonged vasoconstriction can also cause inward eutrophic remodeling has not been clearly established. However, cumulative in vivo and ex vivo studies suggest that prolonged agonist-dependent stimulation for vasoconstriction induces inward remodeling in resistance vessels.
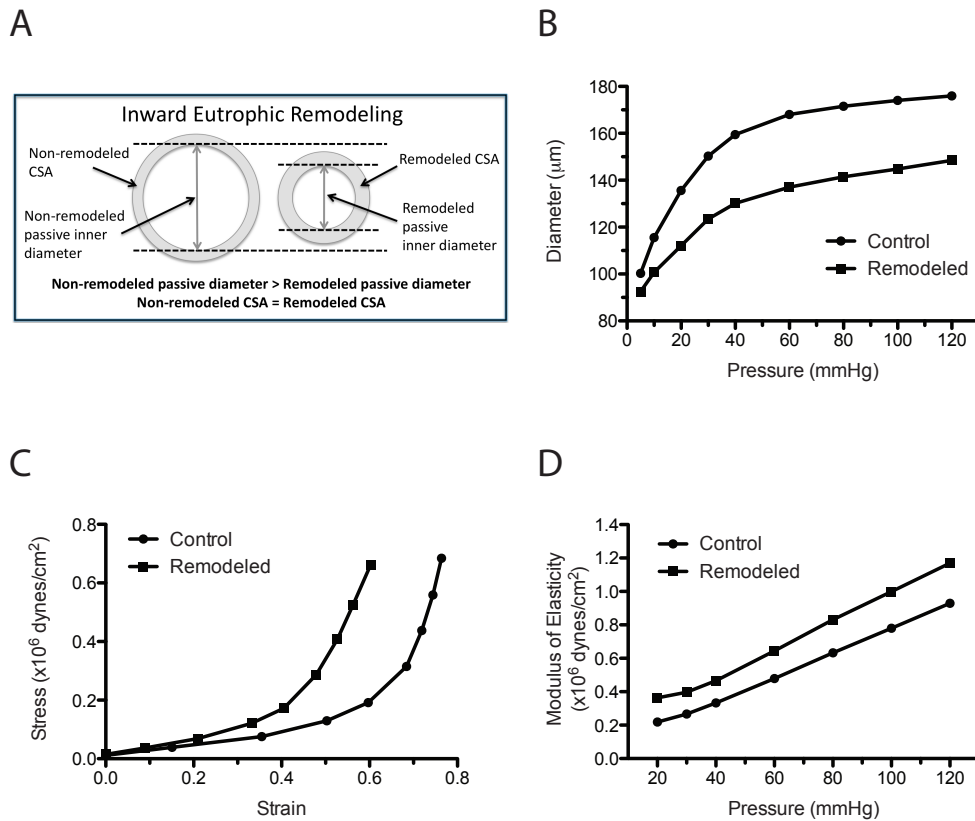
Figure 2.1. Structural and mechanical characteristics of an inwardly remodeled resistance artery. (A) Diagrammatic representation describing the main changes in inner and outer diameters and CSA observed in the arteriolar wall of arterioles with inward eutrophic remodeling. (B) Diagrammatic representation of the intraluminal pressure to passive diameter relationships of a control and an inwardly remodeled arteriole. (C) Diagrammatic representation of the strain–stress relationships of the control and inwardly remodeled arterioles presented in Panel B. (D) Diagrammatic representation of the moduli of elasticity obtained from the control and inwardly remodeled arterioles presented in Panel B.

12

Accordingly, prolonged exposure of isolated arterioles to vasoconstrictors such as endothelin-1, norepinephrine, and angiotensin II has been shown to cause inward remodeling (12, 115). In vivo, prolonged infusion or expression of vasoconstrictor agonists induces inward remodeling as well (37, 71, 209). A number of results suggest that the level of vasoconstriction achieved by the agonists corresponds to the level of reduction in passive diameter observed in the remodeled vessel (115). However, this does not appear to be the case for all agonists (115). Additional studies suggest that, in vivo, the overall influence that vasoconstrictor or vasodilator agonists have on a vascular segment is able to control the remodeling process (122, 168). This is particularly evident in experiments showing that a diminished vasodilator influence caused by a reduction in blood flow and shear stress-dependent production of nitric oxide and activation of transglutaminase activity causes inward remodeling in resistance arteries (11, 13, 51).

The mechanisms associated with the inward remodeling process achieved either by prolonged exposure to vasoconstrictor agonists or a reduction in blood flow have been associated with processes that involve multiple factors, such as reactive oxygen species (ROS), nitric oxide, Rho, Rac-1, matrix metalloproteinases (MMP), and tissue type transglutaminase (TG2) among others (11, 51, 120, 179). All of these factors have the potential to affect cytoskeletal and extracellular matrix structures of the vascular wall. However, how these factors participate in the remodeling process both temporally and mechanistically remains to be fully elucidated. Recently we reported that during the early stages of the inward eutrophic remodeling process, nearly 75% of the reduction in passive diameter observed in isolated arterioles constricted for four hours was reversed following

actin cytoskeletal disruption. Below we present a brief review of some of the known and proposed roles some of the above mentioned factors play on the actin cytoskeleton and potentially on the inward remodeling process.

2.4 Vasoconstriction and actin polymerization

Over the last several years, it has become evident that calcium sensitization and actin polymerization processes participate in the contraction of smooth muscle. These pathways appear to intermingle and collaborate with the classical pathway of constriction induced by increments in intracellular calcium concentration and the subsequent increase in myosin light chain phosphorylation and actomyosin cross bridge cycling (Fig. 2.2). Studies performed in different types of smooth muscle including airway, vascular, and intestinal muscle indicate that exposure to contractile agonists induces the polymerization of actin and that this actin polymerization is required for the development of force (2, 128, 138, 141, 151, 161, 188). Importantly, results also indicate that inhibition of actin polymerization by agents such as cytochalasin-D or latrunculin-A do not affect the signaling pathways that regulate myosin light chain phosphorylation during smooth muscle contraction (43, 161).

Evidence suggests that the actin polymerization pathways taking place upon stimulation for constriction serve to strengthen a scaffold of actin fibers (primarily cortical actin) that allows for contractile fibers to exert force appropriately, and shorten the cell (204). Hypothetically a reversed loosening of these structures occurs during cell

14

relaxation in response to contractile agonists withdrawal or in the presence of relaxing compounds. In support of this hypothesis a recent study reported that the cortical stiffness of isolated vascular smooth muscle cells increases in response to stimulation with the vasoconstrictor agonist angiotensin II, and is reduced upon exposure to a vasodilator (78).
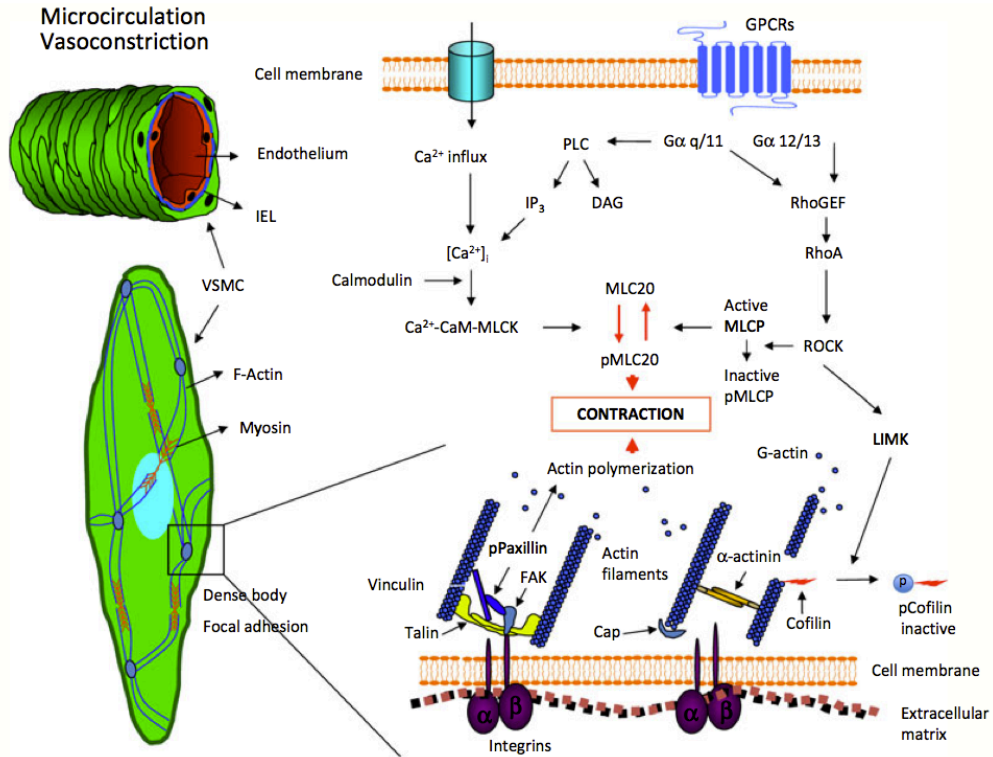
Figure 2.2. Vascular smooth muscle intracellular mechanisms for vasoconstriction. VSMC located in the medial layer of resistance arteries reduce their length to cause vasoconstriction. This process involves mechanisms associated with the phosphorylation of MLC20, and the formation and disruption of actin cytoskeletal structures. The activation of ROCK is an event that potentially links MLC-20 phosphorylation and actin polymerization mechanisms. ROCK inactivates MLCP to maintain MLC-20 phosphorylation and constriction. It also deactivates cofilin and its severing action on actin filaments via the activation of LIMK. Consequently, integrin-linked actin fibers are able to polymerize and strengthen the cytoskeleton through processes that involve the phosphorylation of paxillin and a number of other focal adhesion proteins with and without kinase activity. GPCRs, G-protein coupled receptors; IEL, internal elastic lamina; PLC, phospholipase C; IP3, inositol triphosphate; DAG, diacyl glycerol; RhoGEF, Rho guanine exchange factor; MLCK, myosin light- chain kinase; FAK, focal adhesion kinase. Figure adapted from references (64, 117).

In vascular structures some results suggest that actin polymerization increases as vasoconstriction is prolonged (151). In accordance with those results, we recently reported that stimulation of isolated arterioles for four hours with the vasoconstrictor agonists norepinephrine and angiotensin II increased the ratio of filamentous (F) to globular monomeric (G) actin obtained by differential centrifugation of the tissue (179). Our results further suggest that some actin structures formed during the prolonged exposure to the vasoconstrictor agonists are not readily disrupted by withdrawal of the vasoconstrictor agonists, exposure to vasodilator compounds, or removal of calcium. Only the active severing disruption of actin filaments with mycalolide B was able to allow for vascular relaxation to passive diameters similar to those observed before the prolonged exposure to the vasoconstrictor agonists. We hypothesize that during prolonged periods of vasoconstriction "more permanent" actin cytoskeletal structures are formed through actin polymerization pathways. These "more permanent" cytoskeletal structures may be part of the existing cytoskeleton or may represent new cellular processes of the vascular smooth muscle cells that re-elongate and reposition themselves in the arteriolar wall during the remodeling process (see below). Our results suggest that in the initial stages of the inward remodeling process the establishment of these structures does not allow the vessel to dilate to its previous maximal passive diameter.

The generation of filamentous F-actin occurs via the aggregation of globular G-actin monomers into oligomers that are subsequently elongated to form a polarized filament. During the elongation phase, ATP bound monomers are added to both ends of the growing filament, though the rate of addition is not equal, as the designated plus end

16

adds monomers at a much greater rate than the minus end. Once incorporated into filaments, the actin monomers can undergo nucleotide hydrolysis, thereby increasing the rate at which they disassociate from the filament. This dissociation predominantly occurs at the minus end. As the filament grows, the local concentration of G-actin decreases and the filament achieves a steady state equilibrium in which the rate of actin monomer incorporation at the plus end equals the rate of monomers disassociating from the minus end. Throughout this process a host of proteins interact with G and F-actin to maintain and regulate not only filament assembly and elongation, but also filament stability and disassembly.

The formation of actin dimers and trimers, termed nucleation, appears to be the rate-limiting step in F-actin polymerization. The dissociation constant (K_d) for actin dimers has been estimated to be as high as 4.6 M (175). To overcome this kinetic barrier, cells utilize a number of actin regulators to promote nucleation. To date, three main classes of nucleators have been described in the literature: the Arp2/3 complex, formins and Spire. The activity of the nucleators is controlled by nucleation promoting factors (NPFs). It is well established that in response to vasoconstrictor stimuli actin polymerization is required for maximum force generation as well as for maintenance of constriction in vascular smooth muscle cells (for review see (64)). It is less clear which nucleator (or combination of nucleators) mediates actin polymerization during constriction of resistance arteries. However, the Arp 2/3 complex has been implicated in the process. The NPF, neuronal Wiskott-Aldrich Syndrome Protein (N-WASp), activates the Arp 2/3 complex and promotes nucleation and actin polymerization. In rat mesenteric

arteries exposed to phenylephrine, inhibition of N-WASp association with the Arp 2/3 complex decreases the extent of constriction and dampens the increase in the ratio of F- to G-actin (an indicator of actin polymerization) (8). It has also been shown that the Arp2/3 complex is a component of adhesion complexes that are formed following activation of integrins (48). Integrins are transmembrane receptor proteins that link the extracellular matrix (ECM) to the cytoskeleton and, in addition to other functions, facilitate cell motility by regulating actin polymerization at adhesion sites (23). They also play a role in vascular remodeling, as inhibition of α_V integrins blocked inward eutrophic remodeling in rat resistance vessels (71). Interestingly, formins have also been identified in purified adhesion complexes that promote actin polymerization (29). However, it is not clear what effect, if any, they have on actin polymerization in vascular smooth muscle cells in response to contractile stimulation.

In addition to assembly, actin filament disassembly is also highly regulated. Cofilin-1 is a member of the Actin-depolymerizing factor/cofilin family and, when active, is able to bind adenosine diphosphate subunits in F-actin and sever actin filaments (130). Paradoxically, cofilin's depolymerizing effects are concentration dependent. At relatively high concentrations, the severing activity of cofilin promotes actin nucleation by increasing the availability of free monomers to oligomerize. In addition, it is postulated that direct binding of cofilin with actin dimers promotes their stabilization, thereby decreasing the rate of dimer disassociation (6). Cofilin's ability to bind to actin is inhibited by its phosphorylation at position Ser3 by Lim Kinase (205). Interestingly, the signaling pathways of numerous vasoconstrictor agonists lead to Lim Kinase activation,

as Rho associated kinase phosphorylates and activates Lim Kinase (Fig. 2) (142). It remains to be determined what role cofilin and Lim kinase play in vasoconstriction of resistance vessels, and the subsequent development of inward remodeling. Since actin polymerization is required for inducing inward remodeling in resistance vessels, we are intrigued by the possibility that Lim kinase could potentially regulate the process by inactivating cofilin, thereby shifting the actin dynamics towards increased polymerization.

2.5 Matrix metalloproteinases, inward remodeling and the cytoskeleton

Inward remodeling induced ex vivo by prolonged vasoconstriction of isolated arterioles or in vivo in animal models of hypertension has been associated with the production of ROS and MMP activity (34, 35, 120). MMP activity is for the most part associated with extracellular matrix degradation, but there are a number of ways by which MMPs may modulate cytoskeletal structures. The degradation of extracellular matrix structures creates protein fragments with exposed cryptic sites that activate integrins (118). Integrin activation in turn activates intracellular signals that induce cytoskeletal modifications. Interestingly, the activation of specific integrins is also required for the inward eutrophic remodeling of resistance arteries observed in the Ren2 rat model of hypertension (71). Additional pathways by which MMPs can induce cytoskeletal modifications include the transactivation the epidermal growth factor receptor as it occurs upon stimulation with vasoconstrictor agonists such as norepinephrine and angiotensin II (132, 198). The formation of vasoactive compounds such as the vasoconstrictor fragments of endothelin created by the cleavage of big

19

endothelin-1 (57), is another mechanism by which MMPs could induce cytoskeletal modifications and arteriolar inward remodeling. In isolated arterioles we previously showed that prolonged stimulation with norepinephrine and angiotensin II resulted in an increased expression of MMP-2, and an increased level of gelatinolytic activity that was dependent on the production of ROS (120). Furthermore, we showed that broad MMP inhibition did not affect the production of ROS but prevented the remodeling induced by prolonged vasoconstriction. In contrast, inhibition of ROS prevented both the activation of MMPs and the inward remodeling, suggesting that ROS-dependent activation of MMPs is involved in the development of the remodeling process (120).

2.6 Inward remodeling, transglutaminase activity and the actin cytoskeleton

The role of transglutaminase activity on the inward remodeling process of resistance arteries was first demonstrated in a seminal study by Bakker et al. (11). In that study the authors showed that the inward remodeling induced in vivo by low flow or ex vivo by prolonged exposure to endothelin-1 could be blocked with inhibitors of TG2 activity (11). They also showed that exogenous application of TG2 or its increased expression in response to retinoic acid exposure also induced inward remodeling in isolated resistance arteries (11). The transglutaminases are a family of enzymes that promote transamidation, covalently linking a lysine from one protein with the glutamine of another under high calcium conditions such as those found extracellularly (14). Consequently, the role of TG2 on vascular remodeling has been shown and presumed to

20

include extracellular matrix crosslinking (11, 194). The role of TG2 on remodeling of the vascular extracellular matrix has also been shown to include vascular calcification in conduit arteries (36, 90). However, in addition to the well-known extracellular matrix cross-linking functions of TG2, this enzyme is known to contribute to and catalyze other reactions that impact cytoskeletal structures (137). For example, TG2 has the capability to function as a G-protein, with the potential triggering of pathways that stimulate the activity of small GTPases such as Rho and its downstream effector ROCK leading to the remodeling of the actin cytoskeleton via mechanisms such as the polymerization of actin, the stabilization of existent actin fibers and the inhibition of actin depolymerization (137). The activation of TG2 at the cell membrane and its association with integrin receptors also has the potential to cluster cell adhesion sites and initiate integrin dependent outside in signaling pathways that lead to cytoskeletal remodeling (14, 118). The association that exists between TG2 and intracellular stress fibers suggests that TG2 may also help in the formation and stabilization of those fibers. Therefore the role of the transglutaminases on the inward remodeling process of resistance arteries needs to be further investigated to determine their potential participation on the initial stages of the process, which we have shown includes cytoskeletal modifications, and on the specific extracellular matrix changes TG2 causes on inwardly remodeled vessels.

2.7 Rho, Rac and the role of smooth muscle cell motility in arteriolar remodeling

The majority of smooth muscle cells within the vessel wall are found in a differentiated state called the contractile phenotype. This differentiated state is characterized by low proliferative capabilities, specific cellular morphologies (i.e., elongated and spindle shaped) and by the expression of contractile molecular markers such as smoothelin, α-smooth muscle actin and smooth muscle-myosin heavy chain. During the remodeling of large conduit vessels (e.g., aorta, carotid artery) encountered in vascular injury, hypertension and atherosclerosis, the contractile smooth muscle cells undergo a process of dedifferentiation towards a synthetic phenotype. An important characteristic of the synthetic phenotype is that the smooth muscle cells acquire the capacity to proliferate and migrate in response to extracellular stimuli such as angiotensin II, norepinephrine, and extracellular matrix fragments. In large conduit arteries, vascular smooth muscle cell migratory behavior has been documented both in vitro and in vivo (22, 89, 101). However the role of smooth muscle cell migration in the microcirculation has not been investigated. We have previously reported that repositioning of smooth muscle cells from the medial layer of resistance arteries is one of the mechanisms associated with inward eutrophic remodeling (116). We found that after only four hours of exposure to vasoconstrictor agonists, the vessels manifested structural changes consistent with inward remodeling (115, 116, 120, 179). Using multiphoton microscopy, it was determined that the reduction in luminal diameter was associated with the rearrangement of a number of smooth muscle cells relative to each other. These smooth

muscle cells relengthened and increased their overlapping along their longitudinal axis during the continual exposure to contractile agonists. As mentioned above, in this type of remodeling the cross-sectional area of the vessel wall does not change, while the passive luminal diameter is reduced. This suggests that the reduction in luminal diameter is accomplished by the rearrangement of the same amount of wall material, including smooth muscle cells, around a smaller vascular lumen. Our results suggest that a number of smooth muscle cells reposition around a smaller lumen resulting in luminal narrowing and impaired capacity for dilation. Although the cytoskeleton was not specifically investigated in that study, the repositioning of the smooth muscle cells likely requires a coordinated rearrangement of cytoskeletal structures in addition to the acto-myosin cross bridge cycling associated with smooth muscle cell contraction. Furthermore, the cytoskeletal reorganization is likely coordinated with changes in cell-matrix adhesions (78), as suggested by studies indicating that integrin associated mechanisms are required for the inward eutrophic remodeling process to occur (70, 71).

Actin cytoskeleton reorganization and dynamics are critical for smooth muscle cell movement and are associated with changes in cell shape and polarity (68). The cell movement is coordinated by the key regulators of the cytoskeleton, Rho, Rac and Cdc42. These small GTPases control numerous aspects of actin-filament turnover and assembly (94, 154). Each GTPase can induce different changes in the cytoskeleton. For example, Rho activation results in the formation of stress fibers which contain acto-myosin filaments and are associated with focal adhesion complexes (155). Also, through its downstream target Rho kinase (ROCK), Rho is associated with calcium sensitization

(177). In comparison, Rac activation induces the formation of membrane ruffles and lamellipodia leading to reorganization of the cytoskeleton (135). Cdc42 has been shown to induce the formation of filopodia. Cdc42 activation, induced by exposure to contractile agonists, has also been shown to control actin polymerization and active tension development in tracheal smooth muscle cells (102, 136). In a recent study from our laboratory we investigated the role of the small GTPases in the inward remodeling process of resistance arteries (179). Using isolated vessels, we determined that ROCK or Rac-1 inhibition with the pharmacological agents Y27632 or NSC23766, respectively, prevented the inward eutrophic remodeling induced by prolonged exposure to contractile agonists. ROCK inhibition prevented the maintenance of agonist induced constriction and inward remodeling, while Rac-1 inhibition prevented the remodeling but allowed prolonged vasoconstriction to be maintained. We also found that ROCK inhibition interfered with the maintenance of basal tone. This is consistent with studies showing that in pressurized vessels Rho-ROCK pathways maintain calcium sensitivity in the absence of vasoconstrictor agonists (107, 171, 196), and with studies showing that ROCK affects actin polymerization (42). That the early remodeling process was dependent on actin cytoskeletal modification was corroborated by the observation that actin fiber disruption reversed the inward remodeling caused by prolonged vasoconstriction. However, the pathways involved in inward remodeling that are more likely to be affected by the pharmacological blockade of ROCK or Rac-1 remain to be experimentally determined.

Taken together our studies suggest that the early phases of constriction-induced inward remodeling involve the dynamic reorganization of smooth muscle cells around a smaller lumen. This rearrangement appears to be dependent on the actin cytoskeletal reorganization orchestrated by the small GTPases Rho and Rac. A possible mechanism of remodeling would involve two concomitant processes. First, once the smooth cells are exposed to contractile agonists they begin to constrict and continue to maintain the constriction over time. This process is dependent mainly on the Rho-ROCK pathway. In parallel with this process a number of smooth muscle cells relengthen, readjust their position within the media and increase their cellular overlap. This latter process might be locally and temporally coordinated by the interplay between Rho, Rac and Cdc42 pathways. During this process of readjustment, the cells might extend lamellipodia and filopodia coordinated by Rac and possibly Cdc42, while simultaneously forming stress fibers through Rho activity. This model is consistent with our findings that ROCK inhibition prevents both the maintenance of constriction and remodeling, whereas Rac inhibition only prevents the remodeling without affecting acute or prolonged constriction. However, the validity of this model needs to be confirmed experimentally.

2.8 Conclusions and future directions

A substantial number of studies provide strong evidence that a number of cardiovascular diseases are associated with structural changes in resistance arteries, with inward eutrophic remodeling being the most prevalent in hypertension. Results from recent studies have associated the development of inward eutrophic remodeling with

processes that involve prolonged vasoconstriction, actin polymerization, transglutaminase activity and ROS-dependent activation of MMPs. However, a complete pathway that connects all these phenomena, and provides a full temporal and mechanistic description of the remodeling process is still warranted. Additional studies should therefore investigate the temporal associations and interactions that link prolonged vasoconstriction with actin polymerization pathways, the oxidative state of cells, activation of MMPs and transglutaminase activity. Elucidation of these associations and interactions should provide a clearer view of the mechanisms that control inward eutrophic remodeling and consequently present targets for therapeutic intervention and reduction of the life threatening events associated with resistance vessel remodeling.

CHAPTER 3

THE OBLIGATORY ROLE OF THE ACTIN CYTOSKELETON ON INWARD REMODELING INDUCED BY DITHIOTHREITOL (DTT) ACTIVATION OF ENDOGENOUS TRANSGLUTAMINASE IN ISOLATED ARTERIOLES[‡]

3.1 Introduction

Inward remodeling of arterioles is the most prevalent structural change of the resistance vasculature observed in patients with hypertension and diabetes (69, 157). Its presence is associated with an increased risk for life threatening cardiovascular events including stroke and myocardial infarction (123, 156). However, despite its clinical importance, the mechanism(s) responsible for its development have not been completely elucidated.

Cumulative evidence indicates that prolonged exposure to vasoconstrictor agonists causes inward remodeling of arterioles. Ex vivo, prolonged vasoconstriction induced by exposure of isolated arterioles to endothelin-1, angiotensin II, norepinephrine, or serum causes inward remodeling (15, 16, 115). In vivo, vasoconstriction also appears to be the primary stimulus causing inward remodeling in hypertension, as vasodilation and not a mere reduction in blood pressure is needed to prevent or revert inward remodeling in hypertensive individuals (39, 122). The mechanism(s) responsible for inducing remodeling during prolonged vasoconstriction, however, remain elusive.

A series of recent studies indicates that inward remodeling of arterioles requires transglutaminase activity. In 2005 Bakker et al. showed that the inward remodeling induced by prolonged exposure of isolated arterioles to endothelin-1 was prevented by incubation with the inhibitors of transglutaminase, cystamine, or 5-(biotinamido) pentylamide (11). In vivo, it has also been shown that inhibition of transglutaminase activity with cystamine prevents the inward remodeling observed in mesenteric arterioles of rats subjected to prolonged infusion with phenylephrine or a local reduction in blood flow (11, 53). In conduit arteries, Santhanam et al. (166) showed that the reduced distensibility observed in carotid arteries of mice treated with the nitric oxide synthase inhibitor L-N^Gnitroarginine methyl ester (L-NAME) was greater in wild type animals than in those not expressing tissue-type transglutaminase. They also observed that the increased pulse wave velocity observed in old rats was diminished after treatment with cystamine, suggesting that inhibition of transglutaminase activity reduces aortic stiffness (166).

As transglutaminase activity is known to participate in the crosslinking of extracellular matrix proteins, it has been proposed that inward remodeling and vascular stiffness occur as transglutaminase crosslinks extracellular matrix proteins of vessels with reduced diameters and thus prevents subsequent vessel diameter expansion (11, 166).

Evidence is also accumulating that indicates the process of vasoconstriction involves the activation of small GTP binding proteins and the polymerization of actin within vascular smooth muscle cells (99). Recently we demonstrated that inhibition of actin polymerization or the signaling pathways associated with the activity of the small GTP binding proteins, Rho and Rac, prevents prolonged vasoconstriction from inducing inward remodeling in isolated arterioles (179). Moreover, we showed that nearly 75% of the structural reduction in passive diameter observed in the early stages of vasoconstriction-induced inward remodeling is reversible upon the enzymatic depolymerization of F-actin (179). Other studies have shown that dithiothreitol (DTT) induces inward remodeling in isolated arterioles via the activation of endogenous transglutaminases (194), and that DTT induces vasoconstriction in isolated arteries (59, 60). Moreover, transglutaminase activity is known to activate RhoA (88). Therefore, we designed the present study to test the hypothesis that prolonged activation of endogenous transglutaminase with DTT reduces the passive diameter of arterioles through processes that depend on actin cytoskeletal structures and require actin polymerization and vasoconstriction.

3.2 Materials and methods

3.2.1 Animals

Male Sprague-Dawley rats (~200 g) were used in all experiments. All animal protocols and procedures implemented during these studies were approved by the Animal Care Quality Assurance office (ACQA) and the Animal Care and Use Committee (ACUC) at the University of Missouri-Columbia. Before experimentation rats were housed in pairs under a 12-hour per day illumination regimen and provided with ad libitum access to standard rat chow and water.

3.2.2 Vessel isolation

Rats were anesthetized by means of an intraperitoneal injection of pentobarbital sodium at a dose of 100 mg/Kg. After confirmation that spinal reflexes were lost, both cremaster muscles were excised and placed in a cold (~4°C) physiological saline solution (PSS) containing: 145.0 NaCl, 4.7 KCl, 2.0 $CaCl_2$, 1.0 $MgSO_4$, 1.2 NaH_2PO_4, 0.02 EDTA, 2.0 Pyruvic Acid, 5.0 Glucose and 3.0 MOPS (all concentrations are given in mM) with a final pH of 7.4. First order (1A) feed arterioles from each cremaster were isolated, cannulated and pressurized for experimentation as previously described (115). Briefly, arteriolar segments of ~1mm in length were cannulated onto glass micropipettes within an observation chamber (Living Systems Instrumentation, Burlington, Vermont) filled with PSS. The arterioles were pressurized without flow to 60 mmHg using a Pressure Servo System (Living Systems Instrumentation Burlington, Vermont) and PSS containing 0.15 mM bovine serum albumin. The observation chamber with the

cannulated vessel was transferred to an inverted microscope equipped with a video display and video caliper system (Living Systems Instrumentation Burlington, Vermont) to record measurements of wall thickness and luminal diameter. All experiments were performed at 34.5°C.

3.2.3 Experimental protocols

<u>Assessment of endogenous transglutaminase activation by DTT in isolated arterioles</u>

To determine relative transglutaminase activity, isolated arteriolar segments were incubated with the transglutaminase substrate Alexa Fluor 488 cadaverine. Rat cremaster 1A arterioles were isolated and then transferred to 1.5 mL tubes containing 10μM cadaverine in PSS and incubated over night at 4°C. The next day, vessels were warmed to 37°C and incubated in one of the following treatments: PSS + 10 μM cadaverine (Control), PSS + 200 μM DTT + 10 μM cadaverine (DTT), and PSS + 200 μM DTT + 1.0mM cystamine + 10 μM cadaverine (DTT + cystamine) for 4 hours at 37°C. All subsequent steps were performed at 4 °C. Vessels were washed twice in phosphate buffered saline (PBS), then fixed for 1 hour in 4% paraformaldehyde. Vessels were washed twice in PBS and then incubated for 1 hour in 2.0μM 4',6-diamidino-2-phenylindole (DAPI) in PBS + 10% bovine serum albumin (BSA) to visualize nuclei. Vessels were washed 3 times in wash buffer followed by 2-time wash in PBS. Vessels were then imaged using a Leica SP5 confocal microscope with a 63x/1.2 numerical aperture water objective. Cadaverine was excited with an Argon laser at 488 nm. DAPI was excited with a multi-photon laser at 720 nm. Images were processed and quantified

31

using Imaris software. For quantification, a region of interest (ROI) was selected containing predominantly vascular smooth muscle cells. ROI $\cong$ 40μm x 40μm x 15μm. The mean fluorescent intensity per μm^3 was determined for the ROI, n ≥ 5 for all treatments.

Effects of acute activation of endogenous transglutaminase on arteriolar tone

To determine the acute effect of endogenous transglutaminase activation on arteriolar function, isolated arterioles with spontaneous myogenic tone were exposed abluminally to increasing concentrations of DTT ($10^{-6.5}$ to 10^{-3} M) in the absence or presence of the transglutaminase inhibitor, cystamine (1 mM). Cystamine has been previously used at concentrations of 0.1 and 1 mM to inhibit the activity of transglutaminase in vascular tissues (11, 91). In our experiments designed to inhibit transglutaminase activity, cystamine was added to the superfusate 20 minutes before and at all times during exposure to DTT. In an additional series of experiments, arterioles were incubated with 500 nM cytochalasin-D 20 minutes before and at all times during exposure to increasing concentrations of DTT in order to block actin polymerization (179). To construct vessel diameter response curves, each concentration of DTT was maintained for 5 minutes in the absence or presence of cystamine or cytochalasin-D.

Effects of prolonged activation of endogenous transglutaminase on arteriolar remodeling

To confirm previous observations that prolonged activation of endogenous transglutaminase induces arteriolar inward remodeling (11, 194), isolated arterioles pressurized to 60 mmHg were exposed to 200 μM DTT for 4 hours in the absence or presence of 500 nM cytochalasin-D. We chose a concentration of 200 μM DTT because it induced a submaximal constriction of arterioles that is completely blocked by 1 mM cystamine (Fig. 3.1-C). Before and after the prolonged exposure to DTT arterioles were exposed to Adenosine (10^{-4} M), and then to Ca^{2+}-free PSS containing Adenosine (10^{-4} M) and EGTA (2 mM) to obtain maximum passive diameter. A reduction in the maximal luminal diameter obtained after the prolonged exposure to DTT was considered evidence that inward remodeling had occurred. Presence of cytochalasin-D caused the prolonged vasoconstriction induced by DTT to wane over time. Therefore, as both cytochalasin-D and cystamine prevented DTT from maintaining vasoconstriction, additional experiments were conducted in vessels pressurized to 5 mmHg in order to maintain a reduced diameter during the prolonged exposure to DTT in combination with cytochalasin-D or cystamine. In all experiments where cytochalasin-D or cystamine was used, arterioles were pre-incubated for 20 minutes with the inhibitor and at all times during exposure to DTT.

<u>Effect of prolonged activation of endogenous transglutaminase on actin polymerization</u>

To determine the effect of prolonged activation of endogenous transglutaminase on actin polymerization, we measured the amount of F and G actin present in isolated arterioles exposed for 4 hours to DTT or vehicle control as previously described (179) . Freshly isolated rat cremasteric 1A arterioles were incubated in 1.5 mL vials at 34°C for 4 hours in either PSS (Control), or PSS+200μM DTT. Immediately after treatment, arterioles were homogenized in an F-actin stabilization buffer (Cytoskeleton #LAS01) with ATP, Halt Protease & Phosphatase Inhibitor Cocktail and EDTA (Thermo Scientific #78440),. Subsequently, the homogenized samples were centrifuged for 1 hour at 100,000xg. After centrifugation, the supernatants were transferred into new labeled 1.5 mL vials, while the pellets were incubated and re-suspended for 1 hour in an F-actin depolymerization buffer (Cytoskeleton #FAD02) at 4°C. The supernatant and pellet portions of the samples were subjected to SD-PAGE and proteins transferred to nitrocellulose membranes (BIO-RAD #162-0147). The blots were probed with rabbit polyclonal anti-actin antibody (Cytoskeleton #AAN01 at a 1:1,000 dilution) and protein bands visualized with a ChemiDOC XRS+ (BIO-RAD). Images were analyzed and the signals for supernatants (G-actin) and pellets (F-actin) for each treatment were quantified, and F-actin/Total-Actin ratios were computed and compared (179).

Effect of F-actin cytoskeleton disruption on control and remodeled arterioles

In order to test the effect of F-actin cytoskeleton disruption on the vasculature, and to determine the role of F-actin cytoskeletal structures in vascular remodeling, freshly isolated arterioles and DTT-remodeled arterioles were subjected to a 1-hour incubation with the actin-depolymerizing agent Mycalolide-B (2 µM) in Ca^{2+}-free PSS (160, 179). Subsequently, passive pressure-diameter relationships were determined for each arteriole.

Determination of arteriolar elastic characteristics

To study the elastic characteristics of the arteriolar wall, and to determine the effect of actin cytoskeleton disruption on remodeled arterioles, pressure-diameter curves were obtained under passive conditions (Ca^{2+}-free PSS) before and after every main treatment in the experimental protocols. Pressurizations were performed in steps covering a range between 5 and 120 mmHg. Maximum internal diameter and wall (left and right) thicknesses were recorded at each pressure. This information was later used to determine the circumferential stress, strain and moduli of elasticity curves for each group of vessels.

Chemicals

All chemicals and drugs used in this study were purchased from Sigma (St. Louis, Missouri), except for Mycalolide-B, which was acquired from Wako (Wako Chemicals, USA, Richmond, Virginia); Alexa Fluor 488 cadaverine from Invitrogen; and the chemicals and anti-bodies used for F and G-actin separation were purchased from BIO-RAD, KPL, Cytoskeleton, Chemicon and Thermo Scientific. In preparation for the

experiments, stock solutions of adenosine, cystamine and DTT were prepared in PSS (without Glucose and Pyruvate) at a concentration of 10^{-2} M, 10^{-1} M and 10^{-1} M, respectively. Stock solutions of cytochalasin-D and mycalolide-B were made in DMSO at a concentration of 1 mM and 2 mM, respectively. Stock solutions were diluted in the buffer solution used as superfusate (i.e., PSS or Ca^{2+}-free PSS). The final concentrations reported refer to concentrations in the superfusate.

3.2.4 Data analyses

Data are presented as mean values of multiple experiments (the number of experiments is reported for each experimental series in the results section and The Figures) ± SEM (standard error of the mean). Diameter (μm), wall thickness (μm), pressure (mmHg), circumferential stress (dynes/cm^2), strain and modulus of elasticity (dynes/cm^2) were calculated as previously described (148, 178), and are expressed in absolute values. The circumferential stress was calculated at every pressure as $\sigma_i = P_i D_i / (\tau_{L,i} + \tau_{R,i})$, where P_i is the intraluminal pressure, D_i is the internal diameter; and, $\tau_{L,i}$ and $\tau_{R,i}$ are the left and right wall thicknesses obtained from the 2D projection of the video caliper. The strain was calculated as $\varepsilon_i = (D_i - D_0)/D_0$, where D_0 represents the internal diameter measured at the lowest intraluminal pressure (5 mmHg), and D_i represents the internal diameter measured at greater intraluminal pressures. We calculated the modulus of elasticity as the ratio between stress and strain ($E_i = \sigma_i / \varepsilon_i$) to obtain a measure of the wall stiffness. Repeated measures ANOVA and paired or unpaired T-tests were used to make statistical comparisons between means. Differences were considered significant at values of P ≤ 0.05.

3.3 Results

3.3.1 DTT-induced activation of transglutaminases is blocked by cystamine

In order to assess the activation of endogenous transglutaminases by DTT, and to determine the effectiveness of cystamine to block this activation, we utilized a previously described (194) fluorescent assay that quantifies transglutaminase activity by the incorporation of transglutaminase substrate Alexa Fluor 488 cadaverine in isolated arterioles. The vessels not exposed to DTT had a modest amount of fluorescence indicative of minimal incorporation of cadaverine via transglutaminase crosslinking (Fig. 3.1-A,B). In contrast, DTT treated vessels, displayed a roughly 3-fold increase in fluorescent intensity indicative of cadaverine incorporation into arteriolar structures. The addition of the transglutaminase inhibitor cystamine (1 mM) completely abolished the marked increase in cadaverine incorporation induced by DTT.

3.3.2 Transglutaminase inhibition with cystamine blocks DTT-induced arteriolar constriction

Exposure of isolated and pressurized (60 mmHg) arterioles to DTT induced concentration dependent vasoconstriction with a maximal constriction of 43.8±5.8% from original spontaneous tone at 10^{-3} M DTT (n=5). Inhibition of transglutaminase activity with 1 mM cystamine caused vessels to lose 85.7±11.5% of spontaneous myogenic tone and prevented DTT at all concentrations up to 200 μM from inducing vasoconstriction (n=5) (Fig. 3.1-C). Exposure to cystamine did not prevent a solution containing 80 mM KCl from inducing depolarization-dependent vasoconstriction (Fig. 3.1-D).

A

Control   DTT   DTT + Cystamine
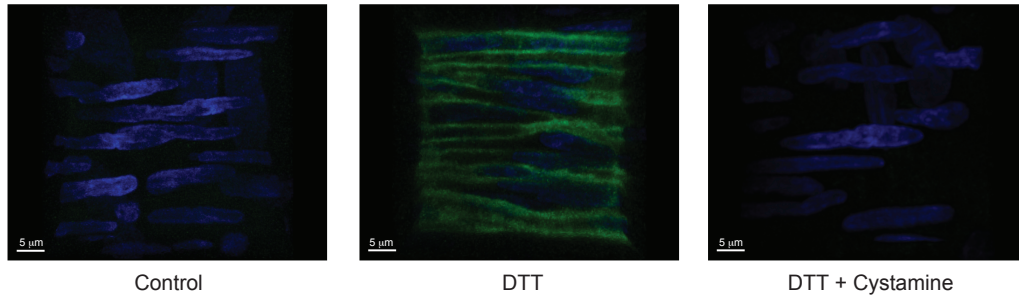
B
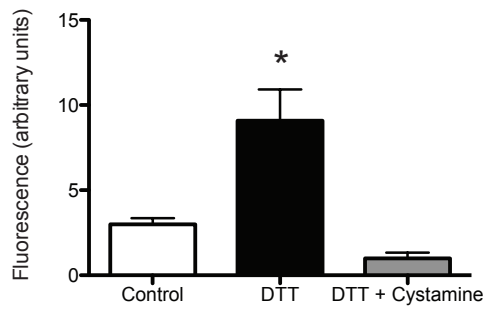
C
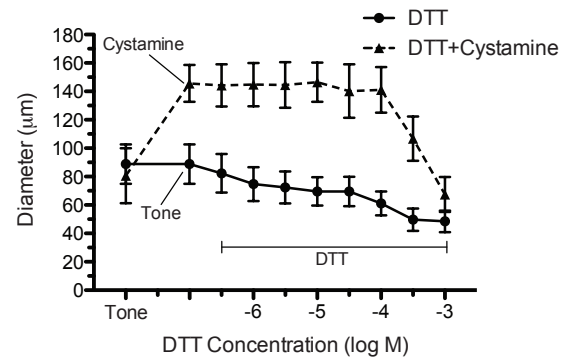
D
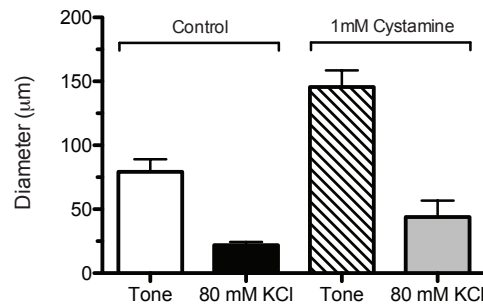
Figure 3.1. Cystamine blocks DTT-dependent activation of endogenous transglutaminases and DTT-induced vasoconstriction but not depolarization-induced vasoconstriction. A: Confocal images of rat cremaster arteriolar walls incubated with Alexa Fluor 488-cadaverine (green) and exposed for 4 hours to vehicle control (left), 200 μM DTT (center), or DTT in the presence of 1mM cystamine (right). Blue shows smooth muscle nuclei stained with 4',6-diamidino-2-phenylindole (DAPI). B: Mean fluorescence intensity

of Alexa Fluor 488 cadaverine in Control (n=5), DTT (n=7), and DTT+Cystamine (n=5) treated arterioles. *P≤0.05 vs. Control or DTT+Cystamine. C: Percent control diameter of isolated arterioles exposed to incremental concentrations of DTT in the absence (n=5) or presence (n=5) of 1mM cystamine. Diameters in the presence of cystamine at DTT $10^{-6.5}$ to $10^{-3.5}$ M were significantly greater than those with DTT alone (*P≤0.05). D: Internal diameter (µm) of isolated and pressurized (60 mmHg) arterioles before (Tone) and after exposure to 80 mM KCl in the absence (n=5) or presence (n=5) of 1 mM cystamine. Data are means ± SEM.

3.3.3 Prolonged exposure to DTT causes inward eutrophic remodeling in isolated arterioles

Exposure of isolated and pressurized (60 mmHg) arterioles to DTT (200 µM) for 4 hours caused a strong (39.5±5.1% from spontaneous myogenic tone) and continuous (entire exposure time) vasoconstriction (Fig. 3.2-A). Arterioles remained constricted by 31.8±6.3% of spontaneous myogenic tone after removing DTT from the perfusate for 10 minutes and by 19.7±8.9% after exposure to the vasodilator adenosine (10^{-4} M). Once arterioles were exposed to Ca^{2+}-free solution, their maximal passive diameter attained was significantly smaller and their media-to-lumen ratio significantly larger than those observed before exposure to DTT (Fig. 3.2-A,B). Passive pressure-diameter profiles obtained before and after exposure to DTT showed that the reduction in inner passive diameter was evident at all pressures (Fig. 3.2-C). Strain-stress profiles showed that the remodeled arterioles had decreased circumferential stress, but no major changes in distensibility (Fig. 3.2-D). Remodeled arterioles had a tendency towards a reduced modulus of elasticity at high pressures that was not significantly different (P>0.05) from controls (Fig. 3.2-E).

39
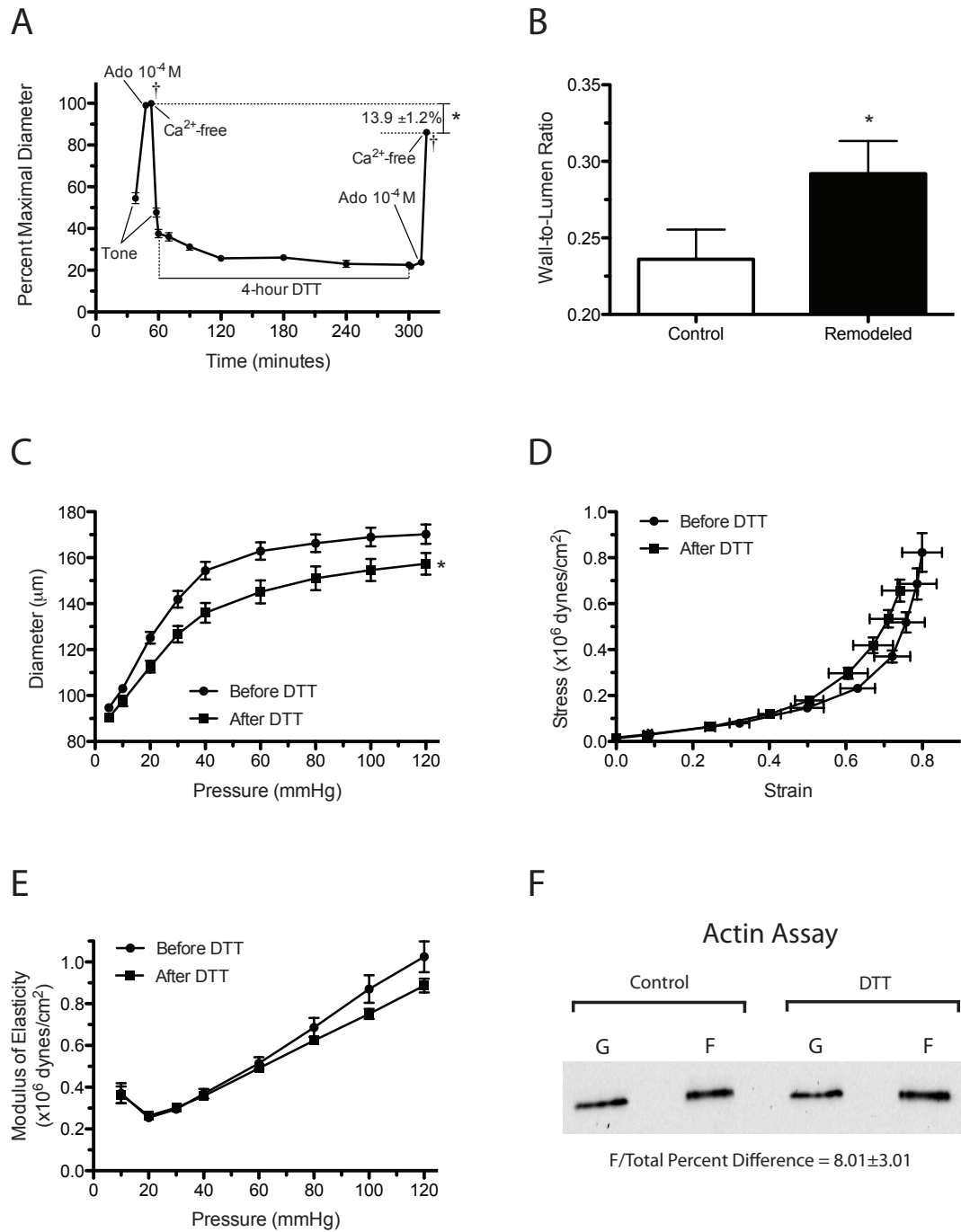
Figure 3.2. Prolonged exposure to DTT induces inward remodeling in isolated arterioles. A: Arterioles were exposed to 200 μM DTT for 4 hours. Before and after the 4-hour exposure to DTT, arterioles were allowed to develop spontaneous tone and subsequently exposed to 10^{-4} M adenosine (Ado) and then to calcium-free solution. Data are means ± SEM of the maximal passive diameter obtained during the first exposure to calcium-free conditions. After the second exposure to calcium-free conditions,

maximal passive diameter was significantly reduced (*P≤0.05, n=5). B: Wall to lumen ratios of arterioles in calcium-free conditions before (Control) and after a prolonged (4-hour) exposure to DTT (n=5). *P≤0.05 vs. control. C: Passive pressure-diameter curves of arterioles obtained before (Before DTT, n=5) and after (After DTT, n=5) exposure (4 hours) to 200 μM DTT. *P≤0.05 vs. Before DTT. D: Passive strain-stress relationships of isolated arterioles before (Before DTT, n=5) and after (After DTT, n=5) exposure (4 hours) to 200 μM DTT. E: Incremental modulus of elasticity vs. pressure in isolated arterioles under passive conditions before (Before DTT, n=5) and after (After DTT, n=5) exposure (4 hours) to 200 μM DTT. F: Representative immunoblot of the F- and G-actin portions of the cytoskeleton from arterioles treated with vehicle control or DTT (200 μM) for 4 hours. Exposure to DTT increased (P≤0.05) the F/Total actin by 8.01±3.01 % vs. controls (n=6 for each treatment).

3.3.4 Prolonged exposure to DTT increases the F/Total actin ratio in isolated arterioles

Use of a differential centrifugation assay to quantify F- and G-actin proportions revealed that a 4-hour incubation in DTT (200μM) increased the F-actin/Total-actin ratio by 8.01% ± 3.01% (n=6) as compared to control arterioles kept in vehicle control for 4 hours (Fig. 3.2-F).

3.3.5 F-actin disruption does not affect the passive diameter or elastic properties of freshly isolated arterioles

In order to determine the role that disruption of the F-actin cytoskeleton has on the elastic characteristics of freshly isolated arterioles, we first confirmed that a one-hour incubation in mycalolide-B completely destroyed F-actin fibers in isolated arterioles using confocal microscopy. Three-dimensional reconstruction images of arterioles exposed for one hour to vehicle control or mycalolide-B stained to visualize F-actin fibers with Alexa Phalloidin 546 are shown in Fig. 3.3-A. Notice that incubation with mycalolide-B caused a complete obliteration of F-actin fibers contained within cells of

41

the arteriolar wall. In comparison, intact F-actin cytoskeletal structures are evident in freshly isolated arterioles exposed to vehicle (Fig. 3.3-A).

Although a one-hour incubation in Mycalolide-B (2 µM) caused complete disruption of F-actin fibers in freshly isolated (non-remodeled) arterioles, no significant changes in the internal passive diameter or the elastic properties of the vessel wall were evident (Fig. 3.3-B-D).

A

Freshly Isolated Arteriole

After 1-hr in Mycalolide-B

B

C

D
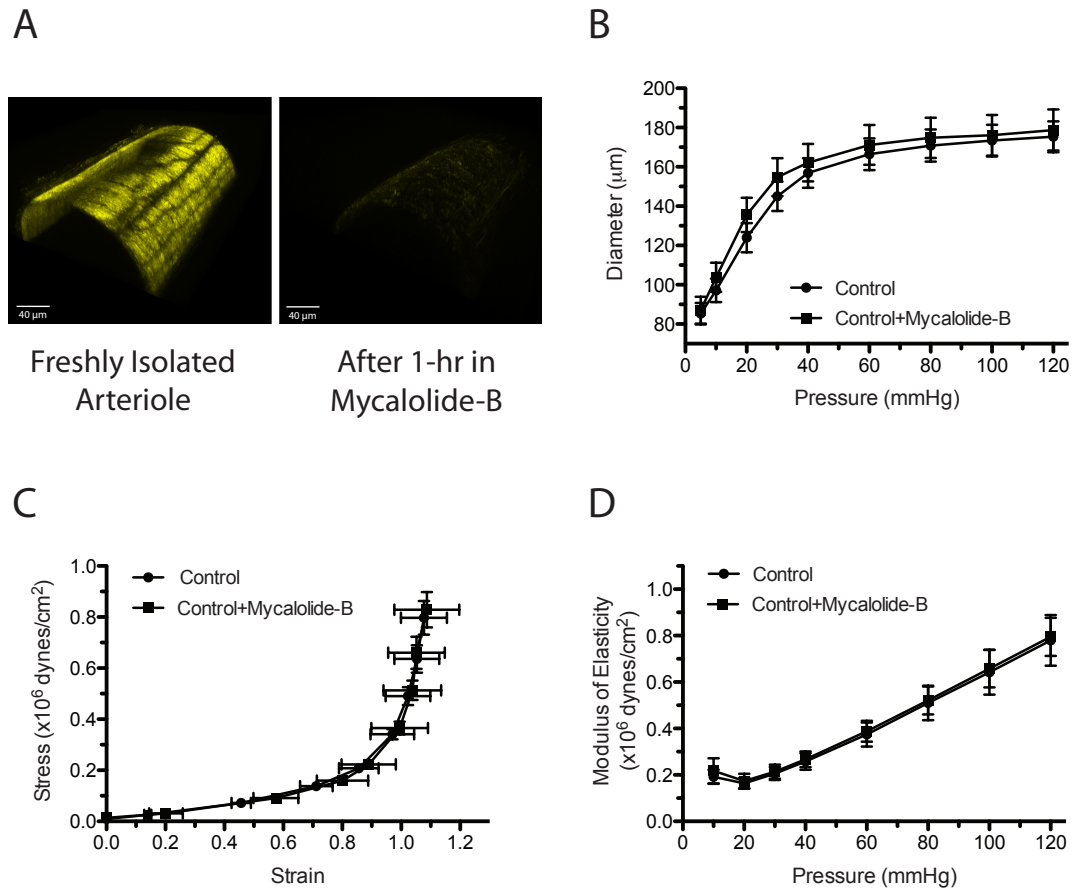
Figure 3.3. Actin cytoskeletal disruption does not affect the passive diameter or elastic characteristics of freshly isolated arterioles. *A:* Three-dimensional confocal images of isolated arterioles exposed to vehicle control (left) or 2 µM mycalolide-B (right) and subsequently stained with phalloidin-Alexa 546 (yellow) to visualize the actin cytoskeleton. *B:* Pressure-diameter curves of freshly isolated

42

arterioles before (Control, n=7) and after (Control+Mycalolide-B, n=7) exposure (1 hour) to 2 μM mycalolide-B. *C:* Strain-stress relationships of freshly isolated arterioles before (Control, n=7) and after (Control+Mycalolide-B, n=7) exposure (1 hour) to 2 μM mycalolide-B. *D:* Incremental modulus of elasticity vs. pressure in freshly isolated arterioles before (Control, n=7) and after (Control+Mycalolide-B, n=7) exposure (1 hour) to 2 μM mycalolide-B.

3.3.6 Disruption of the F-actin cytoskeleton reverts the inward remodeling induced by DTT

The reduction in passive internal diameter induced by prolonged (4 hours) exposure to DTT (200 μM) was completely reverted (97.3±7.2%) after mycalolide-B-induced disruption of the F-actin cytoskeleton. In comparison, exposure to vehicle control only partially reversed the DTT-induced inward remodeling by 57.1±8.0%. Consequently remodeled arterioles exposed to mycalolide-B had significantly greater (P<0.05) passive diameters than those exposed to vehicle control (Fig. 3.4-A,B). Pressure diameter curves showed that inwardly remodeled arterioles had greater passive diameters after vs. before exposure to mycalolide-B at all pressures in the curve (5-120 mmHg). In comparison inwardly remodeled arterioles treated with vehicle control had only greater passive diameters at pressures above 20 mmHg (Fig. 3.4-C,D). With regard to the elastic properties of the arteriolar wall, exposure of remodeled arterioles to mycalolide-B caused reduced distensibility and greater circumferential stress, as well as a 36.7±12.65% increase in stiffness (Fig. 3.4-E,G). In comparison, the stress, strain and stiffness of remodeled arterioles treated with vehicle control were not significantly affected (Fig. 3.4-F,H).
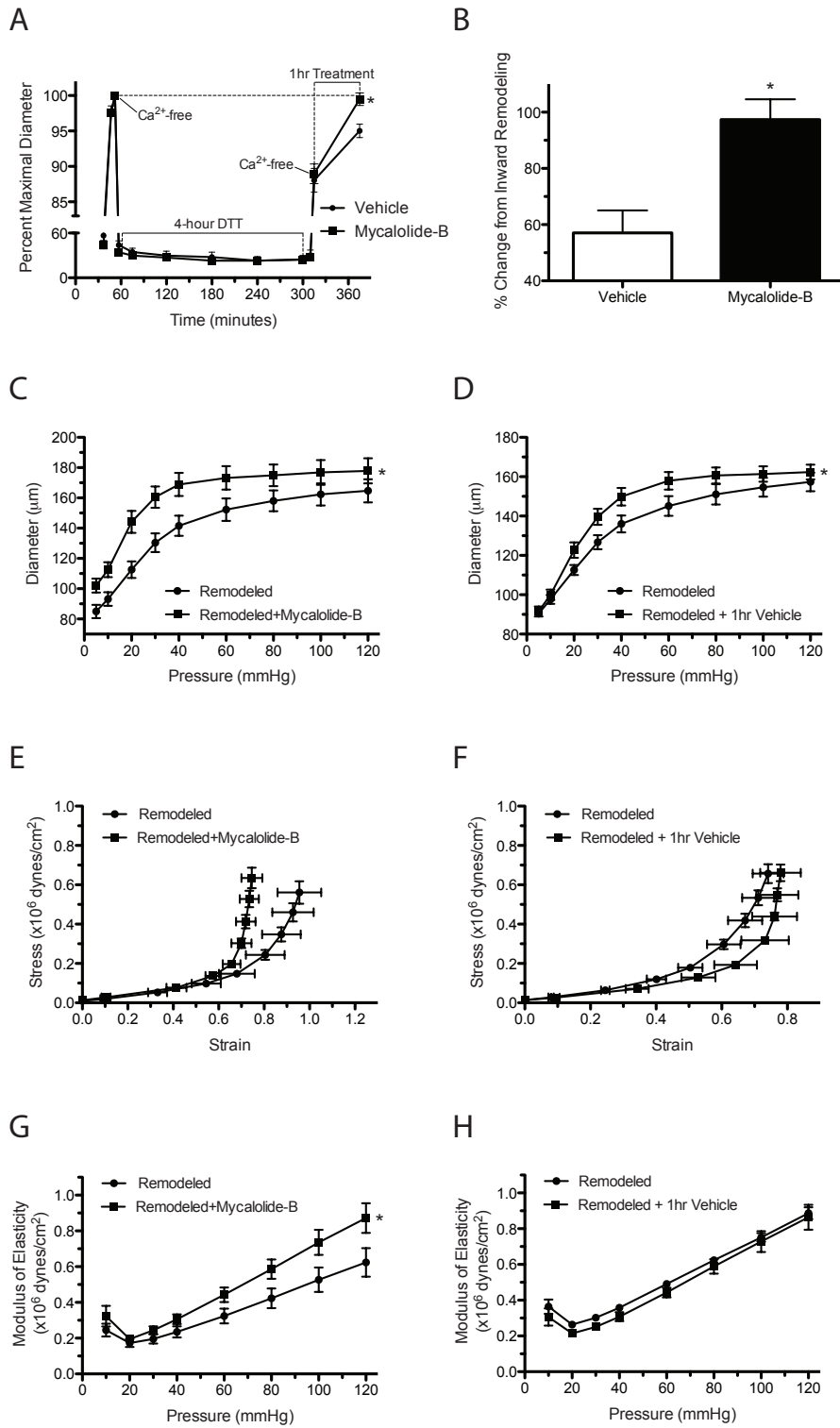
Figure 3.4. Disruption of the actin cytoskeleton reverts the inward remodeling caused by prolonged exposure of isolated arterioles to DTT. A: Arterioles were exposed to 200 µM DTT for 4 hours.

Before and after the 4-hour incubation with DTT, arterioles were allowed to develop spontaneous tone and subsequently exposed to 10^{-4} M adenosine and then to Calcium-free solution. After 5 minutes in the second exposure to calcium-free solution, arterioles were exposed for 1 hour to vehicle control (n=6) or 2 μM mycalolide-B (n=6). Data are means ± SEM of the maximal passive diameter obtained during the first exposure to calcium-free conditions. *P≤0.05 vs. vehicle control. B: Change in diameter caused by 1-hour exposure to mycalolide-B (2 μM) or its vehicle control in arterioles which passive diameter had been reduced by a 4-hour exposure to 200 μM DTT. The percent reversal change was significantly greater in vessels exposed to mycalolide-B vs. vehicle controls (*P≤0.05). C,D: Pressure-diameter curves of DTT-inwardly remodeled arterioles before (Remodeled, n=7 in C and n=5 in D) and after exposure (1 hour) to 2 μM mycalolide-B (Remodeled+Mycalolide-B, n=7) or its vehicle control (Remodeled+Vehicle, n=5). *P≤0.05 vs. Remodeled+Mycalolide-B or Remodeled+Vehicle. E,F: Strain-stress relationships of DTT-inwardly remodeled arterioles before (Remodeled, n=7 in C and n=5 in D) and after exposure (1 hour) to 2 μM mycalolide-B (Remodeled+Mycalolide-B, n=7) or its vehicle control (Remodeled+Vehicle, n=5). G,H: Incremental modulus of elasticity vs. pressure in DTT-inwardly remodeled arterioles before (Remodeled, n=7 in G and n=5 in H) and after exposure (1 hour) to 2 μM mycalolide-B (Remodeled+Mycalolide-B, n=7) or its vehicle control (Remodeled+Vehicle, n=5). *P≤0.05 vs. Remodeled+Mycalolide-B.

3.3.7 Inhibition of actin polymerization blocks DTT-induced arteriolar constriction.

Exposure of isolated and pressurized (60 mmHg) arterioles to cytochalasin-D (500 nM) did not significantly affect vascular tone during the pre-incubation period, but over time caused vessels to lose myogenic tone and dilate. Presence of cytochalasin-D also prevented DTT at all concentrations used from inducing vasoconstriction (Fig. 3.5-A).
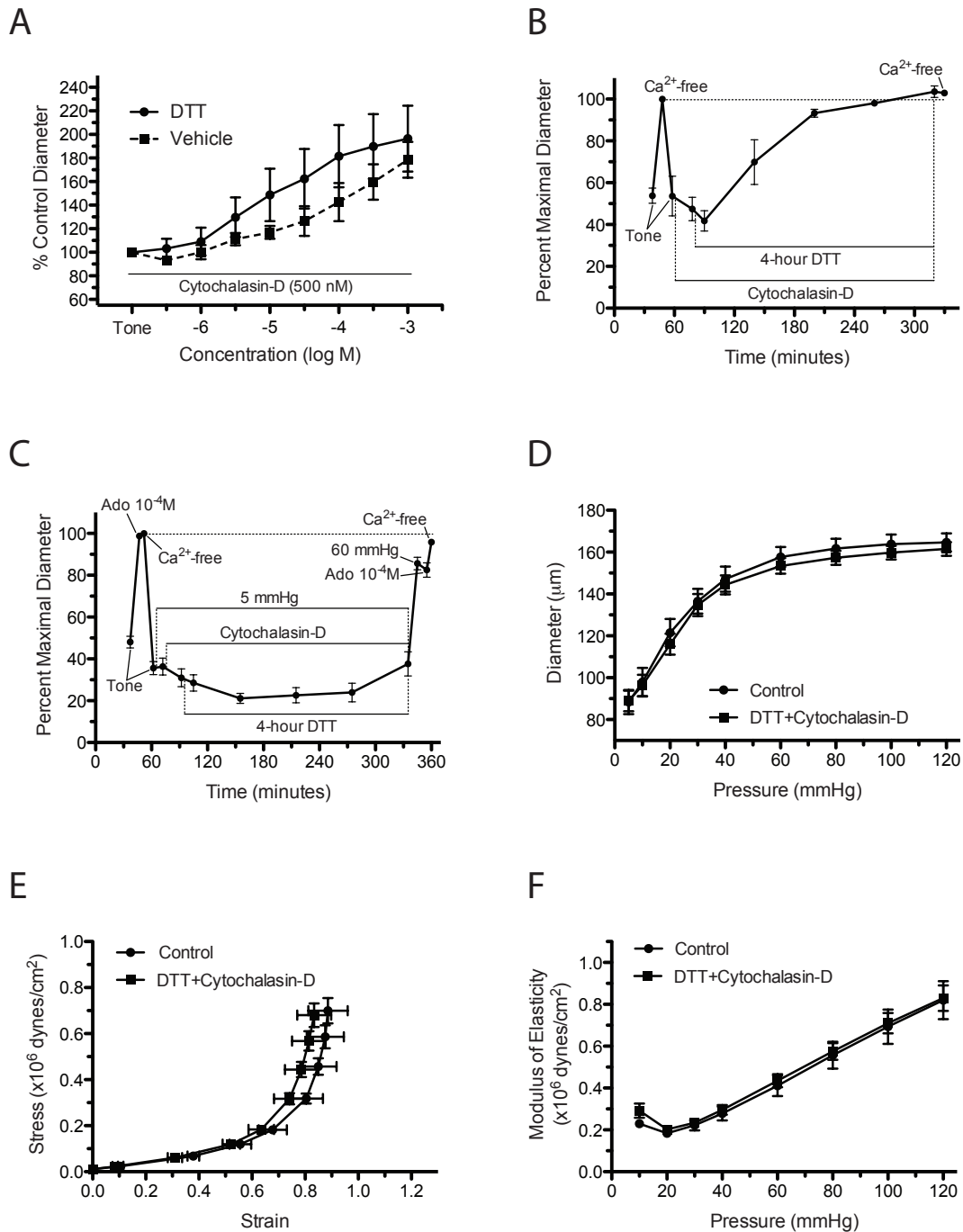
Figure 3.5. Cytochalasin-D inhibits concentration-dependent DTT constriction responses and prevents DTT-induced inward remodeling in isolated arterioles. A: Percent control diameter of isolated arterioles exposed to incremental concentrations of DTT (n=7) or vehicle control (n=5) in the presence of cytochalasin-D (500 nM). B: Arterioles were incubated for 20 minutes with 500 nM cytochalasin-D and then exposed to 200 μM DTT for 4 hours in the presence of cytochalasin-D. Before and after the incubation

46

with cytochalasin-D and DTT, arterioles were allowed to develop spontaneous tone and subsequently exposed to 10^{-4} M adenosine and then to Calcium-free solution (n=4). Data are means ± SEM of the maximal passive diameter obtained during the first exposure to calcium-free conditions. C: Arterioles with intraluminal pressure set at 5mmHg were incubated for 20 minutes with 500 nM cytochalasin-D and then exposed to 200 μM DTT for 4 hours in the presence of cytochalasin-D. Before and after the incubation with cytochalasin-D and DTT, intraluminal pressure was increased to 60 mmHg and arterioles were allowed to develop spontaneous tone followed by exposure to 10^{-4} M adenosine and then to Calcium-free solution (n=6). Data are means ± SEM of the maximal passive diameter obtained during the first exposure to calcium-free conditions. D: Passive pressure-diameter curves of arterioles obtained before (Control, n=6) and after (DTT+Cytochalasin-D, n=6) exposure (4 hours) to cytochalasin-D (500 nM) and DTT (200 μM), while at an intraluminal pressure of 5 mmHg. E: Passive strain-stress relationships of isolated arterioles obtained before (Control, n=6) and after (DTT+Cytochalasin-D, n=6) exposure (4 hours) to cytochalasin-D (500 nM) and DTT (200 μM), while at an intraluminal pressure of 5 mmHg. F: Incremental modulus of elasticity vs. pressure in isolated arterioles under passive conditions obtained before (Control, n=6) and after (DTT+Cytochalasin-D, n=6) exposure (4 hours) to cytochalasin-D (500 nM) and DTT (200 μM), while at an intraluminal pressure of 5 mmHg.

3.3.8 Inhibition of actin polymerization prevents DTT-induced inward remodeling

In isolated arterioles pressurized to 60 mmHg, presence of cytochalasin-D (500 nM) inhibited the constriction induced by 200 μM DTT and caused arterioles to dilate over the 4-hour exposure to the agents (Fig. 3.5-B). At the end of the prolonged exposure to cytochalasin-D and DTT the passive diameter of arterioles did not differ from that obtained before exposure to the agents (Fig. 3.5-B). To ensure that vasodilation or the lack of constriction (reduction in arteriolar diameter) was not an influencing factor in preventing remodeling, an additional series of experiments were performed in arterioles maintained at 5 mmHg of intraluminal pressure. In these vessels, exposure to DTT with cytochalasin-D for 4 hours caused a small but significant constriction. Nonetheless, DTT in the presence of cytochalasin-D failed again to cause a significant reduction in maximal

47

passive diameter measured at 60 mmHg (Fig. 3.5-C). Consequent, no significant changes were observed after vs. before the prolonged exposure to DTT and cytochalasin-D in pressure-diameter profiles, strain-stress curves and elastic moduli of arterioles (Fig. 3.5-D-F).

3.3.9 Transglutaminase inhibition with cystamine blocks DTT-induced inward remodeling

Since cystamine also blocked the vasoconstriction induced by DTT, a series of experiments were performed in arterioles maintained at 5 mmHg of intraluminal pressure to maintain vascular diameter reduced in the presence of cystamine and DTT. In these vessels, exposure to DTT with cystamine induced no significant changes in vascular diameter (Fig. 3.6-A). In addition, prolonged exposure to these agents caused no significant reduction in the maximal passive diameter measured at 60 mmHg (Fig. 3.6-A,B). No significant changes were observed either in the pressure-diameter profiles, strain-stress curves and elastic moduli obtained after the prolonged exposure to DTT and cystamine when compared with those obtained before exposure to the agents (Fig. 3.6-B-D).
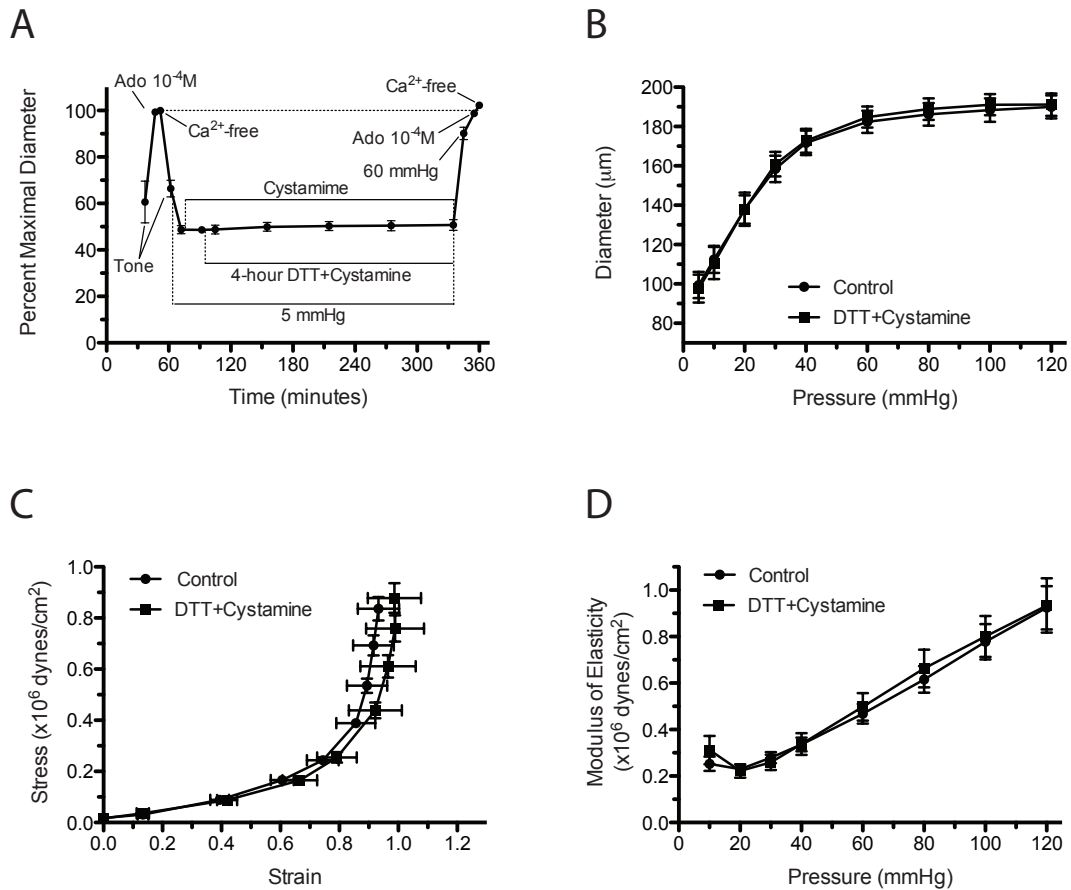
Figure 3.6. Cystamine prevents DTT from causing inward remodeling in isolated arterioles. A: Arterioles with intraluminal pressure set at 5mmHg were incubated for 20 minutes with 1 μM cystamine and then exposed to 200 μM DTT for 4 hours in the presence of cystamine. Before and after the incubation with cystamine and DTT, intraluminal pressure was increased to 60 mmHg and arterioles were allowed to develop spontaneous tone followed by exposure to 10^{-4} M adenosine and then to Calcium-free solution (n=6). Data are means ± SEM of the maximal passive diameter obtained during the first exposure to calcium-free conditions. B: Passive pressure-diameter curves of arterioles obtained before (Control, n=6) and after (DTT+Cystamine, n=6) exposure (4 hours) to cystamine (1 mM) and DTT (200 μM), while at an intraluminal pressure of 5 mmHg. C: Passive strain-stress relationships of isolated arterioles obtained before (Control, n=6) and after (DTT+Cystamine, n=6) exposure (4 hours) to cystamine (1 mM) and DTT (200 μM), while at an intraluminal pressure of 5 mmHg. D: Incremental modulus of elasticity vs. pressure in isolated arterioles under passive conditions obtained before (Control, n=6) and after (DTT+ Cystamine, n=6) exposure (4 hours) to cystamine (1 mM) and DTT (200 μM), while at an intraluminal pressure of 5 mmHg.

3.4 Discussion

The primary finding of the present study is that endogenous transglutaminase activation with DTT in isolated arterioles induces vasoconstriction and inward remodeling that are dependent on actin cytoskeletal dynamics. Based on previous publications that indicated DTT induces vasoconstriction in dog coronary arteries (59, 60) and activation of transglutaminase in mesenteric resistance arteries (194), we first confirmed that DTT induced endogenous transglutaminase activation as determined by the incorporation of Alexa Fluor cadaverine into smooth muscle arteriolar structures. This cadaverine incorporation induced by DTT was inhibited by the presence of the tranglutaminase inhibitor cystamine (Fig. 3.1-A,B). Similar results using a different more specific transglutaminase inhibitor (i.e., L682777) have been previously reported (194). Our current results, therefore, indicate that in isolated rat-cremaster arterioles, DTT induces endogenous smooth muscle transglutaminase activation.

Next, we performed a series of experiments to determine the effect of acute DTT exposure on vascular function in isolated cremaster arterioles. DTT caused a concentration-dependent vasoconstriction that was completely blocked or diminished by the transglutaminase inhibitor, cystamine (Fig. 3.1-C). In comparison, cystamine did not block the vasoconstriction induced by membrane depolarization with KCl (Fig. 3.1-D). This suggests that DTT induces arteriolar vasoconstriction for the most part through the activation of endogenous transglutaminases. The transglutaminases are a group of enzymes which primary function is to deamidate, transamidate and crosslink free amine

50

groups with a protein glutamine (62, 137). Of the eight transglutaminases known to exist in humans, transglutaminase 1, 2 and 4 have been found in blood vessels, where their primary location is within the cytosol of smooth muscle and endothelial cells (14, 91). It has been previously shown that the vasoconstriction induced by a number of agonists depends on transglutaminase activity (46, 92, 199). Putatively, transglutaminases, in particular transglutaminase 2, could exert vasoconstriction via their activity as G proteins, as activators of Rho, or via their transamidation process of a number of cytoskeletal molecules associated with vascular smooth muscle contraction, including, α actin, filamin A and myosin (137, 199). Our results showing that inhibition of actin polymerization with cytochalasin-D blocked the constriction induced by increasing concentrations of DTT (Fig. 3.5-A), suggest that indeed endogenous transglutaminase activation causes vasoconstriction through process that require actin dynamics.

Next, we determined that a prolonged (4-hour) exposure of isolated and pressurized arterioles to DTT induced a strong and sustained vasoconstriction that resulted in the vessels becoming inwardly remodeled, that is, their maximal passive diameter became smaller (Fig. 3.2). We also determined that prolonged exposure to DTT induced actin polymerization, as determined by the increased F-actin/Total-actin ratio observed in DTT-exposed arterioles compared to controls. Previously we showed that a similar 4-hour exposure to the vasoconstrictor agonists norepinephrine and angiotensin-II induces inward remodeling in isolated arterioles (115, 179), and that the remodeling caused by those vasoconstrictor agonists is reversible upon disruption of the actin cytoskeleton (179). Prolonged exposure to vasoconstrictor agonists has also been

51

previously reported to diminish the response of arterioles to adenosine or sodium nitroprusside (115). We have interpreted these reduced responses to endothelium-independent vasodilators as indication that inward remodeling processes are taking place (117). Similarly, in the present study, prolonged exposure to DTT diminished the vasodilatory response of arterioles to adenosine, but the mechanisms responsible for this effect of prolonged vasoconstriction remains to be determined.

To determine whether the inward remodeling induced by the 4-hour exposure to DTT was also dependent on actin cytoskeletal structures, we exposed DTT-remodeled arterioles to the actin-depolymerizing agent, mycalolide-B. Actin cytoskeletal disruption completely reversed the remodeling induced by DTT (Fig. 3.4-A,B), suggesting that changes in actin cytoskeletal structures are responsible for reducing the passive diameter of arterioles during the early stages of the inward remodeling process induced by transglutaminase activation. The observation that incubation with cytochalasin-D also prevented the passive diameter of arterioles exposed for 4 hours to DTT from becoming reduced (Fig. 3.5-B,C), further suggests that actin polymerization is needed during the inward remodeling process induced by transglutaminase activation. Incubation of remodeled arterioles with the vehicle control for mycalolide-B also reversed the remodeling induced by DTT, but to a lesser extent than the complete reversal achieved by the actin-depolymerizing agent (Fig. 3.4-A,B). We previously reported that the vehicle control for mycalolide-B, which contains no calcium and the vasodilator adenosine, does not reverse the inward remodeling induced by a 4-hour exposure of isolated arterioles to norepinephrine and angiotensin-II (179), suggesting that presence of these

52

vasoconstrictor agonists causes a more permanent modification of cytoskeletal structures than that achieved by the mere DTT-dependent activation of endogenous transglutaminases. The observation that the reversal of inward remodeling induced by mycalolide-B or its vehicle control differed in their effects on the elastic characteristics of the vascular wall further suggests that vasodilation alone reverts only a portion of the cytoskeletal changes induced by transglutaminase activation. This is evident by the capacity of mycalolide-B to increase the passive diameter of remodeled arterioles even at intraluminal pressures of 5 and 10 mmHg (Fig. 3.4-C). Disruption of the actin cytoskeleton also reduced the distensibility of remodeled arterioles, and made them stiffer (Fig. 3.4-E,G), while vessels exposed to vehicle control had no changes in these parameters (Fig. 3.4-F,H). These results support out hypothesis that in the early stages of the inward remodeling process induced by prolonged exposure to DTT, changes in the actin cytoskeleton are in part responsible for modifying the elastic properties of the vascular wall. They are also consistent with data indicating that actin fibers are more elastic (pliable) than extracellular matrix structures (191, 192), which more likely determine the elastic characteristics of the arterioles after disruption of the actin cytoskeleton.

To determine whether the involvement of actin cytoskeletal structures in the elastic characteristics of arterioles is only a feature present in remodeled arterioles, we compared pressure-diameter curves, strain-stress relationships and elastic moduli of freshly isolated arterioles before and after exposure to mycalolide-B (Fig. 3.3). Our results indicate that actin cytoskeletal structures have no significant role on the passive

elastic characteristics of non-remodeled arterioles, and that involvement of the actin cytoskeleton on reducing the passive diameter of arterioles is a common feature in the early stages of the inward remodeling induced by direct activation of endogenous transglutaminase or exposure to prolonged vasoconstrictor agonists.

Previously, van den Akker et al. (194) reported that exposure of non-pressurized resistance arteries to DTT for 24 hours induces inward remodeling through processes dependent on the activation of transglutaminase 2. Their data suggest that the reduction in passive diameter occurs as extracellular matrix components of the vascular wall are crosslinked by transglutaminase activity around a reduced vascular diameter. Because our experiments in which DTT was incubated with cytochalasin-D caused vessels to dilate to near maximal passive diameter during the 4-hour exposure to the agents, we performed a series of experiments in which vessel diameter was maintained reduced at 5 mmHg of intravascular pressure during the exposure to DTT with cytochalasin-D (Fig. 3.5-B,C). Results from those experiments indicate that inhibition of actin dynamics and not vasodilation or the lack of constriction was the reason why vessels did not remodeled inwardly. We also performed experiments in which vessels were incubated for 4 hours in DTT with the transglutaminase inhibitor cystamine while maintained at 5 mmHg of intravascular pressure to keep a reduced vascular diameter (Fig. 3.6). Those vessels also failed to remodel inwardly, indicating that indeed endogenous transglutaminase activation was responsible for changing actin cytoskeletal structures and reducing the passive diameter of arterioles exposed for 4 hours to DTT. Overall, these results suggest that in the early stages of the inward remodeling process induced by endogenous

54

transglutaminase activation, reduction of the passive diameter requires changes in actin cytoskeletal structures. Our results do not rule out that later on in the remodeling process, extracellular transglutaminase activity may solidify the reduced structural diameter of vessels by crosslinking extracellular components of the vascular wall. An additional potential explanation of our results could be that disruption of actin cytoskeletal structures prevents transglutaminase translocation to the cell membrane and extracellular environment. However, this is highly unlikely based on our observation that once inward remodeling induced by DTT had occurred, it was completely reversed upon actin disruption with mycalolide-B.

The physiological relevance of our findings rely on previous reports indicating that inhibition of transglutaminase 2 activity blocks or retards the development of inward remodeling in resistance arteries exposed to low blood flow (11, 13), and reduces the stiffness of conduit arteries that occurs in advanced age (166). The novelty of our findings is that changes in vascular structure associated with endogenous transglutaminase activation start at the level of the cytoskeleton and not with extracellular matrix components. This is particularly important in light of recent reports that indicate vascular smooth muscle cellular stiffness plays a more important role in hypertension than previously thought (149, 173, 211). Although the methods of activation and inhibition of transglutaminase used in our experiments have been used extensively in the past (11, 53, 92, 166, 194, 199, 208), a limitation of our study rests on the potential non-specific effects of DTT and cystamine. Nonetheless, our results are consistent with an increasing body of evidence that indicates intracellular transglutaminase activation

participates in vascular pathology (21, 36, 124, 165). A better understanding of the pathways associated with transglutaminase-dependent cytoskeletal changes should provide new therapeutic avenues for controlling vascular remodeling and the adverse cardiovascular events associated with it.

CHAPTER 4

FUNCTIONAL AND STRUCTURAL CHARACTERISTICS OF SKELETAL MUSCLE AND MESENTERIC RESISTANCE ARTERIES FROM OLD SPONTANEOUSLY HYPERTENSIVE RATS (SHR) AND WISTAR-KYOTO RATS (WKY)

4.1 Introduction

Hypertension is a chronic medical condition characterized by the presence of elevated arterial blood pressure. In most of the cases, hypertension is *essential*; that is, there is no obvious/apparent reason that can be established for the development or presence of the disease. Hypertension increases the risk for developing various cardiovascular diseases. Cardiovascular diseases are considered the major life threatening health conditions. That is why it is important to study and understand all the factors that are involved and that play an important role in the development of hypertension; as well, as to study and understand the physiological and structural changes that occur in the vasculature and are associated with this disease.

The spontaneously hypertensive rat (SHR) is the most commonly used animal model for the study of cardiovascular diseases associated with essential hypertension. These SHRs are Wistar-Kyoto rats that have been bred for high blood pressure. The early development of hypertension in SHR starts within the first few weeks of life (5-6 weeks). When adult, SHRs can reach systolic pressures of about 180-200 mmHg. These rats commonly develop cardiovascular diseases, such as vascular and cardiac hypertrophy, after 40 weeks of age.

In this chapter we focus on the study and understanding of the major functional and structural changes associated with essential hypertension and age. A comparison between 65-week-old SHRs and WKY rats is presented and the major results are discussed.

4.2 Materials and methods

All animal procedures were performed in accordance with the Animal Use and Care Committee at the University of Missouri-Columbia and National Institutes of Health guidelines. SHRs and Wistar-Kyoto WKY rats 65-week-old were used for the studies here included. WKY rats were used as normotensive controls. Animals in both groups were maintained in a control (regular rat chow) diet.

Rats were anesthetized via an intraperitoneal injection of pentobarbital sodium (100 mg/Kg). After confirmation that spinal reflexes were lost, the mesenteric vasculature and both hind legs as well as a portion of the mesentery were excised and placed in a cold (~4°C) physiological saline solution (PSS) containing (in mM): 145.0 NaCl, 4.7 KCl, 2.0 CaCl2, 1.0 MgSO4, 1.2 NaH2PO4, 0.02 EDTA, 2.0 Pyruvic Acid, 5.0 Glucose and 3.0 3-(N-morpholino) propanesulfonic acid at pH 7.4. Third order (3A) mesenteric arterioles (from the mesenteric vasculature) and the gracilis artery (from each hind leg) were isolated, cannulated and pressurized for experimentation as previously described (32, 33, 115). Experiments were performed at 37°C. After warming up for about 1 hour, vessels were exposed to a PSS containing 80 mM KCl to test viability by inducing depolarization of vascular smooth muscle cells membranes and vasoconstriction. Subsequently, vessels were exposed to increasing concentrations of phenylephrine to test for adrenergic vasoconstriction responses. Vasodilation responses to increasing concentrations of acetylcholine or sodium nitroprusside (SNP) were performed after vessels were pre-constricted with 10^{-6} M phenylephrine. These agonists tested endothelium-dependent and -independent vasodilatory responses, respectively.

To study the elastic characteristics of the arterial wall, pressure-diameter curves were obtained under passive conditions (in vessels exposed to Ca^{2+}-free PSS containing 2 mM ethylene glycol tetra-acetic acid and 10^{-4} M adenosine) at the end of each experiment. Changes in intraluminal pressure were performed in steps covering a range between 5-120 mmHg. Maximum internal diameter and wall (left and right) thicknesses were recorded at each pressure. After experimentation, this information was used to calculate

the circumferential stress, strain and modulus of elasticity curves for each group of vessels (32, 33).

Post experimentation, vessels were fixed with 4% paraformaldehyde, while pressurized at 70 mmHg for 1 hour. For imaging, cannulated vessels were incubated for 1 hour in 0.5μg/mL 4',6-diamidino-2-phenylindole (DAPI), 0.2μM Alexa Fluor 633 Hydrazide (Molecular Probes) and 0.02 μM Alexa Fluor 546 phalloidin (Molecular Probes) in PBS. Alexa Fluor 633, which stains elastin, was excited with a 633 nm HeNe laser. Alexa Fluor 546 phalloidin, which stains the actin cytoskeleton, was excited with a 543 nm HeNe laser. DAPI, was used to image nuclei, was excited with a multi-photon laser at 700 nm. Second-harmonic image generation was used to image collagen by utilizing a multi-photon laser at 850 nM. A Leica SP5 confocal/multiphoton microscope with a 63x/1.2 numerical aperture water objective was used to obtain confocal/fluorescence images of the vessels under study. Images were processed and all channels were quantified to determine the total volume occupied by VSMCs nuclei, elastin, actin (within the media) and collagen. The image processing was performed with an in-house built algorithm on the MATLAB (The Mathworks, USA) environment.

4.3 Results

4.3.1 Adrenergic vasoconstriction responses in arterioles from old WKY and SHR are similar

When assessing adrenergic-receptor dependent vasoconstriction in mesenteric arterioles from WKY and SHR rats, no significant differences were found in the vasoconstriction levels reached at the different increasing concentrations of phenylephrine between groups. Similarly, when gracilis arteries where exposed to the same range of increasing concentrations of phenylephrine, the constriction at the maximum concentration was not different between groups; however, at low concentrations (specifically 10^{-7} M) gracilis arteries from SHR showed a reduced constriction when compared to arteries from WKY (Fig. 4.1).
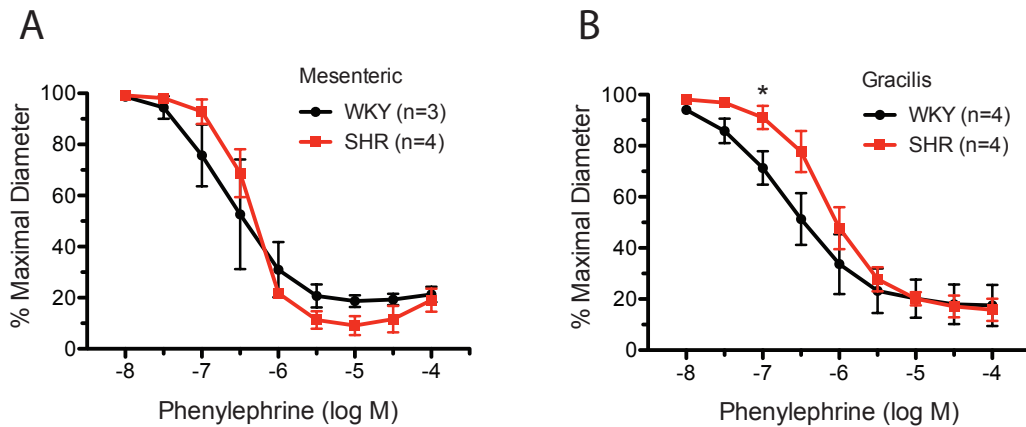
Figure 4.1. Vasoconstriction measurements at different increasing-concentrations of phenylephrine. Values are expressed as a percent of the maximal diameter. Results are given as mean ± SEM. * $p<0.05$ vs WKY.

4.3.2 Differences in endothelium-dependent vasodilation for arterioles from WKY and SHR

Endothelium-dependent vasodilation was assessed on gracilis and mesenteric arterioles by exposure to increasing concentrations of acetylcholine. Although, no significant differences were observed in maximal dilation in either of the two vascular beds between groups (Fig. 4.2), the EC50s associated with the vasodilatory respectively dose-response for mesenteric arterioles from WKY rats and SHRs were significantly different. EC50s were calculated at -7.891±0.016 for WKY and -6.995±0.199 for SHR (Fig. 4.2-A).
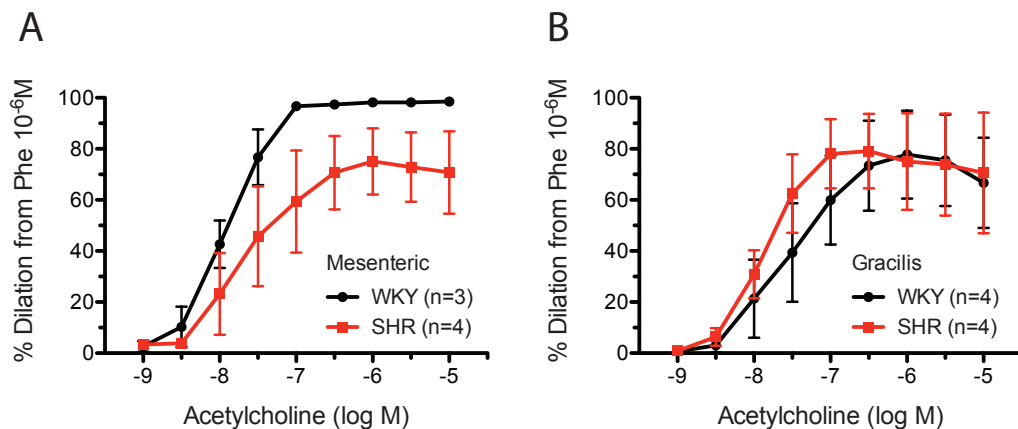
Figure 4.2. Endothelium-dependent vasodilation at different increasing-concentrations of acetylcholine. Relaxation is expressed as percent dilation from the constriction level at phenylephrine 10^{-6} M. Results are given as mean ± SEM.

4.3.3 Mesenteric arterioles from SHRs have heightened SNP-vasodilation

When exposing mesenteric arterioles to increasing concentrations of the endothelium-independent vasodilator SNP, arterioles from SHR showed an increased relaxation ($p<0.05$) at every concentration compared to arterioles from WKY (Fig. 4.3-A). No significant differences in the dilation induced by SNP in gracilis arteries were observed between groups (Fig. 4.3-B).
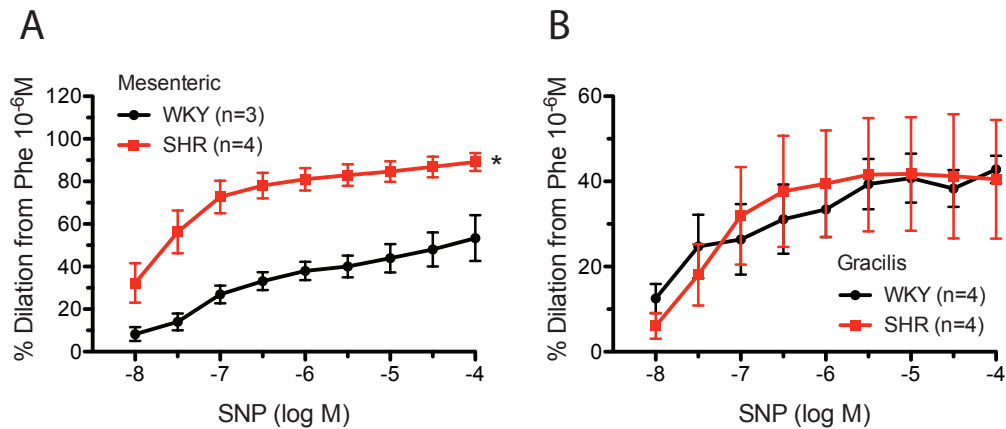
Figure 4.3. SNP vasodilation at different concentrations ranging from 10^{-8} to 10^{-4} M. Values are expressed as percent dilation from the constriction level at phenylephrine 10^{-6} M. Results are given as mean ± SEM. * $p<0.05$ vs WKY.

4.3.4 Arterioles from SHRs are inwardly remodeled

Mesenteric and gracilis arterioles from SHRs showed significantly reduced ($p<0.05$) luminal diameters under passive conditions when compared with the control group (WKY). The arterioles from SHRs also had significantly larger wall-to-lumen ratios. These are both structural markers indicative of inward remodeling (Fig. 4.4).
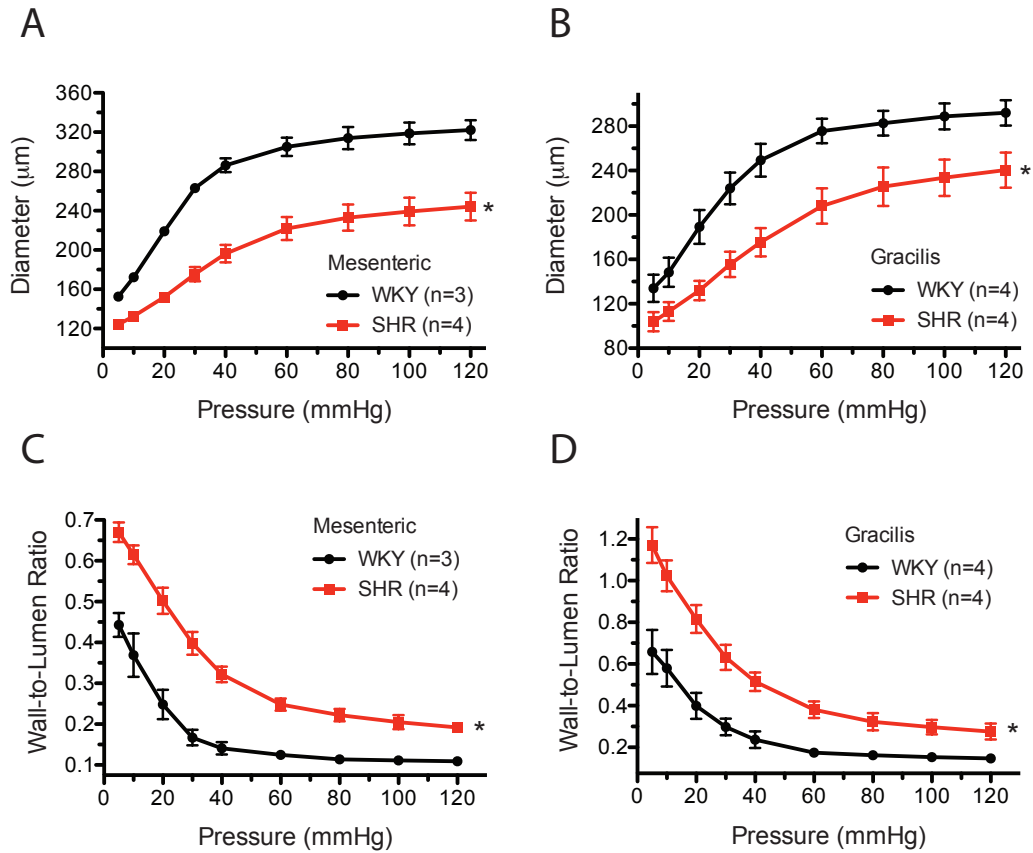
Figure 4.4. (A, B) Characterization of the maximum passive luminal diameter at different intraluminal pressures for mesenteric and gracilis arteries from WKY and SHRs. (C, D) Wall-to-lumen ratios at every pressure for mesenterics and gracilis arterioles, respectively. Results represent means ± SEM. * $p < 0.05$ vs WKY.

4.3.5 Arterioles from SHRs have reduced compliance indicative of increased stiffness

When assessing the elastic properties of the arterioles included in this study, vessels from the SHRs showed a significantly reduced circumferential wall stress in the entire pressure range, but it was more evident at larger pressures ($\geq$60 mmHg) (Fig. 4.5-A,B). However, the cross-sectional compliance, which is inversely proportional to the

stiffness, as a function of intraluminal pressure showed that, in the lower range of pressure, arterioles from SHR had significantly reduced compliance, which is indicative of increased stiffness. (Fig. 4.5-C,D).
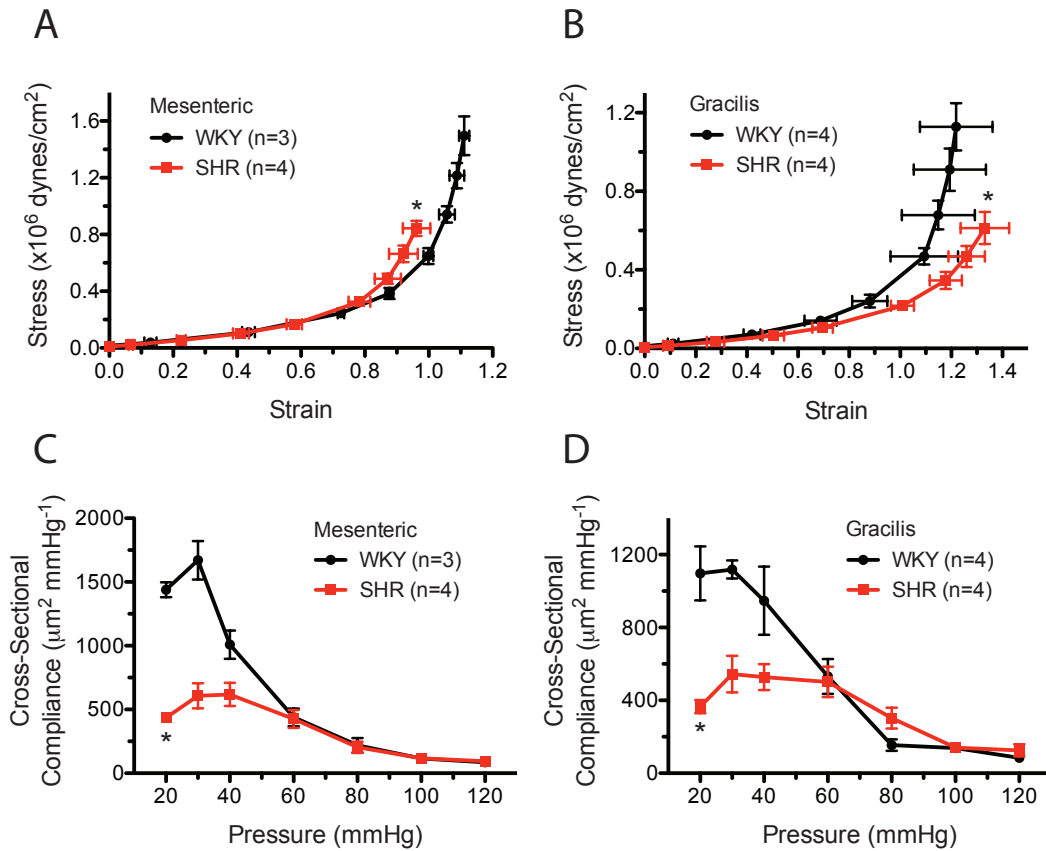
Figure 4.5. Assessment of elastic properties of arterioles obtained from WKY and SHRs. Panels A and B show the calculated Stress as function of the Strain. The cross-sectional compliance as a function of pressure is shown in panels C and D. Values represent means ± SEM. * $p<0.05$ vs WKY.

4.3.6 Arterioles from SHRs have increased media thickness, medial cross-sectional area and number of smooth muscle cells

Analysis of the structural modifications occurring in arterioles from SHRs, via fluorescence and confocal microscopy, showed that vessels from these rats have a

significantly larger gap between their internal and external elastic laminas (media thickness) (Fig. 4.6-A). The cross-sectional area associated with the media was significantly increased in SHR, indicative of hypertrophic remodeling of the vascular wall (Fig. 4.6-B). When quantifying the number of nuclei associated with vascular smooth muscle cells, arterioles from SHR had a significantly increased number of nuclei, indicative of these arterioles undergoing hyperplasia (Fig. 4.6-C).
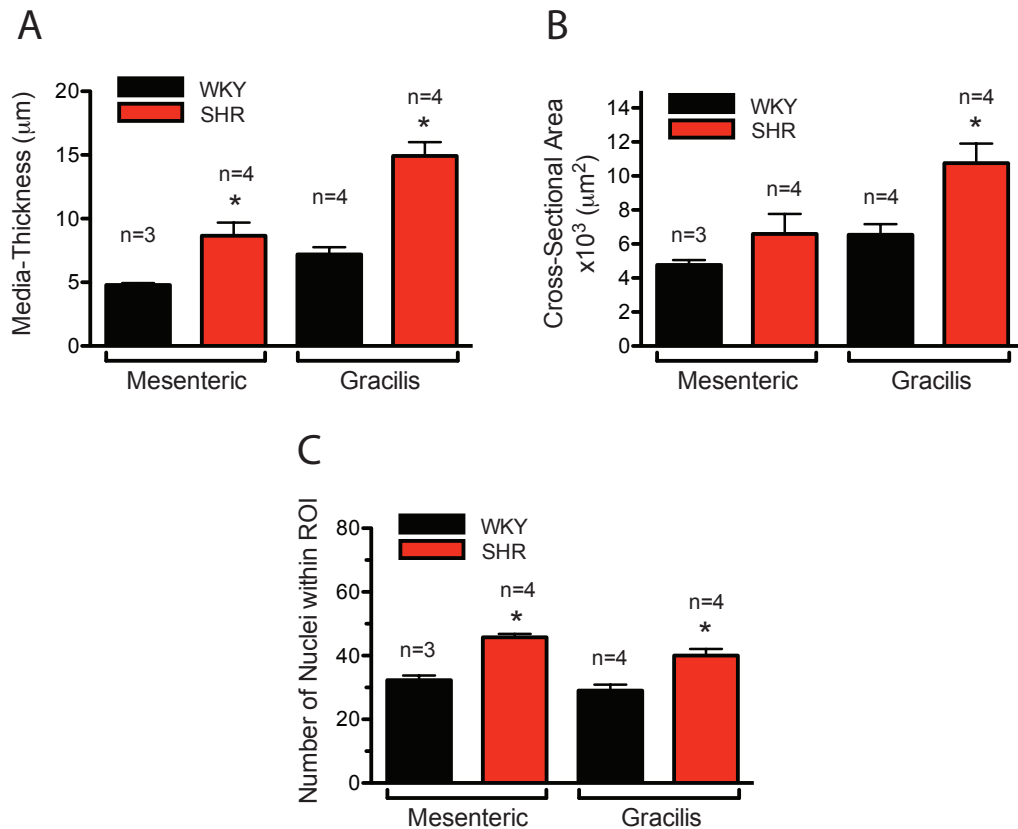
Figure 4.6. (A) Media thickness. These values represent the measured distance from the internal elastic lamina to the external. These measurements were performed on elastin stained vessels imaged by confocal microscopy. (B) Cross-sectional area associated with the media layer of the vascular wall. (C) Number of vascular smooth muscle nuclei within a region of interest. Values represent means ± SEM. * $p < 0.05$ vs WKY.

4.3.7 Arterioles from SHRs have smaller fenestrae in their internal elastic lamina

Characterization of the elastic laminas in arterioles from SHRs and WKY rats showed that the fenestrae present in both mesenteric (Fig. 4.7-A) and gracilis (Fig. 4.7-B) resistance arteries from SHRs are significantly smaller in size.
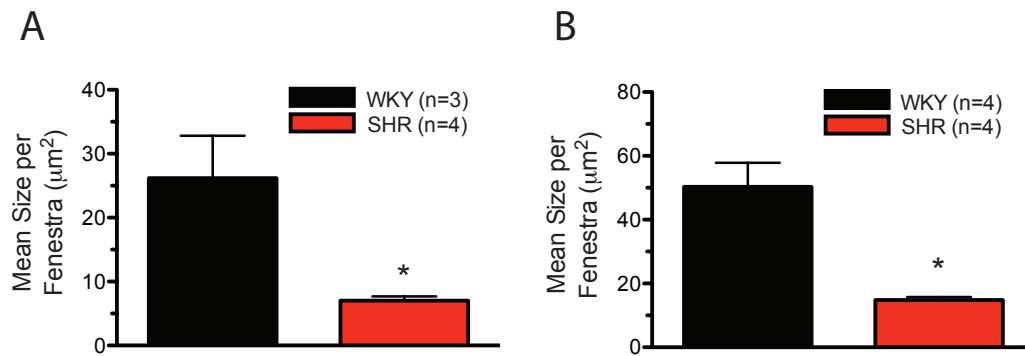
Figure 4.7. Mean size per fenestrae in mesenteric (A) and gracilis (B) arteries from SHRs and WKY rats. Results are given as means ± SEM. * p<0.05 vs WKY.

4.4 Conclusions and discussion

In essential hypertension, one of the major structural changes of the vasculature associated with this condition is the inward remodeling of resistance vessels. The inward remodeling of the small blood vessels is also deemed an important predictor for the development of cardiovascular diseases (e.g. stroke, myocardial infarction, etc.). When assessing the functional response of arterioles, we found that although the constriction at the maximum concentration of phenylephrine was not different between groups, blood

vessels from SHRs showed a tendency to present a reduced constriction to phenylephrine at lower concentrations. This suggests that adrenergic vasoconstrictor pathways are impaired in old rats with essential hypertension. This effect was more evident in gracilis arteries, where the difference in constrictions reached a significant level at a phenylephrine concentration of 10^{-7} M. Endothelium-dependent dilation assessed via exposure to a range of increasing concentrations of acetylcholine showed similar dilations for both groups and in both vascular beds under study. SNP is an endothelium-independent vasodilator, the pathways through which SNP induces dilation are not all completely understood; however, it is primarily considered a NO donor (1, 87, 95, 147, 172). SNP, therefore, acts directly on the smooth muscle cells. Our results suggest that in adult normotensive aged rats, some of the pathways through which SNP induces dilation are affected, decreasing the sensitivity for NO. This loss in sensitivity is not present in SHRs. Mesenteric and gracilis arteries from SHRs had a significantly smaller luminal diameters with increased wall thickness, increased wall-to-lumen and increased cross-sectional area associated with the media layer of the vascular wall. These observation are indicative of inward hypertrophic remodeling of the resistance arteries. The number of nuclei was also increased in the SHR model, indicative of hyperplasia. In the low range of intraluminal pressures, the cross-sectional compliance, which is inversely proportional to the stiffness, was significantly reduced in arterioles from spontaneously hypertensive rats. These are all common findings in essential hypertension and major predictors for cardiovascular diseases.

CHAPTER 5

DIET-INDUCED OBESITY IS ASSOCIATED WITH AUGMENTED ELASTIN CONTENT AND INCREASED STIFFNESS OF MESENTERIC RESISTANCE ARTERIES IN MICE

5.1 Introduction

Consumption of a western diet (WD), high in fat and sugar, has led to a dramatic increase in the prevalence of obesity (body mass index $\geq$ 30 kg/m^2) over the last decades in the US, and worldwide (45, 145). Obesity is associated with impaired cardiovascular function and is a risk factor for a range of pathologies including hypertension, atherosclerosis, and type II diabetes (7, 63, 126). Consumption of excess nutrients and associated overweight/obesity is also linked with increased cardiovascular stiffness. In mice, we recently reported that consumption of a WD caused cardiac fibrosis and diastolic dysfunction (26). Using aortic pulse wave velocity as a measurement of arterial stiffness, others have shown that abdominal body fat is positively correlated with a faster pulse wave, indicative of stiffer arteries (184). Additional studies have also found a

positive correlation between body mass index and pulse wave velocity, suggesting there is an association between obesity and arterial stiffening (113, 186, 187, 203).

Arterial stiffening is characterized by a reduction in the ability of an artery to expand and contract in response to luminal pressure changes (32). This stiffening causes a decreased level of distensibility at a given pressure that has important pathological implications, as a number of cardiovascular diseases are associated with increased stiffness in conduit and coronary arteries, including hypertension (146, 197) and atherosclerosis (52, 195). Arterial stiffness is also prevalent in type II diabetes, where the subsequent development of cardiovascular disease is the main cause of death (83, 180). The mechanism(s) leading to arterial stiffness have not been fully elucidated, in particular at the level of the microcirculation, where the majority of resistance to blood flow occurs. Moreover, it is unclear whether arterial stiffening is a maladaptive process in response to a disease state, or whether it precedes cardiovascular disease and plays a causative role in initiating cardiovascular dysfunction. In the case of hypertension, recent data suggests the latter. In a longitudinal study, arterial stiffening was associated with a higher risk for developing hypertension, in contrast, initial blood pressure was not a risk factor for the subsequent development of arterial stiffness in subjects four to ten years later (93). In a mouse model for WD-induced obesity, it was demonstrated that aortic stiffening precedes systolic hypertension (200). We have previously reported that there is a marginal increase in systolic blood pressure in mice fed a WD (134), however it is not known whether this increase is associated with changes in function and/or stiffness at the level of the resistance vasculature.

One of the mechanisms proposed to initiate arterial stiffening is a change in the structural organization of the extracellular matrix (ECM) within the arterial wall. Elastin and collagen fibers are the main structural ECM components of the vascular wall. Elastin in particular is the most abundant ECM in vascular elastic laminas. It allows the vessel to expand and return to its original diameter in response to pressure changes. In the resistance arteries of rodents, the internal elastic lamina (IEL) is an intact sheet perforated with holes, termed fenestrae. These openings provide portals for communication between the endothelium and vascular smooth muscle cells (VSMCs) via direct cell-cell membrane contacts (108) or through the diffusion of vasoactive agents. It was demonstrated that the size of these fenestrae as well as their number are reduced in inwardly remodeled vessels from angiotensin-II treated rodents, and this coincided with an increase in mesenteric arterial stiffness and the development of hypertension in rats (28). In a pig model of atherosclerosis, the number of fenestrae was also decreased in atherosclerotic coronary arteries (106). Together these observations suggest that dynamic changes to the fenestration of the IEL could be an early structural modification and lead to the subsequent development of cardiovascular disease. The goal of this study was to determine if a WD, linked to the rising incidence of obesity and hypertension, induces functional changes and/or structural remodeling of the ECM in resistance arteries. A second goal was to identify potential triggering mechanism(s) for the development of arterial stiffness and cardiovascular disease associated with obesity.

5.2 Materials and methods

5.2.1 Animal care and use

All animal procedures were performed in accordance with the Animal Use and Care Committee at the University of Missouri-Columbia and National Institutes of Health guidelines. C57BL6/J males were obtained from The Jackson Laboratory. Groups of 4-week-old male mice were fed a WD (TestDiet 5APC, Test Diet, St. Louis, MO) consisting of high fat (46%) and high carbohydrate as sucrose (17.5%) and high-fructose corn syrup (17.5%) for 16 weeks (134). A parallel group of age-matched male controls were fed a normal diet (ND), i.e. regular mouse chow, for the same time (TestDiet 5APD, Test Diet, St. Louis, MO). Both cohorts were provided water ad libitum while housed in pairs under a 12-hour/day illumination regimen.

5.2.2 Vessel isolation and functional assessments

Mice were anesthetized by isoflurane inhalation. After confirmation that spinal reflexes were lost, the mesenteric vasculature was excised and placed in a cold (~4°C) physiological saline solution (PSS) containing (in mM): 145.0 NaCl, 4.7 KCl, 2.0 CaCl2, 1.0 MgSO4, 1.2 NaH2PO4, 0.02 EDTA, 2.0 Pyruvic Acid, 5.0 Glucose and 3.0 3-(N-morpholino) propanesulfonic acid at pH 7.4. First order (1A) feed mesenteric arteries were isolated, cannulated and pressurized for experimentation as previously described (115). Briefly, arteriolar segments of ~3mm in length were cannulated onto glass micropipettes within an observation chamber (Living Systems Instrumentation, Burlington, Vermont) filled with PSS. The arteries were pressurized without flow to 70

mmHg using a Pressure Servo System (Living Systems Instrumentation Burlington, Vermont) and PSS containing 0.15 mM bovine serum albumin. The chamber was transferred to an inverted microscope equipped with a videodisplay and video caliper (Living Systems Instrumentation Burlington, Vermont) to record vascular wall thickness and luminal diameter. All experiments were performed at 37°C. Warmed vessels were exposed to PSS containing 80 mM KCl equimolarly substituted for NaCl to induce depolarization and vasoconstriction and test viability. Subsequently, vessels were exposed to increasing concentrations of phenylephrine to test for adrenergic vasoconstriction responses. Vasodilation responses to increasing concentrations of insulin or sodium nitroprusside (SNP) were performed after vessels were pre-constricted with 10^{-6} M phenylephrine. Responses are reported as percent of maximal constriction, percent reduction in maximal passive diameter, or as percent of phenylephrine pre-constriction. Maximal passive diameter was obtained at the end of each experiment by exposing vessels to Ca^{+2}-free PSS in the presence of 2 mM ethylene glycol tetra-acetic acid and 10^{-4} M adenosine.

5.2.3 Determination of arterial elastic characteristics

To study the elastic characteristics of the arterial wall, pressure-diameter curves were obtained under passive conditions (Ca^{2+}-free PSS) at the end of each experiment. Changes in intraluminal pressure were performed in steps covering a range between 5-120 mmHg. Maximum internal diameter and wall (left and right) thicknesses were recorded at each pressure. This information was used to determine the circumferential stress, strain and modulus of elasticity curves for each group of vessels.

5.2.4 Confocal/multiphoton fluorescence microscopy imaging

At the end of each experiment, vessels were fixed with 4% paraformaldehyde, while pressurized at 70 mmHg for 1 hour. For imaging, vessels were rinsed twice in phosphate buffered saline (PBS) and once in 0.1M Glycine for 5 minutes each time. Cannulated vessels were flushed with 1 mL PBS to rinse their lumen, and permeabilized via incubation in 0.5% TritonX100 for 20 minutes. Vessels were washed twice in PBS and incubated for 1 hour in 0.5µg/mL 4',6-diamidino-2-phenylindole (DAPI), 0.2µM Alexa Fluor 633 Hydrazide (Molecular Probes) and 0.02 µM Alexa Fluor 546 phalloidin (Molecular Probes) in PBS. After being washed 3 times in PBS, vessels were imaged using a Leica SP5 confocal/multiphoton microscope with a 63x/1.2 numerical aperture water objective. Alexa Fluor 633, to image elastin, was excited with a 633 nm HeNe laser. Alexa Fluor 546 phalloidin, to image actin components, was excited with a 543 nm HeNe laser. DAPI, to image nuclei, was excited with a multi-photon laser at 720 nm. Collagen was imaged via second-harmonic image generation using a multi-photon laser at 850 nM.

5.2.5 Image processing

Images were processed and all channels were quantified to determine the total volume occupied by VSMCs nuclei, elastin, actin (within the media) and collagen. The image processing was performed with an in-house built algorithm on the MATLAB (The Mathworks, USA) environment. The four channels corresponding to Elastin, Actin, Nuclei and Collagen were saved as individual slices that formed 3D data sets.

First, the Elastin channel was processed to estimate the boundaries of the vessel. Pre-processing of the data was required to reduce the noise. Each slice of the 3D data set was

reduced in dimensions with a standard Quad Tree averaging: the intensities of a four neighboring elements were averaged and assigned to a new image (61). In this way, the noise is reduced at the expense of a reduced spatial resolution. The reduction was carried out twice, therefore subsequent calculations were performed on data sets with 256×256 pixels as the channels consisted of images with 1024×1024 pixels. In order to estimate the boundaries of the Elastin, it was assumed that the Elastin fibers formed half a cylinder, which was "stretched out" to a planar form by transforming between Cartesian and Polar coordinates. Once stretched; the boundaries were assumed to be at the two peaks of maximum intensity over each column, and then these points were translated back to the Cartesian coordinates. The two boundaries were returned to the original dimensions of 1024×1024 to be used to quantify the expression of the other channels relative to the position of the boundaries.

Since the intensity levels of the pixels from the DAPI channel varied considerably, the intensity segmentation with a single threshold would have merged some of the bright regions, which corresponded to two separate nuclei, while discarding the dim nuclei. To prevent this, the segmentation was performed in 2 stages, first with a high threshold to detect the bright regions, then with a low threshold to detect faint regions. In addition, to improve the segmentation, a hysteresis thresholding was used for both bright and dim Nuclei. Hysteresis thresholding (73) uses a double threshold in the following way; pixels below a low threshold are considered as background and pixels above the high threshold are considered as nuclei. Pixels in between the two thresholds are considered as nuclei only if they are in contact with pixels above the high threshold. The thresholds of all

slices were derived from the threshold levels calculated with the algorithm proposed by Otsu (143). A final post-processing stage was to remove all nuclei with a predetermined volume of 15 voxels.

The regional quantification of expression of the proteins was calculated in the following way: images of each channel were segmented with a single threshold. The total number of segmented voxels was counted, as well as number of segmented voxels that were located within the two boundaries of the Elastin. From these values, the relative expression for each channel was calculated. Figure 5.1 shows the results of the segmentation process. The Elastin Boundaries are displayed as two surfaces with different shades of gray, the locations where the expression was located is shown in different colors. The Nuclei were divided in three groups and counted relative to their location with the boundaries: (a) in contact with the boundaries, (b) in between the two boundaries, (c) outside the boundaries. These classifications are indicated by different colors in Figure 5.1 (c).

In a separate analysis, for the DAPI and Alexa 633 channels, a region of interest (ROI) was selected (95 μm x 143 μm for DAPI and 60 μm x 121 μm for Alexa 633) and the total number of nuclei and fenestrae were calculated using an Image-J macro.
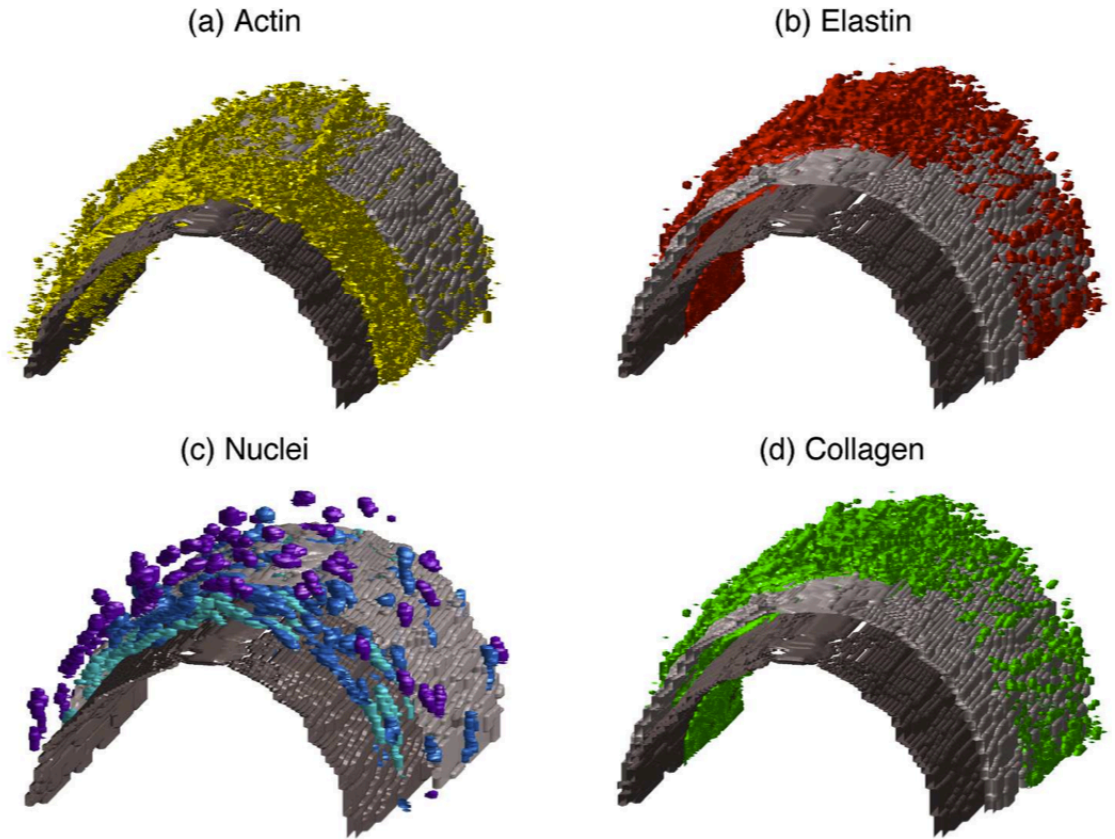
Figure 5.1. *Representative processing of a mouse mesenteric resistance artery image.* Segmentation of four channels was used to quantify the expression of four different proteins: (a) Actin, (b) Elastin, (c) Nuclei, (d) Collagen. The boundaries of elastin are shown in gray, the inner in a darker shade than the outer boundary. The nuclei were classified according to their location relative to the boundaries; purple is outside the boundaries, blue is in contact with the boundaries and cyan is in between the two boundaries. To aid the visualization, the outer boundary has been retracted as well as the components. The inner boundary is shown complete.

5.2.6 Assessment of insulin resistance

Glucose and Insulin levels were determined as previously described (210). Briefly, venous blood was drawn from fasting mice and assessed for glucose concentrations using a G-6-PDH assay, and insulin levels with a mouse specific Elisa. Insulin resistance was calculated using the homeostasis model assessment (HOMA-IR) formula: HOMA-IR =

fasting glucose (mg/dL) × fasting insulin (μU/ml)/405 (125). HOMA-IR has been shown to be strongly correlated with the insulin sensitivity index derived from the standard euglycemic hyperinsulinemic clamp method (54). In the HOMA-IR model, insulin levels are expressed in international units. Within the literature, there is a discrepancy on the concentration of insulin that equals 1 μU activity (72). We used the potency factor (28,698 U/g) provided by the manufacturer of Novolin R (Novo-Nordisk), thus the conversion from mass units to units of activity was 6.00 ρmol/l = 1μU/ml.

5.2.7 Real-time quantitative PCR

Total RNA was extracted from mesenteric arteries using Arcturus PicoPure RNA Isolation Kit (Life Technologies, Carlsbad, CA, USA), equal amounts of total RNA extracts were then reverse transcribed to generate cDNAs using SuperScipt III First-Strand Synthesis System (Life Technologies). Real time TaqMan PCR assays were performed using a Mastercycler EP Realplex^2 (Eppendorf-North America, Westbury, NY, USA) and TaqMan Fast Advanced Master Mix (Life Technologies). Probes and primers for amplification of elastin and the housekeeping gene, β-2-microglobulin, were purchased from Life technologies (Mm00514670_m1 for elastin, Mm01178820 for TGF-β1, Mm00437762_m1 for β-2-microglobulin). Reactions were performed in 20 μl, comprised of 10 μl master mix, 1 μl probe and primers, 1 μl of cDNA template and 8 μl DNase-free water. Thermal cycling conditions were as follows: 50°C for 2 min, 95°C for 20 sec, repeat for 40 cycles of 95°C for 3 sec and 60°C for 30 sec. Realplex software (Eppendorf-North America) was used to collect and analyze the data. The following equation was used to determine the relative mRNA expression level (R) for Elastin or

TGF-β1 normalized to β-2-microglobulin expression: $R= 2^{-\Delta\Delta Ct} = 2^{-(\Delta Ct \ elastin \ - \ \Delta Ct \ \beta-2-microglobulin)}$ as previously described (111, 119).

5.2.8 Protein expression

Aortas were isolated from mice, and homogenized with a bead rupture (Omni Bead Ruptor, Omni International, Keenesaw, GA) in 200 μl radio-immunoprecipitation lysis buffer containing HALT Protease Inhibitor Cocktail (Pierce, Thermo Scientific, Rockford IL). Homogenates were centrifuged (13,000 × g for 10 min at 4°C) to remove debris. Protein content was determined with a BCA Protein Assay Kit (Pierce). Protein extracts (12 μg) were heated at 94°C for 5 minutes, separated on a 10% gel, and transferred to a nitrocellulose membrane. The blot was blocked for 45 minutes at room temperature in 0.5% Tween 20 Tris-buffered saline + 5% milk. Membranes were incubated over night at 4 °C with anti-TGF-β 1-2-3 at 1:500 dilution and subsequently with horseradish peroxidase-conjugated secondary antibody (1:10,000; room temperature for 2 hours). Stripped membranes were re-probed with an antibody specific to β-actin for normalization. For TGF-β, peroxidase activity was visualized with the Super Signal West Femto (Pierce) and LumiGlo (KPL, Baltimore, MD) for β-actin. Signal was visualized using a Bio-Rad Chemi-Doc Imaging System. TGF-β and β-actin protein bands were quantified using the Bio-Rad Chemi-Doc software. Results are expressed as a ratio of TGF-β to β-actin.

5.2.9 Data analyses

Data are expressed as means ± SEM. The number of experiments represents the number of animals in each experimental group. Statistical analyses included T-test, or ANOVA followed by Bonferroni post hoc test where appropriate. A value of $P<0.05$ was considered significant. All statistical analyses were performed using GraphPad Prism 5 software.

5.3 Results

5.3.1 Feeding a western-diet induced significant weight gain, increased plasma insulin levels and caused insulin resistance

Feeding mice a WD high in fat and sugar for 16 weeks after weaning resulted in substantial weight gain compared to mice fed a ND. The average body weight of 20 week-old WD-fed mice was significantly greater ($P<0.05$) than that of mice fed a ND (Fig. 5.2-A). In addition, there was a significant increase ($P<0.05$) in fasting plasma insulin levels in the WD cohort (Fig. 5.2-B), which in turn resulted in insulin resistance as assessed by HOMA-IR (Fig. 5.2-C). Plasma glucose levels were not significantly different between the two cohorts (data not shown).
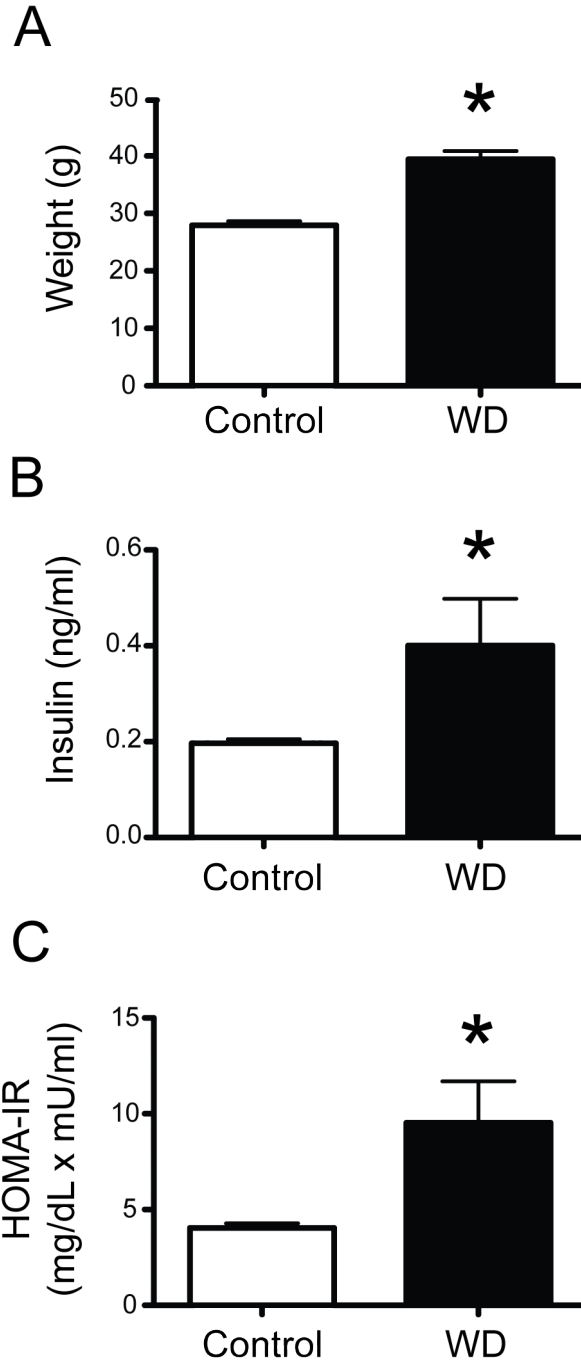
Figure 5.2. *Mice fed a WD were significantly heavier than ND-fed mice and had elevated fasting insulin levels.* (A) Mean body weights of control ND-fed mice (n=9) and WD-fed mice (n=10). Mean body weight was greater in WD-fed mice, *$P< 0.05$. (B) Plasma concentration of insulin from mice following 4 hrs of fasting, was significantly elevated in mice fed a WD (n=10) vs. control mice fed a ND (n=10), *$P<0.05$. (C) HOMA-IR (fasting glucose ((mg/dL x fasting insulin uU/ml)/405) index was significantly higher for WD-fed mice (n=10) vs. control mice fed a ND (n=10), *$P<0.05$. Data are means ± SEM.

5.3.2 Western-diet did not affect receptor-dependent or receptor-independent vasoconstriction

To assess if the WD affected vascular α1-adrenergic receptor activation, isolated mesenteric arteries were exposed to increasing concentrations of phenylephrine (10^{-8} M – 10^{-4} M). There was not a statistically significant difference in percent maximum constriction between arteries from WD- and CD-fed mice, or in the half maximal effective concentration for the drug (Fig. 5.3-A). To determine if receptor-independent vasoconstriction was affected by the WD, we exposed isolated arteries to 80 mM KCl. Depolarization-induced vasoconstriction with high K^+ was not statistically different between WD and CD mice (Fig. 5.3-B).

5.3.3 Western-diet reduced basal myogenic tone in mesenteric resistance arteries

Mesenteric arteries from mice fed the WD had a decreased level of spontaneous myogenic tone compared to arteries from mice fed the ND. The arteries from WD-fed mice developed tone at 88.62 ± 2.04% of maximal passive diameter vs. 79.50 ± 2.42% of the ND-fed mice (P<0.05) (Fig. 5.4).
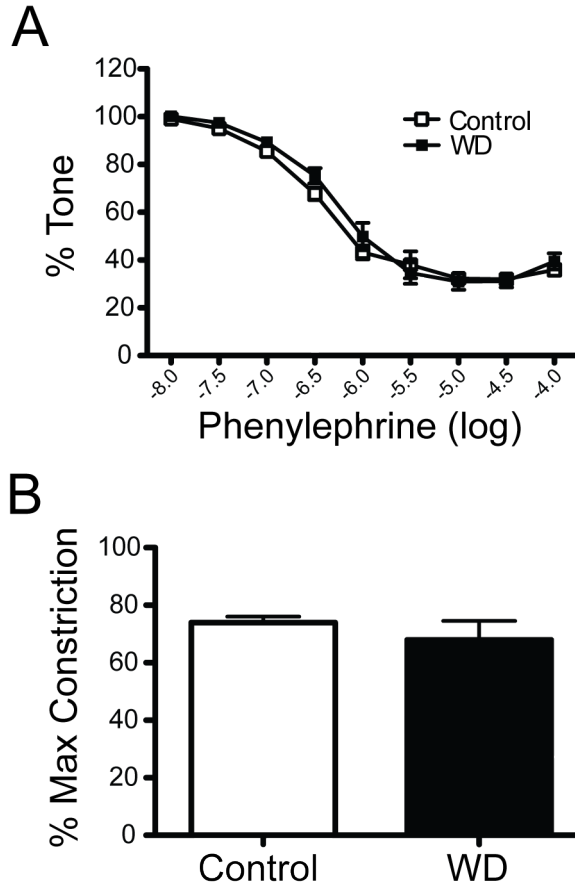
Figure 5.3. *Constriction to adrenergic stimulation was unaffected by a WD.* (A) Vessels were allowed to develop tone, and maximum passive diameter was determined in Ca^{2+}-free PSS. Vessels were exposed to increasing concentrations of phenylephrine and arterial diameter was assessed and expressed as a percent of basal myogenic tone. (B) Vessels, from A, were assessed for constriction to KCl (80 mM) and constriction expressed as percent maximal constriction ((Maximal passive diameter–Diameter at 80 mM KCL)/(Maximal passive diameter)) x 100). Data are means ± SEM, Control (n=9), Obese (n=10).
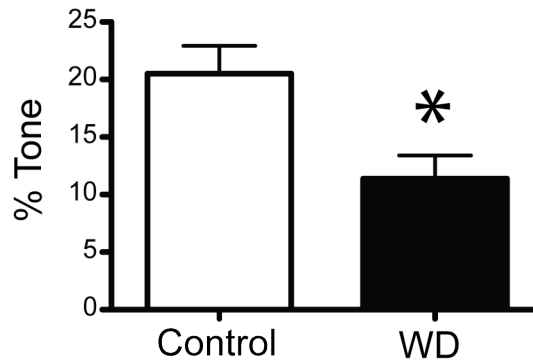
Figure 5.4. *Effect of WD on Myogenic tone. B*asal myogenic tone expressed as percent reduction in maximal passive diameter. Comparisons are between control ND-fed mice (n=9) and WD-fed mice (n=10). Data are means ± SEM. *P<0.05 vs. control

5.3.4 Effect of diet-induced obesity on vasodilatory signaling pathways

As illustrated in Figure 3C, the WD cohort was insulin resistant. In obese human subjects, insulin resistance is associated with an impaired vasodilatory response to insulin in peripheral arteries (185). To determine if the WD-fed mice had an impaired vasodilatory response to insulin, isolated mesenteric arteries were pre-constricted with 10^{-6} M phenylephrine and exposed to increasing concentrations (10^{-9} – 10^{-5} M) of insulin. There was no significant difference in the insulin-induced dilation for arteries from WD-fed mice vs. the ND-fed cohort (Fig. 5.5-A). To assess if endothelium-independent relaxation pathways were affected by the WD, pre-constricted vessels were exposed to increasing concentrations (10^{-8} - 10^{-4} M) of SNP. There was not a significant difference between the two groups for SNP induced vasodilation (Fig. 5.5-B). At low concentrations of both insulin and SNP, vessels from CD-fed mice had a tendency to relax better than those from WD-fed mice, but the differences were not significant (P=0.06).
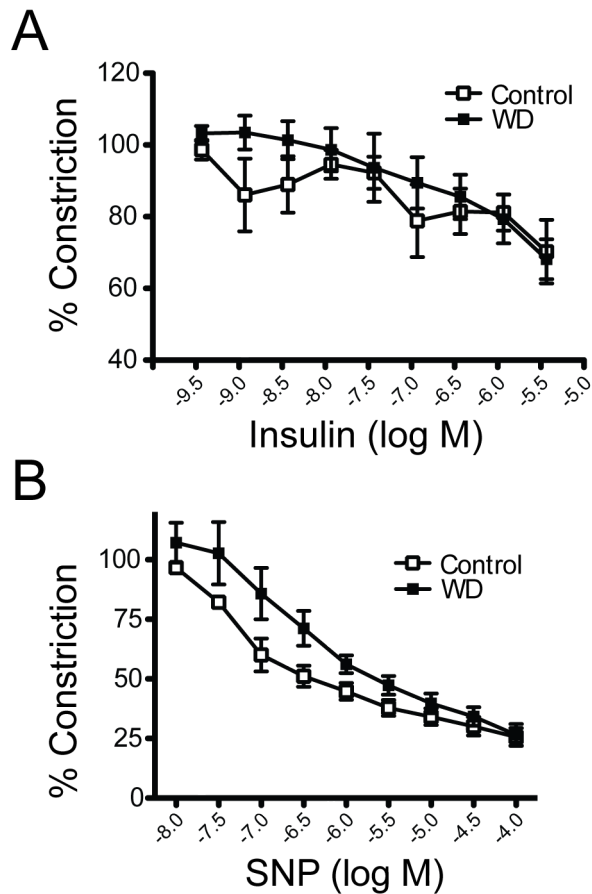
Figure 5.5. *Effect of a WD on vasodilation to receptor-dependent and receptor-independent agonists.* Mesenteric arteries from control ND-fed mice (n=9) and WD-fed mice (n=10) were pre-constricted with 10^{-6} M phenylephrine, and their internal diameters assessed in the presence of increasing concentrations of (A) insulin and (B) SNP. Data are means ± SEM, and expressed as percent constriction to 10^{-6} M phenylephrine.

5.3.5 Effects of a western-diet on the structure and elastic properties of resistance arteries

Obese individuals have been shown to have increased arterial stiffness (increased pulse wave velocity). Moreover, in the same strain of mice used in this study, aortic stiffness had been shown to be increased after 1 month of exposure to a WD (200). To

determine if the WD also affects the stiffness of resistance vessels, we examined the elastic properties of mesenteric arteries from the WD- and ND-fed mice under passive conditions. There were no significant differences in wall stress as a function of strain in vessels from WD- vs. ND-fed mice. However there was a not significant (P=0.07) tendency for arteries from the WD-fed mice to have greater stress at the highest levels of strain (Fig. 5.6-A). This in combination with a tendency for the arteries from the WD-fed mice to be less distensible (reduced strain) resulted in these arteries being stiffer, that is they had a greater (P<0.05) modulus of elasticity than vessels from the ND-fed mice (Fig. 5.6-B).
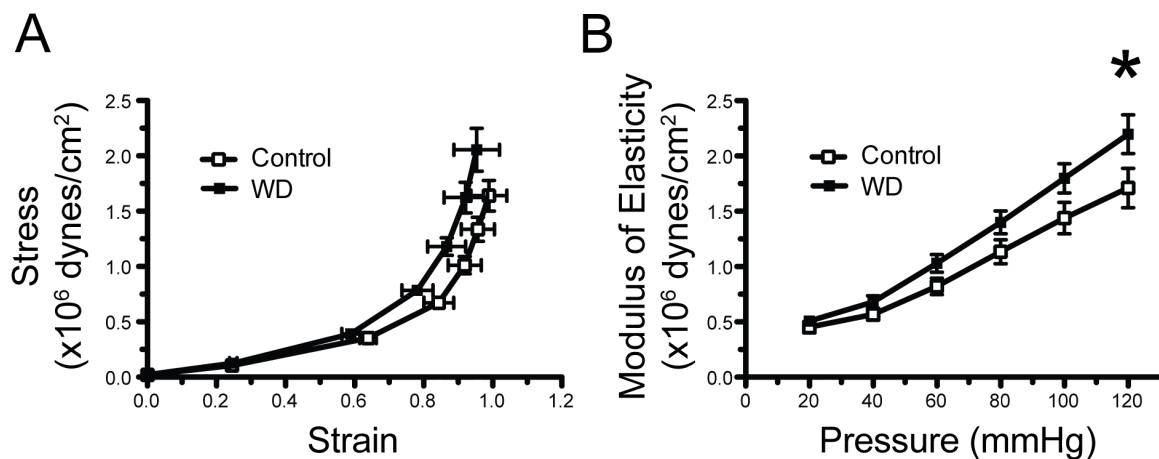
Figure 5.6. Stress strain characteristics of ND and WD cohorts. (A) Strain-stress relationship curves of mesenteric arteries from control ND-fed mice (n = 9) and WD-fed mice (n = 10). (B) Incremental modulus of elasticity vs. pressure from the same set of arteries in panel A. *P<0.05 vs. control.

5.3.6 Effect of a western-diet on resistance artery remodeling

To assess vascular remodeling, we obtained pressure-diameter curves in isolated vessels under passive conditions and also calculated wall area to lumen ratios. No differences in the pressure-diameter curves were observed between arteries from the WD- vs. the ND-fed mice at any pressure (Fig. 5.7-A). No significant differences in wall/lumen ratios were found either. However, there was a not significant tendency (P=0.08) for the WD-fed cohort to have lower ratios (Fig. 5.7-B). Because our wall thickness measurements do not take into account cellularity, we fixed the isolated arterioles and stained with DAPI to identify VSMC nuclei and with phalloidin to measure actin content in the vascular media. There were no significant differences in the number of VSMC nuclei or actin content in the media from mesenteric arteries derived from the WD-fed vs. the ND-fed mice.
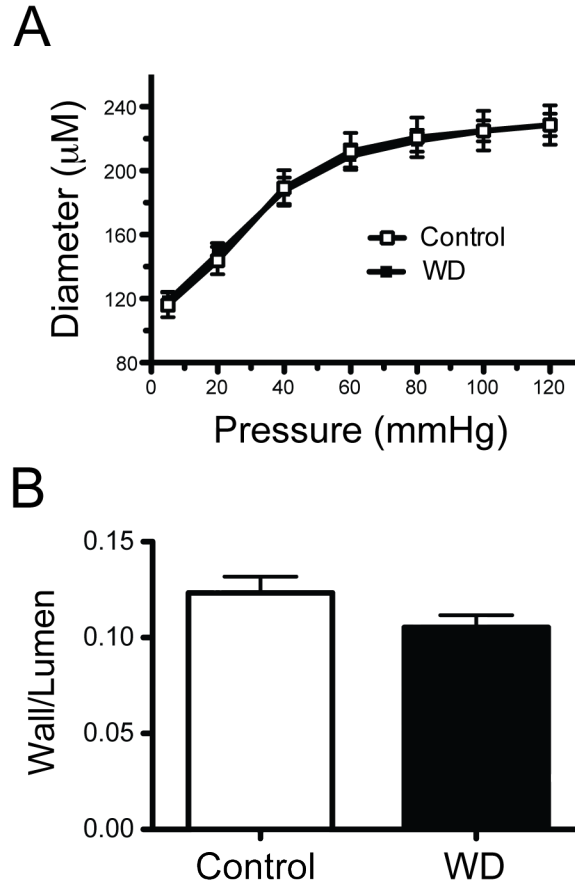
Figures 5.7. *Effect of a WD on passive diameters and media to lumen ratios of mesenteric resistance arteries.* (A) Internal passive (Ca^{2+}-free PSS) diameters obtained at different intravascular pressures in mesenteric resistance arteries isolated from mice fed either a control diet (n=9) or a western diet (WD, n=10). Data are means ± SEM. (B) Comparison of mean media to lumen ratios for mesenteric arteries from control ND-fed mice (n = 9) and WD-fed mice (n = 10). Data are means ± SEM. Measurements were made at 70mmHg in Ca^{2+}-free PSS.

5.3.7 Effect of a western-diet on collagen and the internal elastic lamina

Mesenteric arteries from WD- and ND-fed mice were isolated, fixed and stained for elastin, actin and nuclei (Fig. 5.8-A-D). Alexa633 was used to visualize the internal elastic lamina (Fig. 5.8-B). Staining with elastin specific antibodies revealed the same staining pattern as Alexa633 ((41) and data not shown). The volume occupied by Alexa633 fluorescence was greater in vessels from WD- vs. ND-fed mice (P<0.05),

indicating an increase in elastin volume for the WD cohort (Fig. 5.8-F). Collagen, actin and nuclei were imaged concomitantly using multiphoton second-harmonic image generation, phalloidin and DAPI, respectively. There was not a significant difference in the amount of collagen, actin, or nuclei between the two groups, nor was there a difference in the actin to nuclei ratio (Fig. 5.8-E,G,H,J). The elastin to collagen ratio was also calculated, and was significantly higher for the WD cohort (Fig. 5.8-I). The number of fenestrae present in the IEL for each group was also determined. Mesenteric arteries from mice fed the WD had significantly ($P<0.05$) less fenestrae per unit area than vessels from the ND-fed mice (Fig. 5.9-A,B). The average size of each fenestra was not significantly different between the groups, but there was a shift in the distribution of fenestrae size towards smaller diameters (~1 μm^2) in vessels from the WD-fed mice as assessed by the Gaussian distribution of fenestrae sizes (Fig. 5.9-C). Overall, the fenestrae total area was also significantly greater ($P<0.05$) in the WD vs. the ND group (Fig. 5.9-D).
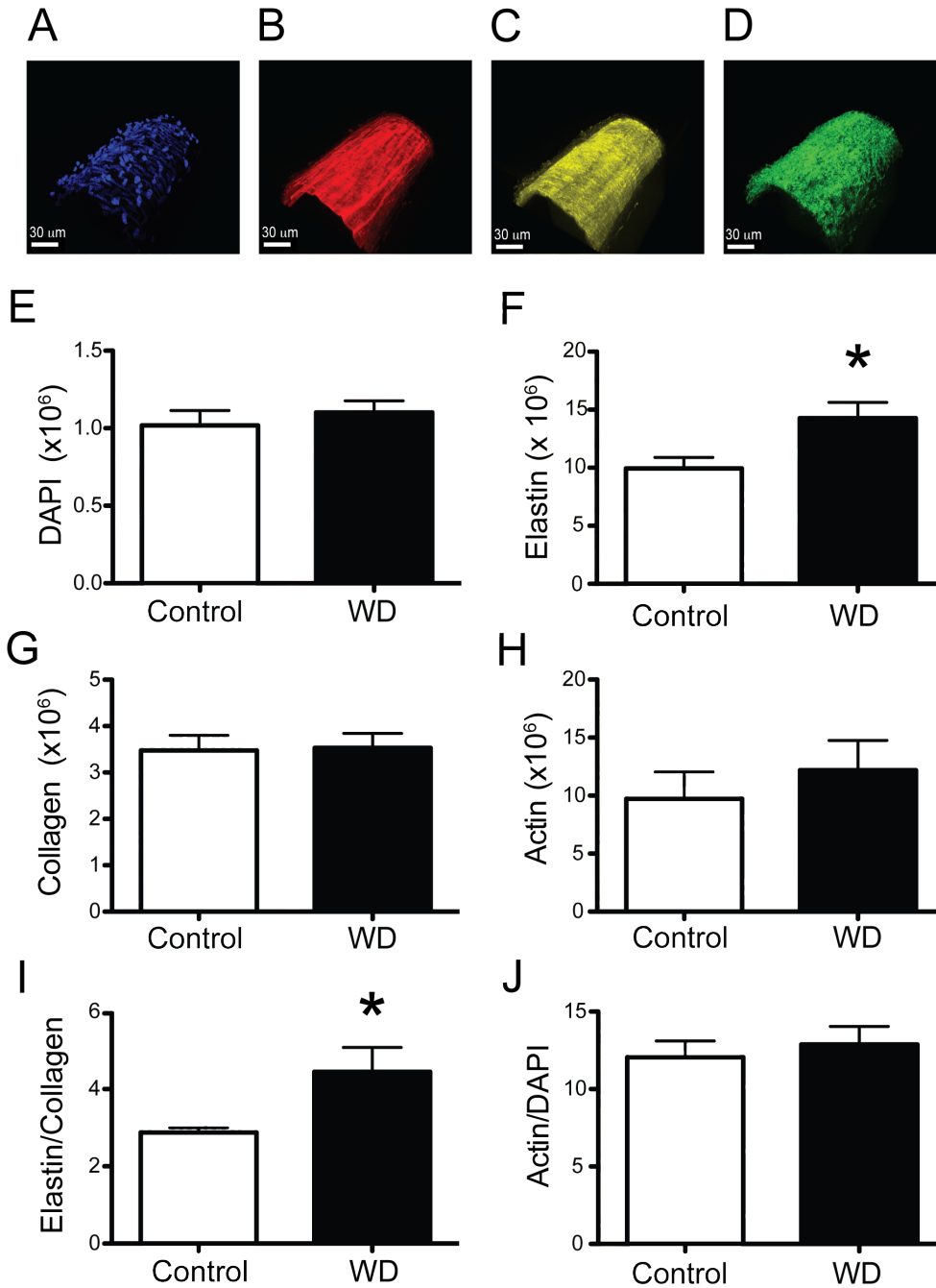
Figure 5.8. *Effect of a WD on the ECM of mesenteric artery structure.* Mesenteric arteries from both diet cohorts were imaged for nuclei, elastin, actin and collagen. Representative image of a vessel with (A) DAPI to image nuclei, (B) Alexa633 to image elastin, (C) phalloidin to image actin and (D) second harmonics to image collagen, scale bar = 30μm. (E) Comparison of mean number of voxels containing DAPI fluorescence above threshold for mesenteric arteries from control and WD-fed mice, (F) Comparison of mean number of voxels containing Alexa633 fluorescence above threshold, (G) Comparison of mean number of voxels containing second harmonic fluorescence above threshold, (H) Comparison of mean

number of voxels containing phalloidin 546 fluorescence above threshold, (I) Comparison of the ratio of the number of voxels containing elastin fluorescence above threshold vs. the number of voxels containing collagen fluorescence above threshold for the control ND and WD cohorts. *P<0.05 vs, control. (J) Comparison of the ratio of the number of voxels containing actin fluorescence above threshold vs. the number of voxels containing DAPI fluorescence above threshold for the control ND and WD cohorts. For panels E-J, ND (n = 9) and WD (n = 10). Data are means ± SEM.
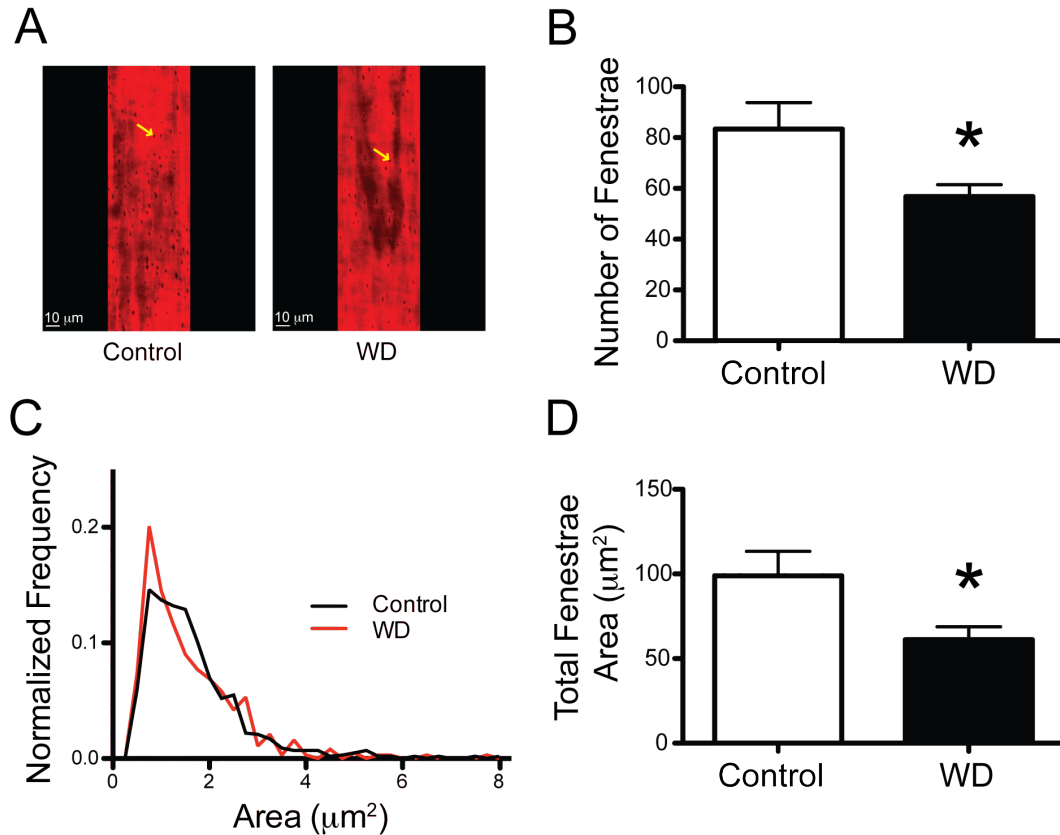
Figure 5.9. *Effect of a WD on IEL fenestrae.* (A) Representative image of elastin staining with fenestrae readily discernible in mesenteric resistance arteries from a control ND-fed mouse and a WD-fed mouse. (B) Comparison of the mean number of fenestra per unit area in mesenteric arteries isolated from control ND- (n = 9) and WD-fed (n = 10) mice. Data are means ± SEM. (C) Frequency distribution of the number of fenestrae by area for control ND- (left panel, n = 9) and WD-fed (right panel, n = 10) mice. The red and blue lines represent the best Gaussian distributions for fenestrae sizes in vessels from ND (red peak = 0.82 μm^2, blue peak = 1.34 μm^2) and WD-fed (red peak = 0.78 μm^2) mice. (D) Comparison of the mean total fenestra area per unit area in control ND- (n = 9) and WD-fed (n = 10) mice. Data are means ± SEM. *P<0.05 vs. control.

5.4 Discussion

In the present investigation, a WD (high in fat and sugar) was used to promote over nutrition in mice. To the best of our knowledge, this is the first report to examine ECM structural changes in the microvasculature as a consequence of a WD and subsequent over nutrition/obesity. Our primary finding was that the number of fenestrae within the IEL of mesenteric resistance vessels is significantly decreased, as is the total area occupied by fenestrae in vessels isolated from male mice fed a WD for 16 weeks. This was associated with an increased amount of elastin present in the vascular wall and an augmented modulus of elasticity, indicating that mesenteric resistance arteries from the WD-fed mice were significantly stiffer. However, the distensibility of these arteries was only modestly affected, as there were only marginal changes in the stress/strain characteristics of the vessels from WD-fed mice. A previous study examining structural changes in mesenteric arteries in a different model of obesity that is associated with diabetes (db/db mice) also found a significantly increased modulus of elasticity in the obese cohort (178). The authors of that study also report that arteries from the obese cohort displayed outward hypertrophic remodeling and a decreased wall to lumen ratio. Though we did not observe outward remodeling, we found a trend for a reduction in wall to lumen ratios for the WD cohort, suggesting that similar structural alterations are manifest in the mesenteric vasculature of db/db mice and mice fed a WD. The major functional difference observed in mesenteric arteries from WD-fed mice in our study was a significantly reduced level of spontaneous myogenic tone. A significantly reduced level of myogenic tone responsiveness to changes in intraluminal pressure has been shown to

occur in resistance vessels isolated form diabetic rats (75). The mechanisms associated with the reduced myogenic response observed in diabetic rats was associated with an attenuated level of VSMC intracellular calcium at a given intravascular pressure (206). Whether a similar mechanism is responsible for the reduced level of myogenic tone we observed in the arteries isolated from mice fed a WD remains to be determined. However, the physiological significance of this finding may be similar to that proposed to be responsible for the outward remodeling found in the mesenteric arteries of db/db mice (178), that is, to increase blood flow to a highly active intestinal wall. We did not find any additional functional changes between mesenteric vessels from WD- vs. ND-fed mice as neither their constriction (KCl, phenylephrine) or relaxation (insulin, SNP) responses were significantly different. This suggests that, in animals fed a WD, structural alterations to the IEL and vascular stiffness precede functional changes to vasoactive stimuli, though additional WD studies of longer duration that test additional vasoconstriction and vasodilation pathways will need to be performed to confirm this.

A reduction in the number and area of fenestrae in the IEL of vessels from hypertensive rodents has been previously reported (28). To our knowledge this is the first description of such a finding in WD-fed mice. The mechanism(s) leading to a decrease in total fenestrae, as well as the reduction in total fenestrae area, is/are yet to be determined. In this study, the changes in the fenestration of the mesenteric vasculature coincided with an increase in elastin volume. A similar link between decreased fenestra area and increased elastin content has been reported in two separate rat models of hypertension. Neonatal spontaneously hypertensive rats were found to have increased elastin-derived

fluorescence in carotid arteries and this was associated with a decrease in the size of individual fenestrae (9). A 2-week infusion of angiotensin II to induce hypertension in Wistar rats also resulted in a reduced number of fenestrae and a reduction in the total fenestrae area in the mesenteric vasculature and this coincided with an increase in the relative area occupied by elastin (28). The current observation of increased deposition and/or reorganization of elastin within the IEL and a decrease in the number of fenestrae suggests a mechanism in which elastin deposition is targeted to sites of fenestration. It has previously been shown that in developing mice aorta, newly synthesized elastin preferentially accumulates at extant fenestrae (44). Though, how this occurs is unclear. Conceivably the borders of fenestrae are biochemically favorable for the polymerization/crosslinking of newly synthesized tropo-elastin monomers. Alternatively, the enzymes that facilitate polymerization of tropo-elastin monomers, such as fibulins and lysyl oxidase (80) and/or transglutaminase 2 (97), could preferentially be targeted to sites of fenestration. Additional studies are necessary to define how and where newly synthesized elastin is deposited in the microvasculature. Regardless of the underlying mechanism of deposition at sites of fenestration, depending upon the amount of elastin deposited, one would expect the size of the fenestrae to be reduced as well as eventually the overall number of fenestrae. This is consistent with our finding that the distribution of fenestrae in vessels from the WD-fed mice was shifted towards smaller sizes.

To determine if signaling for elastin synthesis was increased in the WD-fed mice, we used real-time quantitative PCR to measure mRNA levels of tropoelastin in mesenteric arteries from the WD- and ND-fed mice. There was not a significant

difference in the level of mRNA between the two cohorts (Fig. 5.10). Thus, it is likely that if an increase in elastin production signaling occurs in the WD-fed group, this increase occurs during the initial periods of WD feeding at a younger age.
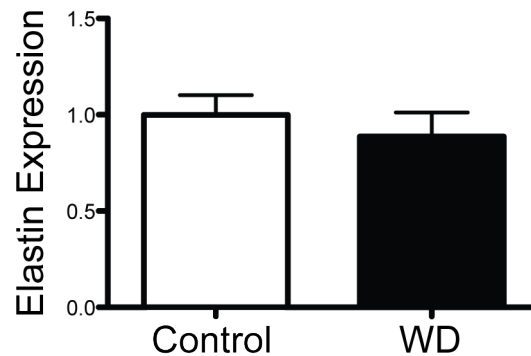
Figure 5.10. *Real-time quantitative PCR analysis of elastin gene expression.* Bars represent the relative fold mRNA expression levels for elastin detected in mesenteric resistance arteries isolated from mice fed either a CD (control, n=10) or a WD (n=10) for 16 weeks. Data are means ± SEM.

It may also be possible that changes the equilibrium of elastin synthesis/degradation to favor increased elastin deposition may occur that do not reflect an increase signaling for elastin synthesis. Elastin synthesis is regulated at multiple levels including: DNA transcription, mechanisms that affect the stability of existing elastin mRNA, mechanisms that affect the enzymes that mediate tropo-elastin monomer polymerization and also via mechanisms that regulate ECM proteases that actively degrade elastin (98). In particular, the cytokine transforming growth factor–beta (TGF-β) has been implicated in elastogenesis via transcriptional as well as post-translational modification mechanisms. It stabilizes elastin mRNA in rat (127) and human lung fibroblasts (104) via a pathway that includes Smads, protein kinase C, and p38 (105). ECM enzymes required for polymerization of tropo-elastin monomers are

transcriptionally up regulated (103) and secreted (24) in response to TGF-β. It has also been shown that TGF-β suppresses elastin degradation via inhibition of matrix metalloproteinase-9 (5). There is also considerable evidence that obesity triggers increased expression of proinflammatory cytokines, including TGF-β in adipose tissue in rodents (77, 82, 162, 163), as well as humans (4, 56, 81, 96). To test the possibility that TGF-β expression may be increased in the WD-fed mice, we performed real-time quantitative PCR and Westerns to measure mRNA and protein levels of TGF-β in the mesenteric arteries isolated from these mice. We found no differences in TGF-β mRNA or protein between arteries from the WD-fed vs. the ND-fed mice (Fig. 5.11). This suggests that at the age and time of feeding we measured (20 weeks of age/16 weeks on WD) the cytokine, cells within the vasculature are not producing more TGF-β in response to WD feeding. It remains to be determined if this is also true at younger ages.

In addition to the release of inflammatory cytokines such as TGF-β, diet-induced obesity is also associated with decreased insulin sensitivity and hyperinsulinemia (134). In C57Bl/6J mice fed a high fat diet, there was a significant increase in serum insulin concentrations versus control fed mice at 30 weeks of age (76). We have demonstrated that the diet protocol used in this study leads to a significant increase in plasma insulin levels and increased HOMA-IR values, a surrogate index of insulin resistance (Figure 1). Interestingly, activation of the insulin receptor via low doses of insulin has recently been implicated in inducing the synthesis of tropo-elastin in human aortic smooth muscle cells in culture, via transcriptional activation and up-regulation of the secretory pathway that delivers tropo-elastin from the endoplasmic reticulum to the cell surface (176). As

96

demonstrated in this study, the vasodilatory response of mesenteric arteries to insulin was not affected by the WD. This suggests that signaling via the insulin receptor was not impaired within the resistance vasculature of these obese mice. Therefore, the observed increase in elastin content within the wall of mesenteric resistance arteries may be due to elevated serum insulin concentrations that positively regulate elastogenic pathways via activation of insulin receptor signaling.

The physiological significance of reduced total fenestrae area is poorly understood. One investigative group reported that conduit/carotid arteries from 1-week old spontaneously hypertensive rats had decreased fenestration and this was coincident with increased arterial stiffness compared with age matched control rats (9). Moreover, these ECM differences were manifest prior to any significant changes in blood pressure between the controls and spontaneously hypertensive rats. In the Weisbrod paper, they as well report that arterial stiffening increased prior to the onset of hypertension in mice fed a WD. Using radio telemetry, we previously demonstrated that the WD used here induced a modest increase (8.2%) in systolic blood pressure, in a different cohort of mice at the same age (134). In humans, a classification of hypertension entails an approximate 16% increase in systolic blood pressure (120 mmHg for normotensive vs. 140 mmHg for hypertensive). Thus, we infer that the mice in this study were in the process of developing hypertension. In contrast, the observed ECM remodeling was well progressed, as the difference in elastin content and IEL fenestration were substantial between the two treatment groups, and likely was the result of incremental increases in elastin deposition or reduced degradation over time. Therefore, our findings that remodeling of the ECM

via decreased fenestration occurred prior to the onset of full-blown hypertension suggest that reorganization of the ECM may be one of the first pathological events that triggers stiffening and the subsequent development of hypertension in diet induced obesity. Within the mesenteric resistance arteries, fenestrae allow for the exchange of macromolecules between endothelial cells and the VSMCs that comprise the media. They also allow for the projection of endothelial cell membranes to make contact with VSMC membranes. It is posited that these myo-endothelial interfaces allow for the transmission of vasoactive elements across the IEL (164, 181). A reduction in total fenestra area would likely affect the time it takes for diffusible substances to transit between the intima and medial layers, and decreases in the number of fenestrae would decrease the number of contacts for the transmission of vasoactive compounds across the IEL. Nitric oxide (NO) is one of the main signaling molecules that diffuses across the IEL, and limiting its availability has been shown to promote vascular stiffness (131, 187). It has recently been postulated that arterial stiffness could arise, in part, from changes in the actin cytoskeleton that affect the intrinsic mechanical properties of individual VSMCs, as actin depolymerizers reduce VSMC stiffness (174). NO has been shown to facilitate F-actin depolymerization in VSMC (167). However, whether the reduced fenestration we observed in the mesenteric arteries of WD-fed mice affects transmission of vasoactive compounds across the IEL and changes the elastic properties of VSMCs or their capacity to develop spontaneous myogenic tone remains to be determined.
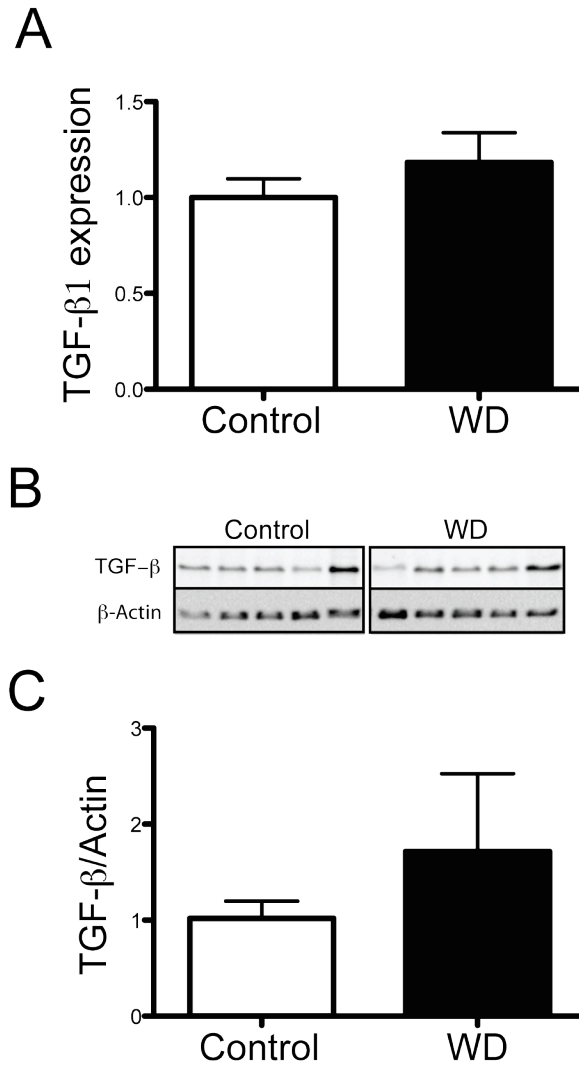
Figure 5.11. *Real-time quantitative PCR and Western blot analyses of TGF-β gene and protein expression in blood vessels.* (A) Relative fold mRNA expression levels for TGF-β1 detected in mesenteric arterioles isolated from mice fed a CD (control, n=10) or a WD (n=10) for 16 weeks. Data are means ± SEM. (B) Western blot showing protein expression of TGF-β and β-Actin in aortas isolated from mice fed a CD (control, n=5) or a WD (n=5) for 16 weeks. (C) Bars represent the relative TGF-β protein expression normalized to β-Actin. Data are means ± SEM.

In conclusion, we demonstrate here that a WD rich in fat and sugars induces obesity, hyperinsulinemia, insulin resistance, and remodeling of the ECM in mesenteric resistance arteries characterized by an increase in elastin volume and a concomitant

99

decrease in fenestrations within the IEL. These changes are associated with a reduced level of basal myogenic tone and stiffening of the vascular wall in these resistance arteries, in the absence of functional responses to vasoactive agonists. Our results further suggest that the changes we observed in elastin content and fenestration of the IEL are not associated with an increased message for synthesis of elastin or TGF-β within the vasculature of 20-week-old mice.

5.5 Perspectives

In this study, we demonstrate that a WD rich in fat and sugars induces remodeling of the ECM in mesenteric resistance arteries via an increase in elastin content. These changes are associated with an increased stiffening of the resistance vasculature and appear to precede functional changes to vasoactive agents. We hypothesize that chronic release of pro-inflammatory cytokines associated with consumption of the WD and the obese state in addition to hyperinsulinemia initiates remodeling of the ECM within the vasculature, which subsequently participates in the development of vascular dysfunction and adverse cardiovascular pathologies.

CHAPTER 6

JEJUNAL SUBMUCOSAL ARTERIOLES FROM BARIATRIC PATIENTS WITH DIABETES HAVE BLUNTED VASODILATORY RESPONSE TO INSULIN BUT NOT TO ACETYLCHOLINE

6.1 Introduction

Obesity represents a major health problem affecting millions of people worldwide. In United States of America obesity has increased considerably in the last decades. Recent studies (139, 140) have shown that in the U.S. about 34.9% of the adults (20 years old and over) are obese. In adults between the ages of 40-59 years the obesity levels reach their maximum at 39.5%. In average, 27.4% of the adults (25 years old and over) die every year as a consequence of heart disease or stroke (74). Obesity increases the risk of several pathophysiological conditions, being hypertension and type-2 diabetes two of the most important. Type-2 diabetes and obesity are associated with cardiovascular disease, which is considered the number-one cause of death nowadays (accounting for

more than 24% of the deaths); and endothelial dysfunction, of which the mechanisms leading to aberrant insulin-dependent vasodilation have not been completely understood.

In an effort to reduce the incidence of diabetes, cardiovascular diseases and other obesity-related morbidities, an increasing number of obese individuals are opting for bariatric surgery to reduce their body weight and body mass index (BMI).

Roux-En-Y Gastric Bypass (RYGB) is a type of bariatric surgery in which the stomach is first divided into two parts, a smaller upper pouch and a larger lower stomach bypassed section. Then the small intestine is re-arranged and re-connected to both parts of the stomach, adopting a "Y" shape. This surgical procedure reduces the amount of food that can be ingested per meal, limiting the calorie intake and reducing the amount of nutrients that are absorbed by the intestines. This helps obese individuals lose weight. Furthermore, through mechanisms that still remain to be completely understood, the RYGB has been shown to improve cardiovascular function and glucose homeostasis (3, 31, 49, 100, 150, 159).

Type II diabetes is associated with obesity, and it is characterized by systemic insulin resistance. However, not all obese individuals are diabetic, therefore we hypothesize that insulin-dependent vasodilation is impaired only in obese individuals with diabetes, but not in obese non-diabetic individuals. This would suggest that there is an insulin-endothelial specific dysfunction that is directly associated with systemic insulin resistance and independent of the degree of obesity.

6.2 Materials and methods

6.2.1 Individuals

Prior to surgery, consent from bariatric-surgery patients was obtained to use a section of their jejunum for medical research. This jejunal section is commonly dissected and discarded during surgery as part of the RYGB procedure. Individuals included in this study were of adult age and had an average BMI of 47.3 ± 0.9 Kg/m^2 (Fig. 6.1). Females and males were both included in these experiments.
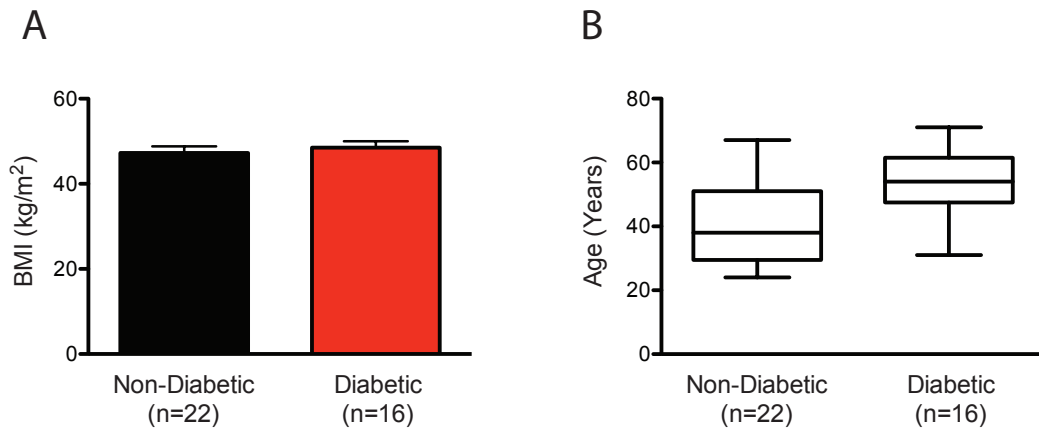
Figure 6.1. BMI (A) and age (B) for non-diabetic and diabetic groups. The number (n) of individuals included in each group is indicated in parenthesis. The results are presented as means ±SEM.

6.2.2 Tissue collection and vessel isolation

During the RYGB surgical procedure, a section of approximately 3 inches of the jejunum and mesenteric tissue/fat was excised and placed in a cold (~4°C) physiological saline solution in a sealed container that was kept in ice for tissue storage and transportation from the surgery room to the laboratory where the experiments were performed. For tissue dissection and vessel isolation, the jejunum sample was transferred

103

onto a cooled dissection chamber and placed on a physiological saline solution (PSS) containing: 145.0 NaCl, 4.7 KCl, 2.0 CaCl$_2$, 1.0 MgSO$_4$, 1.2 NaH$_2$PO$_4$, 0.02 EDTA, 2.0 Pyruvic Acid, 5.0 Glucose and 3.0 MOPS (all concentrations are given in mM) with a final pH of 7.4. From a small section of the jejunal wall, submucosal arterioles were isolated. Mesenteric veins and arteries were also isolated from the jejunal tissue samples from each individual. Right after isolation, a set of one mesenteric vein and one mesenteric artery was snap frozen and stored at -70°C, and later used for western blotting and xMAP multi-plexing. A second piece of mesenteric artery was cannulated, pressurized at 80 mmHg and fixed in 4% paraformaldehyde. Fixed arteries were sliced, mounted on glass slides and used for various immunohistochemistry and fluorescence studies.

6.2.3 Experimental protocols

<u>In-vitro characterization of the functional responses of isolated arterioles</u>

In order to measure and characterize the contractile and vasodilatory responses, isolated jejunal submucosal arterioles were cannulated and pressurized for experimentation as previously described (115). Briefly, arteriolar segments of ~1-2mm in length were cannulated onto glass micropipettes within an observation chamber (Living Systems Instrumentation, Burlington, Vermont) filled with PSS. The arterioles were pressurized without flow to 70 mmHg using a Pressure Servo System (Living Systems Instrumentation Burlington, Vermont) and PSS containing 0.15 mM bovine serum albumin. The observation chamber with the cannulated vessel was transferred to an

inverted microscope equipped with a video display and video caliper system (Living Systems Instrumentation Burlington, Vermont) to record measurements of wall thickness and luminal diameter. After arterioles were warmed up to 37°C and allowed to stabilize for 1 hour, their viability was tested by inducing depolarization of the cell membrane via exposure to a PSS containing 80 mM KCl. Subsequently, their functional responses to increasing concentrations of phenylephrine (10^{-8} to 10^{-5} M), insulin (10^{-9} to 10^{-5} M) or acetylcholine (10^{-8} to 10^{-5} M), and sodium nitroprusside (SNP) (10^{-8} to 10^{-4} M) were recorded. Exposure to phenylephrine tests for adrenergic vasoconstriction, while insulin, acetylcholine and SNP test for vasodilatory responses. Insulin and acetylcholine are both endothelium-dependent vasodilators and SNP an endothelium-independent one (1, 17, 55, 87, 95, 129, 147, 172).

Assessment of the elastic properties of arterioles

The elastic characteristics of the arteriolar wall were studied by performing measurements of the diameter at different levels of intraluminal pressure obtained under passive conditions (in a Ca^{2+}-free PSS containing EGTA and Adenosine). These measurements were obtained for each arteriole at the end of every experiment. The intraluminal pressure was varied in increasing steps ranging from 5 to 120 mmHg. Maximum internal diameter and wall thickness were recorded, and these data were later used to calculate, as previously reported (32, 33), the circumferential stress, strain and modulus of elasticity for all vessels included in this study.

<u>Confocal fluorescence microscopy for the quantification of the main components of the arteriolar wall</u>

After the assessments of functional responses and elastic properties of the arterioles were completed, all vessels were kept at 70 mmHg of intraluminal pressure and fixed using 4% paraformaldehyde for 1 hour at room temperature. For imaging, vessels were uncannulated rinsed twice in pH 7.3 phosphate-buffered saline (PBS) and once in 0.1M Glycine for 5 minutes each time to remove any residual paraformaldehyde. Vessels were then cannulated onto glass micropipettes within an observation chamber (same as when assessing arteriolar functional responses) containing PBS and flushed with 1 mL of the same solution to rinse the lumen. Subsequently, vessels were permeabilized via incubation in 0.5% TritonX100 in PBS for 20 minutes. After that, vessels were washed and their lumens flushed twice with PBS and incubated for 1 hour in a solution containing: 0.5µg/mL 4',6-diamidino-2-phenylindole (DAPI), 200 nM Alexa Fluor 633 Hydrazide (Molecular Probes) and 33 nM Alexa Fluor 546 phalloidin (Molecular Probes) in PBS. After incubation and in preparation for imaging, vessels were washed/flushed 3 times using PBS. Fluorescence images were obtained using a Leica SP5 confocal/multiphoton microscope with a 63X/1.2NA water objective. Alexa Fluor 633 Hydrazide, which stains elastin, was excited with a 633 nm HeNe laser. Alexa Fluor 546 phalloidin binds to actin and was excited with a 543 nm HeNe laser. Nuclei imaging was achieved by exciting DAPI using a multi-photon laser at 700 nm. Collagen structures were imaged by capturing their characteristics produced with second-harmonic generation (SHG) using a multi-photon laser at 850 nM.

106

<u>Immunohistochemistry of the insulin receptor</u>

Using mesenteric arteries that were fixed in 4% paraformaldehyde at 80 mmHg of intravascular pressure right after dissection, the amount of the different structural-components of the insulin receptor (IR) were quantified by means of immunohistochemistry assays as previously described (66, 67, 201, 202). Briefly, ethanol-series rehydrated paraffin-embedded arterial sections were blocked in 5% of BSA, 5% of donkey serum and 0.01% of sodium azide in HEPES buffer for 4 hours in a humidified chamber. Following a brief HEPES-rinse, sections were incubated overnight with 1:40 of Insulin Receptor-Alpha (rabbit polyclonal) Antibody and Insulin Receptor-Beta (rabbit polyclonal) Antibody (Cat. No. 250723 and 250724 from Abbiotec, respectively). Incubation in primary antibodies was performed in humidity chambers at room temperature. Then, the sections were thoroughly washed with HEPES wash buffer (3x 5-minute per wash) and incubated with 1:300 of appropriate secondary antibodies, Alexa Fluor Donkey anti-Rabbit (Invitrogen A31572) for 4 hours. After washing, the sections were mounted with Mowiol and sealed with nail polish for further examination under a confocal microscope. Signal intensities were analyzed with MetaVue and ImageJ. Similarly, sections of the same mesenteric arteries were immunostained for quantification of the amount (total amount of protein) of the four different substrates of the IR. Other sections were stained with Verhoeff-Van Gieson (VVG). Brightfield microscopy images were obtained from these sections and analyzed to measure luminal diameter and media thickness of these mesenteric arteries.

<u>xMAP-multiplexing for quantification of MMPs and TIMPs</u>

Arteries (~3-5mm long sections) isolated from the mesenteric fat located in the vicinity of the jejunum were snap frozen and stored at -70°C. Later, samples from all the patients included in this study were taken out from the freezer and transferred into 0.5 mL homogenizer tubes (Omni International) containing 400 µL of RIPA buffer with halt protease and phosphatase inhibitor cocktail (Thermo Scientific #78440). Arteries were then homogenized using 1.4 mm zirconium oxide beads (20 per tube) and an Omni Bead Ruptor 24 (Omni International). Subsequently, homogenates were transferred into new tubes and centrifuged for 3 minutes at 10,000 rpm using an Eppendorf 5415D centrifuge. Supernatants were then collected and transferred into new tubes for re-centrifugation at 13,000 rpm for 10 minutes to ensure proper debris precipitation. Finally, homogenates were split into two parts and ran as duplicates in a BioPlex 200 system using the Milliplex Map kits Human MMP (Matrix Metalloproteinase) Panel 2 Magnetic Bead Kit and Human TIMP (Tissue Inhibitors of Matrix Metalloproteinase) Panel 2 Magnetic Bead Kit respectively. These kits allowed for the quantification of the amount of MMPs (MMP-1,2,7,9,10) and TIMPs (TIMP-1,2,3,4).

6.3 Results

6.3.1 Smooth-Muscle-Cell (SMC) membrane depolarization- and adrenergic-induced vasoconstrictions were not affected by presence of diabetes

Depolarization of the SMC-membrane via exposure of isolated and pressurized jejunal submucosal arterioles to an 80 mM KCl PSS induced strong and sustained

vasoconstriction. Similar, not statistically significantly different, constriction levels were observed in arterioles from diabetic and non-diabetic individuals (Fig. 6.2-A). Correspondingly, exposure to increasing concentrations of phenylephrine (10^{-8} to 10^{-5} M) induced similar adrenergic-receptor dependent vasoconstriction in both diabetic and non-diabetic groups (Fig. 6.2-B).
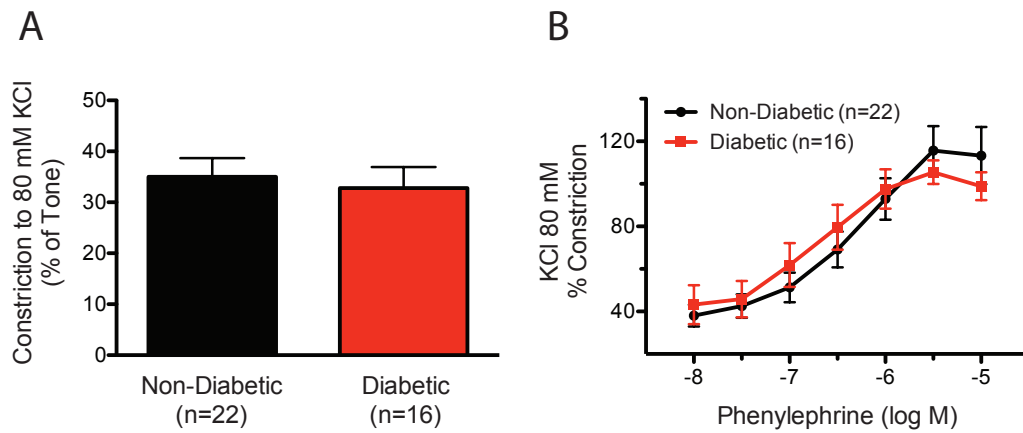
Figure 6.2. (A) Viability of jejunal arterioles was assessed by exposure to a PSS containing 80 mM KCl. Constriction to KCl is presented as a percent of the tone prior exposure. (B) Adrenergic-receptor dependent vasoconstriction at different increasing concentrations of phenylephrine. Constriction is reported as a percent of the maximum vasoconstriction achieved at 80 mM KCl. The results represent means ±SEM of the n number of experiments that were performed.

6.3.2 Arterioles from bariatric patients with diabetes have blunted response to insulin but not to acetylcholine

Endothelium-dependent vasodilation was tested on jejunal arterioles by exposing them to increasing concentrations of either insulin or acetylcholine and subsequently to SNP. Vasodilatory responses were assessed after pre-constriction with phenylephrine (10^{-6} M). When testing insulin-vasodilation, a blunted vasodilatory response was observed

for arterioles from bariatric diabetic-patients. In the diabetic group, the maximal insulin-dependent vasodilation (dilation to insulin 10^{-5} M) was $23.6 \pm 6.9\%$ smaller ($p < 0.05$) than that in the group of non-diabetic patients (Fig. 6.3-C,D). However, the vasodilation induced by acetylcholine or SNP were not significantly different between these two groups (Fig. 6.3-A,B).
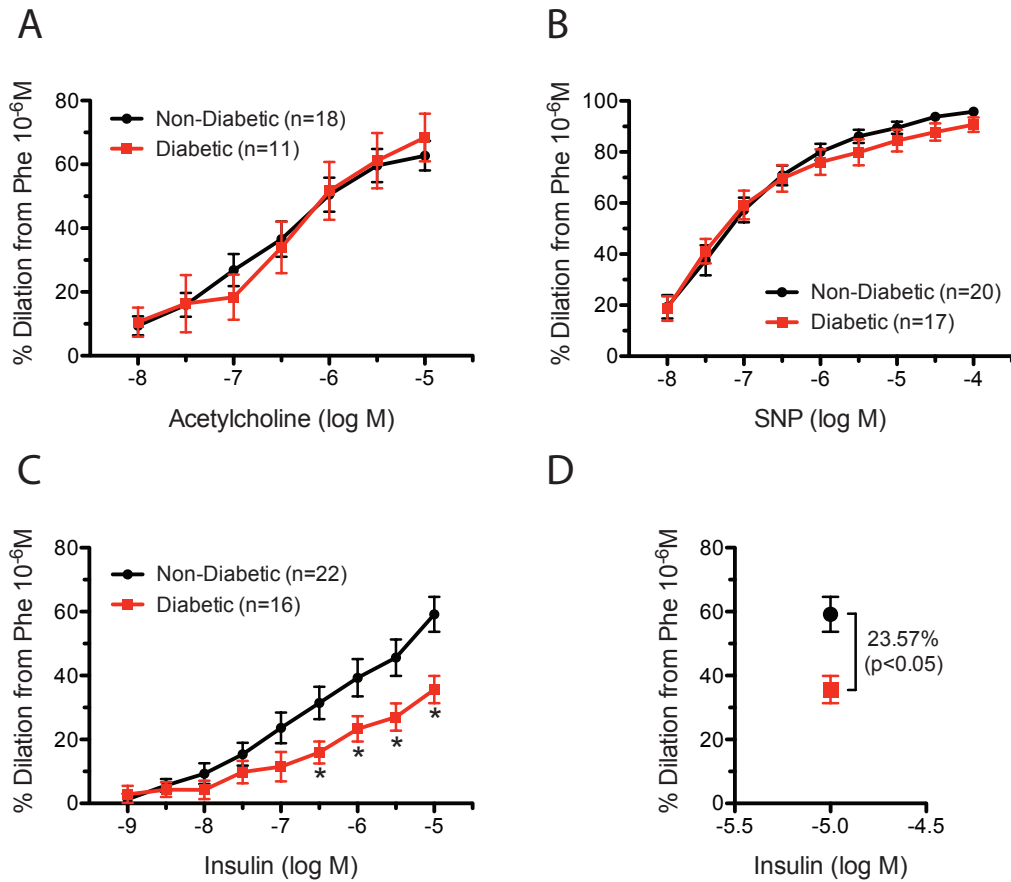
Figure 6.3. Endothelium-dependent vasodilation was assessed by means of exposure to increasing concentrations of acetylcholine (A) and insulin (C). (B) Characterization of endothelium-independent vasodilation using increasing concentrations of SNP. Panel (D) shows the mean difference in vasodilation at the maximum concentration (10^{-5} M) of Insulin. The results represent the means ± SEM. * $p < 0.05$ vs non-diabetic group.

6.3.3 Elastic and mechanical properties of jejunal submucosal arterioles from bariatric patients

Assessment of the elastic/mechanic properties of the jejunal submucosal arterioles after characterization of their functional responses showed that arterioles from diabetic patients had a tendency to have an increased stiffness when compared to those vessels from non-diabetics (Fig. 6.4). However, these results were not significantly different.
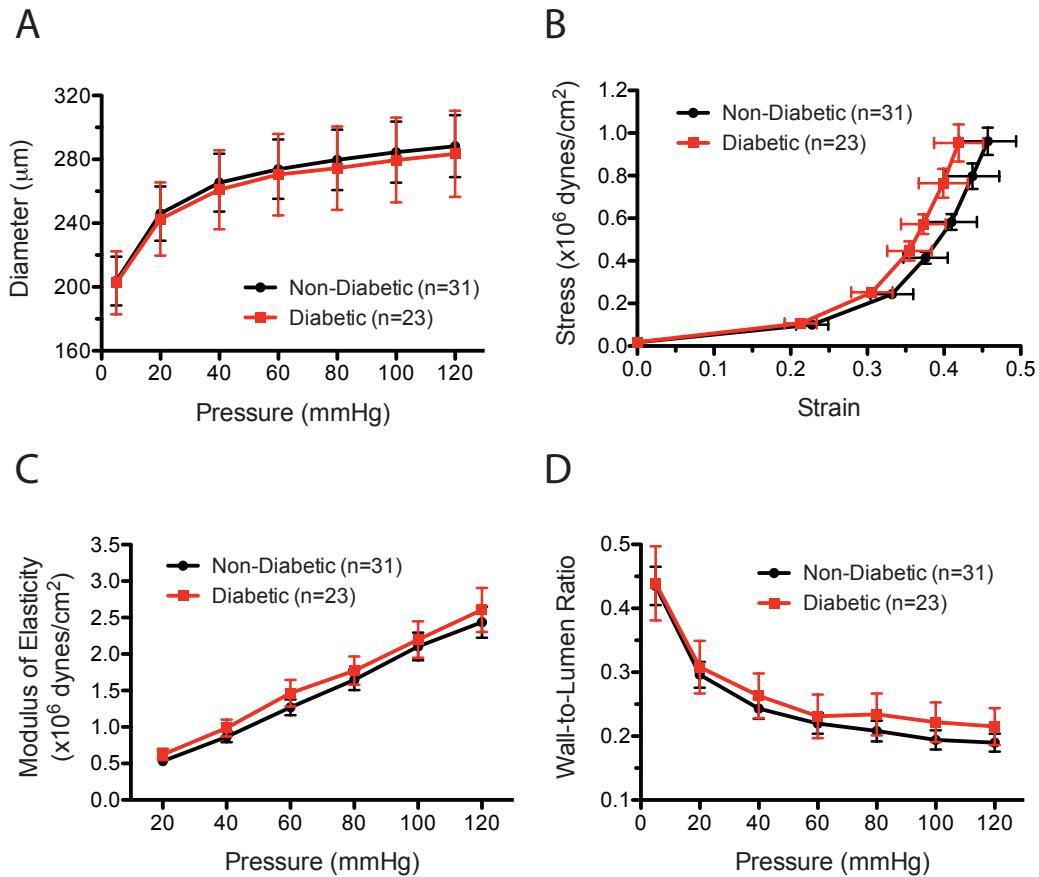
Figure 6.4. Assessment of the elastic properties of jejunal arterioles from non-diabetic and diabetic individuals. (A) Luminal diameter as a function of the intraluminal pressure. (B) Strain-stress relationships. (C) Modulus of elasticity at different intraluminal pressures. (D) Wall-to-Lumen ratios for both groups as functions of pressure. These results represent the mean ± SEM.

6.3.4 Vascular-wall media thickness and cross-sectional area of jejunal arterioles are increased in diabetics, while densities of actin and SMCs nuclei are reduced

Although the raw measurements of total expression of actin, elastin, nuclei and collagen were not statistically different between diabetics and non-diabetics, the normalized amounts of actin and nuclei-volume per unit of vascular-wall volume were found significantly smaller in arterioles from diabetic patients (Fig. 6.5-A,B). This is consistent with the fact that although these arterioles had similar luminal diameters, they had significantly increased wall thickness increasing the cross-sectional area of the arteriolar wall; in particular, arterioles from diabetics had more volume between the elastic laminas (Fig. 6.6-A,B). By implementing a Matlab script, images of the elastin fibers that conform the elastic laminas where analyzed to look at the different angles of orientation. These fibers seem to be oriented in a preferential orientation, at 15 degrees; however there was no difference between groups (Fig. 6.6-C,D).
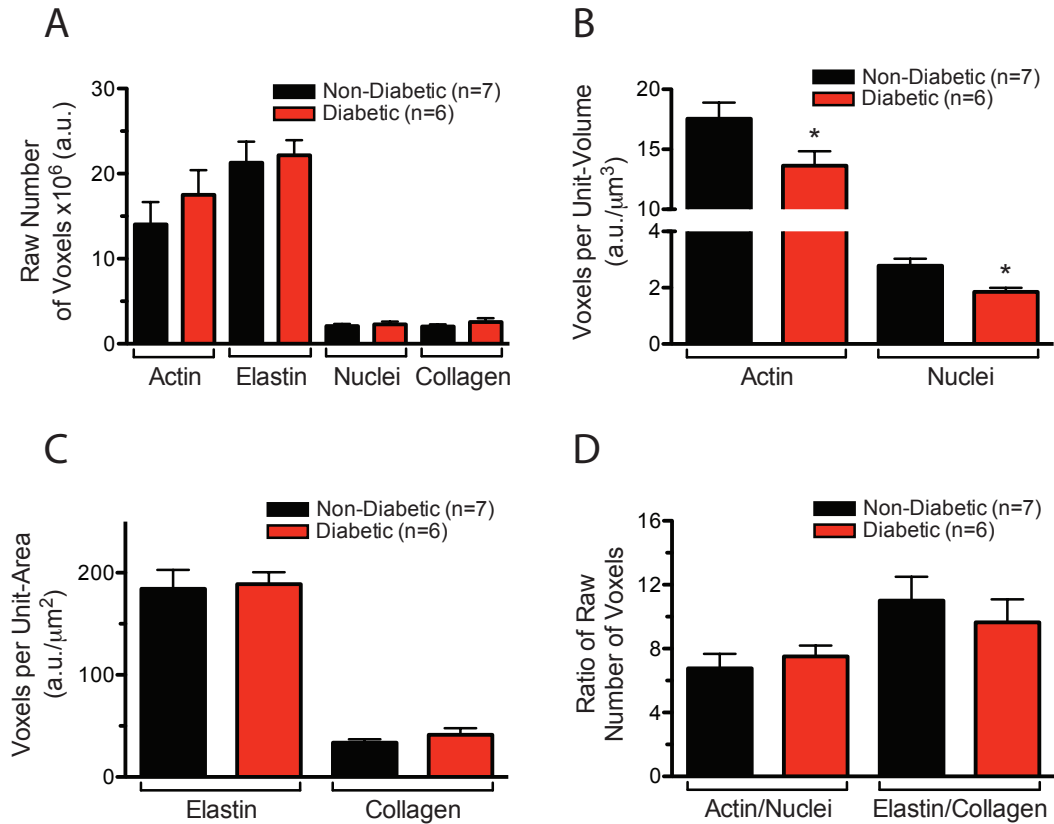
Figure 6.5. Quantification of actin, elastin, nuclei and collagen by confocal microscopy in jejunal arterioles. (A) Raw number of voxels with expression of actin, elasitn, nuclei or collagen. (B) Density of voxels per unit-volume of the vascular wall. These results represent the values on panel (A) normalized to the total available volume within the internal and external elastic laminas. (C) Density of voxels per unit-area of the elastic laminas. These results represent the raw numbers for elastin and collagen from panel (A) normalized to the total surface area associated with the internal and external elastic laminas in the case of elastin; and to the total surface area of the external elastic lamina for collagen. Results are means ± SEM in each case. * $p < 0.05$ vs non-diabetic group.
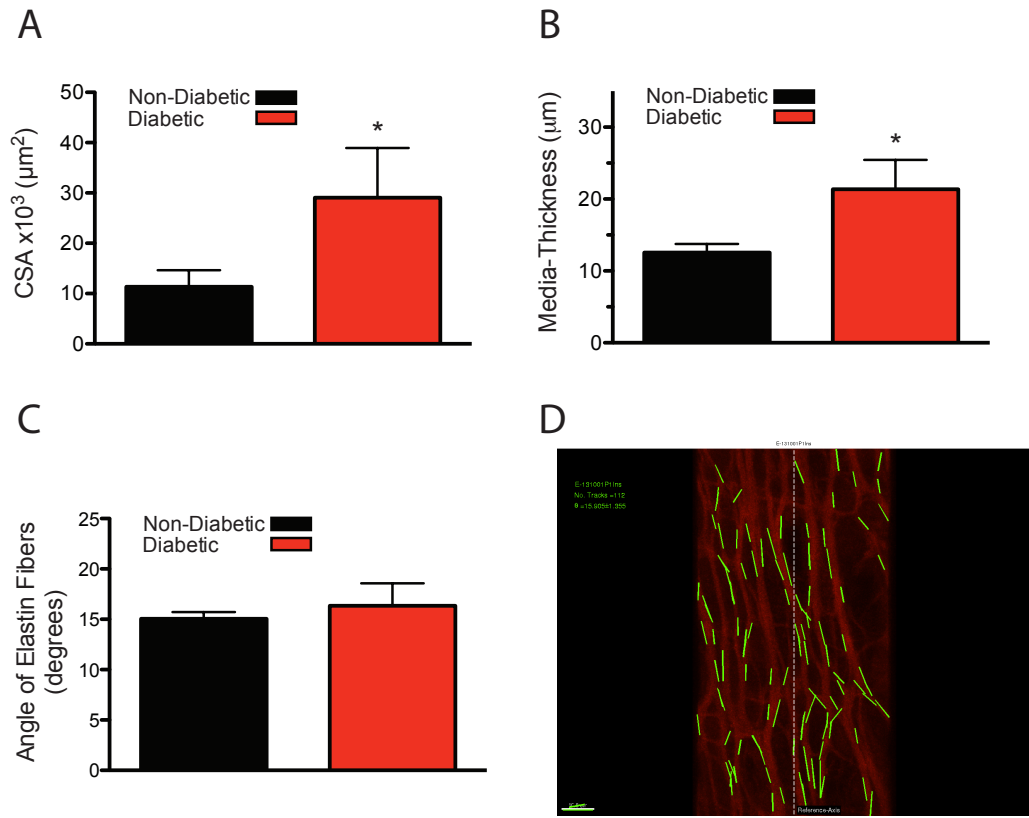
Figure 6.6. (A,B) Cross-sectional area (CSA) and media thickness (C,D). Orientation-angles of the elastin fibers with respect to the longitudinal direction. Mean ± SEM for each group. * $p<0.05$ vs non-diabetic group.

6.3.5 The extracellular subunit of the insulin receptor is cleaved in arteries from diabetic bariatric patients

Immunohistochemistry and fluorescence microscopy techniques were utilized on mesenteric arteries to look at the amount of the two different subunits (extracellular α-subunit and transmembrane β-subunit) that constitute the insulin receptor (IR). The results showed a reduced amount of the extracellular subunit on mesenteric arteries from bariatric patients diagnosed with diabetes (Fig. 6.7-A,C). No significant differences were observed for the amount of the transmembrane subunit (Fig. 6.7-B,D). The reduction in the α-subunit of the IR was consistently observed through all the layers (i.e. intima, media and adventitia) of the vascular wall (Fig. 6.7-C).

6.3.6 Presence of the insulin receptor substrates is similar in patients with and without diabetes

Immunohistochemistry and confocal microscopy was also used to quantify the amount (total amount of protein) of the four known different substrates of the IR in mesenteric arteries from diabetic and anon-diabetic patients. Fluorescence quantification showed non-statistically significant differences in the amount of protein associated with all substrates between the groups (Fig. 6.8).
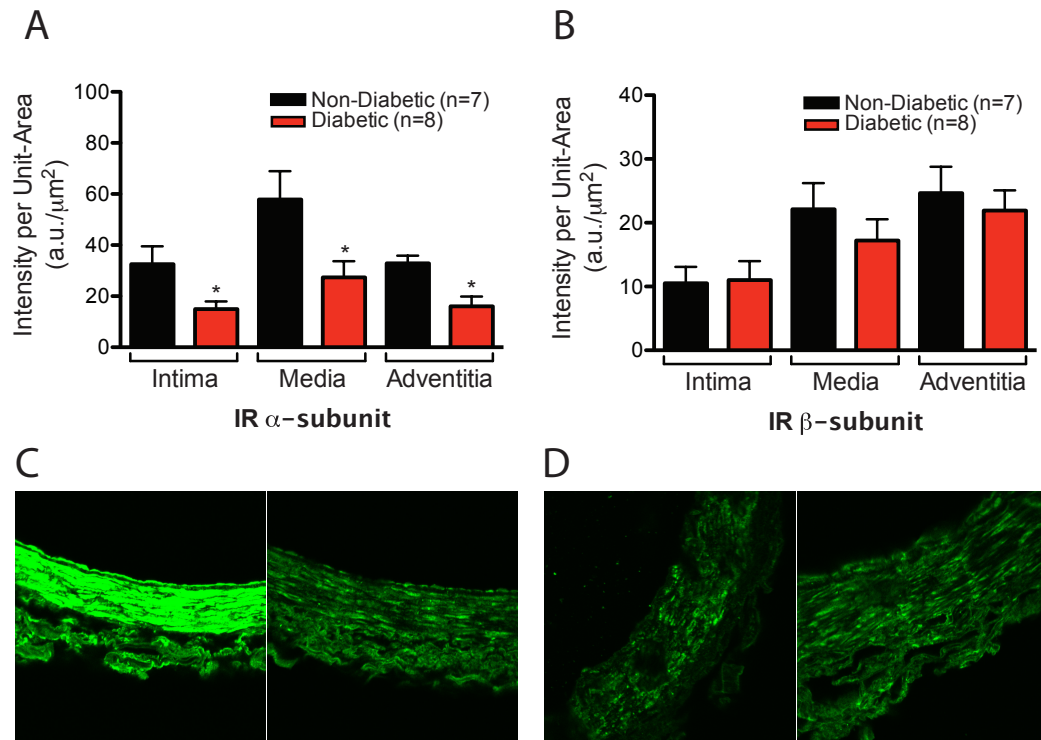
Figure 6.7. Immunohistochemistry and confocal microscopy to quantify: the amount of the extracellular insulin receptor α subunit (A) and the transmembrane insulin receptor β subunit (B). The quantification is expressed as total intensity per unit-area in the different sections of the vascular wall (intima, media and adventitia), and the results are presented as means ± SEM. * $p<0.05$ vs non-diabetic group.
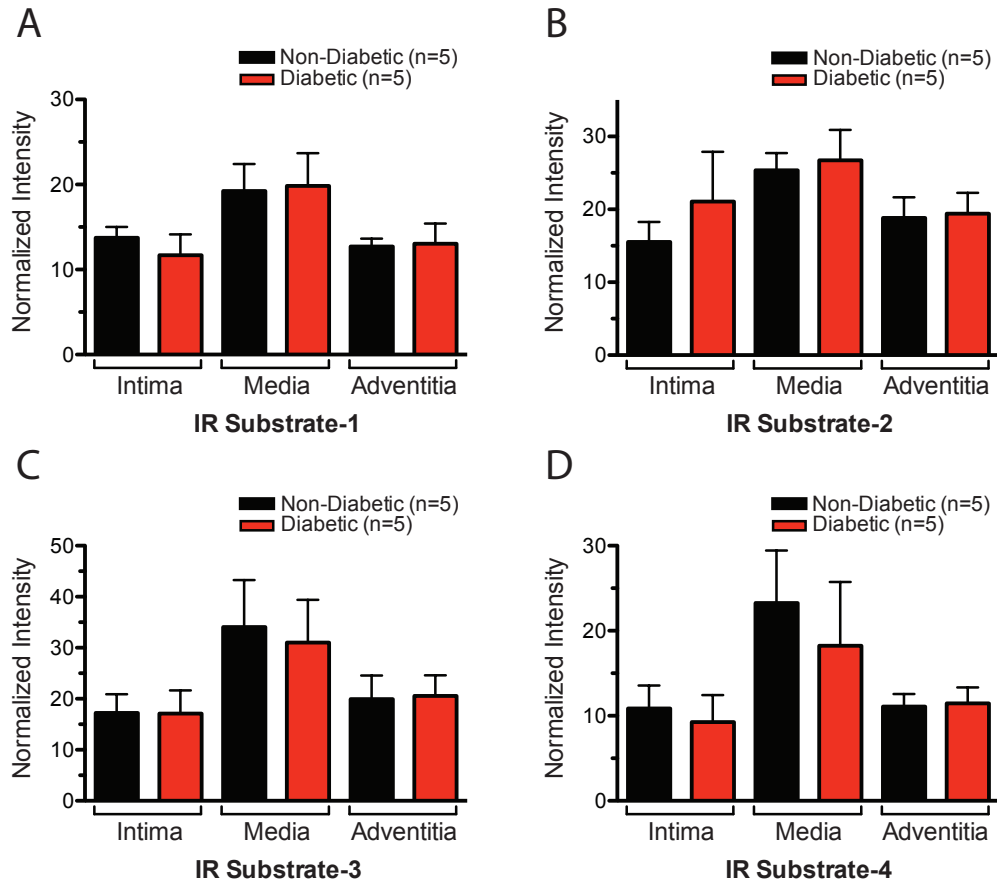
Figure 6.8. Quantification of the four insulin-receptor substrates in mesenteric arteries from diabetic and non-diabetic bariatric patients using immunohistochemistry and confocal microscopy. Total amount of protein associated with each substrate was quantified. The results are expressed as means ± SEM.

6.3.7 Matrix-Metalloproteinase-9 (MMP-9) is reduced in mesenteric arteries from diabetic patients

Multi-plexing assays to measure the amount of MMPs (MMP-1,2,7,9,10) and their tissue inhibitors (TIMPs 1-4) on homogenates from mesenteric arteries. The results showed that from the various MMPs that were assessed, the amount of MMP-9 present in arterial-tissue from diabetic patients was significantly reduced compared to non-diabetic samples (Fig. 6.9-A). No significant differences were observed when assessing the

presence of the different tissue inhibitors of the MMPs (Fig. 6.9-B). The ratios of the MMPs 2,9 to the different TIMPs were calculated. MMP-9/TIMP-1 and MMP-9/TIMP2 were significantly smaller in the arteries from diabetics (Fig. 6.9-D).

6.3.8 Mesenteric arteries from diabetic patients have increased media thickness and increased media-to-lumen ratio

Sliced sections, from the same mesenteric arteries used for the quantification of the IR subunits and IR substrates, were stained following the Verhoeff-Van Gieson (VVG) staining protocol. The results from brightfield microscopy imaging showed that mesenteric arteries from both, diabetics and non-diabetics have similar luminal diameters. However, the arterial-wall media was significantly increased in thickness, resulting in presence of increased media-to-lumen ratios in arteries from diabetic patients (Fig. 6.10).
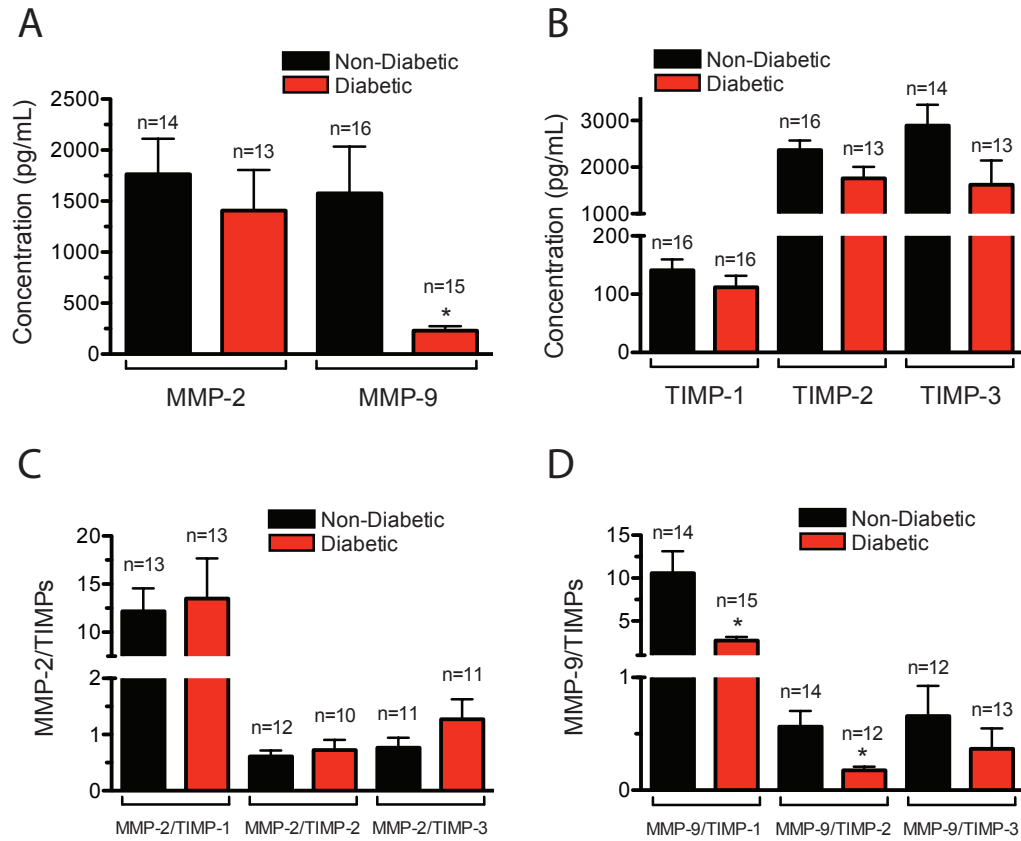
Figure 6.9. Quantification of the levels of MMPs and TIMPs in homogenized mesenteric arteries using multiplexing. These results represent the concentration measurements per unit of volume (mL). The results are expressed as mean ± SEM for diabetic and non-diabetic groups respectively. * $p<0.05$ vs non-diabetic group.
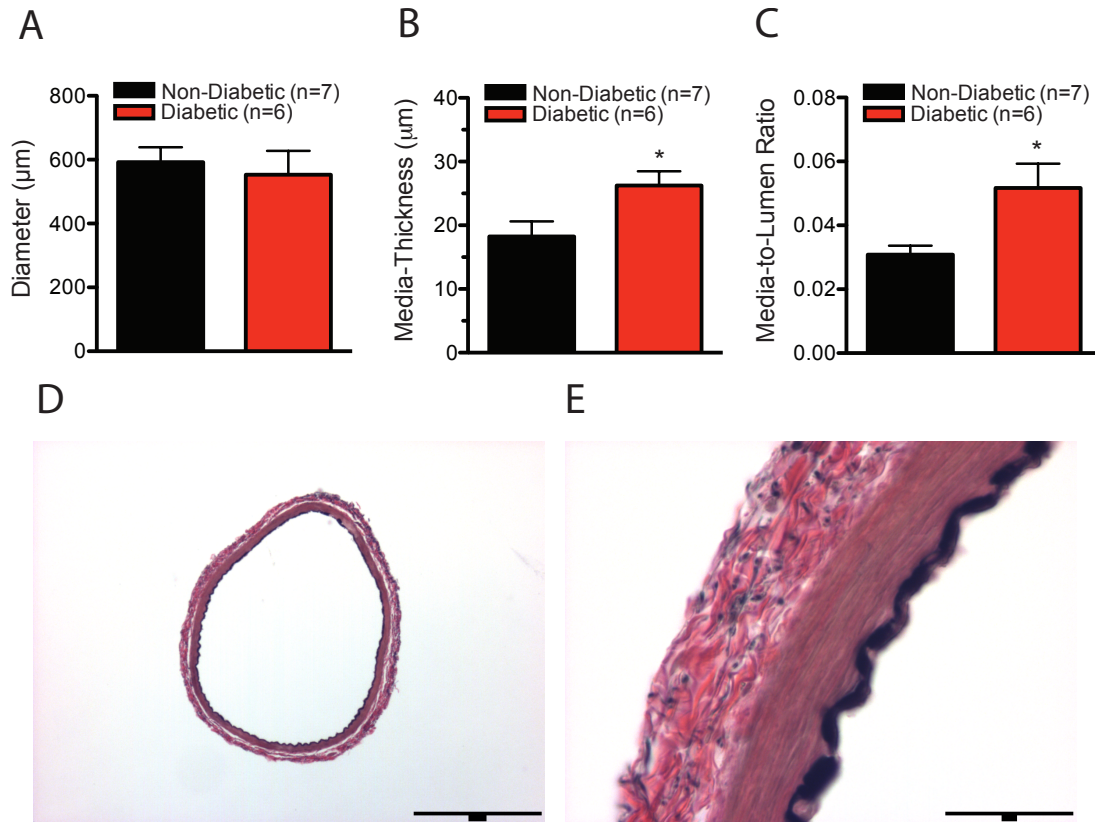
Figure 6.10. Morphometric analysis of mesenteric arties from diabetic and non-diabetic bariatric patients stained with VVG. The diameter results in panel (A) represent the reconstructed values from perimeter measurements. (B) Media thickness. (C) Media-to-Lumen ratio. (D,E) Representative images of a sliced mesenteric artery using 4x and 40x objectives (400 and 40 μm scale-bars) respectively. * $p < 0.05$ vs non-diabetic group.

6.4 Conclusions and discussion

The connection between obesity and vasculature-related diseases has been widely studied. The effects of obesity on large arteries have been shown to increase the risk factors for myocardial infarction, stroke and hypertension (25, 158). Structural and functional changes in the microvasculature have also been shown to increase in obesity (30, 65, 84). Obesity has been also associated with diabetes; furthermore, these two

diseases have been associated with insulin resistance and endothelial dysfunction. However, whether insulin resistance and endothelial dysfunction are directly associated in obesity, and whether one is a necessary condition for the other, remains unknown; and, the mechanisms through which the microvasculature is damaged in obesity remain to be fully understood.

In this manuscript, we showed that micro-vessels from the jejunal submucosa of diabetic obese bariatric-patients presented a reduced dilation to increasing concentrations of insulin, when compared to non-diabetic obese individuals. In contrast, dilations to increasing concentrations of acetylcholine remained at similar levels for both groups. This blunted-response to insulin occurring in the absence of an abnormal acetylcholine-induced dilation suggests that the mechanisms responsible for this endothelial dysfunction are upstream of eNOS activation. The problem may be found at the level of the insulin-receptor itself. Indeed our results indicate that the extracellular portion of the IR is significantly reduced in diabetic vs. non-diabetic vessels. Because the transmembrane portion of the receptor was not reduced, this suggests that the extracellular portion was likely cleaved or shed from the cell membrane. Originally, we suspected that changes in the activity or proportion of MMPs, TIMPs and ADAMs (A disintegrin and metalloproteinases), known for their sheddase-properties in cleaving extracellular portions of transmembrane receptors, could be responsible for cleaving the IR extracellular component (10, 47, 133, 169). Our results indicate that there are changes in the proportion of MMP in the vascular wall of diabetic patients and suggest that, the responsible mechanism(s) may be associated with changes in the activity of matrix

metalloproteinases. As already mentioned, our results on the quantification of the expression of the different subunits of the IR support our original idea of the cleavage of the insulin receptor subunits (reduced extracellular subunit-α); however, contrary to what we expected, MMPs, in particular MMP-9, were reduced in mesenteric arteries from diabetic patients. This reduced expression of MMPs (specifically MMP-9) suggests that, in Type-2 diabetes, the mechanism(s) responsible for a blunted-response to insulin may be related with the expression/activity of MMPs (58, 79, 109, 144, 189, 207). We suspect that MMPs are indeed increased in diabetes, and may be the responsible for the shedding of the insulin receptor, but they are being secreted and released into the blood stream, increasing the concentration of circulating MMPs. Meanwhile the amount of MMPs present in the actual tissue, as in our case, may be reduced.

Although we did not observe a significant change in the elastic properties of jejeunal submucosa arterioles between groups, we did observe a tendency for arterioles from diabetics to be stiffer and have increased wall thickness and increased wall-to-lumen ratios. These results were confirmed by means of fluorescence/confocal microscopy, where it was shown that the density of expressed-voxels per unit of volume of the vascular wall (available volume between elastic laminas) for actin and nuclei were both significantly reduced in arterioles from diabetic individuals. The actin-to-nuclei ratio did not change between groups, meaning that the total amount of actin present per smooth muscle cell was the same. It was just the available volume within elastic laminas that was increased. This result was confirmed when the thickness of the media was measured and was found significantly increased in diabetic vessels. These observations

are consistent with the results from VVG-stained sliced-sections of mesenteric arteries. There we found that luminal diameters did not change between diabetics and non-diabetics, but the media thickness was significantly increased in the diabetic groups.

The results reported in this document suggest that in obesity, the vascular wall, specifically the media, undergo structural modifications that result in an increased volume, while the amounts of actin and number/volume of nuclei remain unchanged. Perhaps collagen of a type other than the one we measured here is filling this space. Furthermore, our results suggest that in obesity and type-2 diabetes, the endothelial dysfunction that results in a reduced dilation to insulin accompanies the systemic insulin resistance that is associated with type-2 diabetes, but this endothelial dysfunction is independent of the degree of obesity that an individual presents.

REFERENCES

1.   Adachi T. Modulation of vascular sarco/endoplasmic reticulum calcium ATPase in cardiovascular pathophysiology. *Advances in pharmacology* 59: 165-195, 2010.

2.   Adler KB, Krill J, Alberghini TV, and Evans JN. Effect of cytochalasin D on smooth muscle contraction. *Cell motility* 3: 545-551, 1983.

3.   Ahn SM, Pomp A, and Rubino F. Metabolic surgery for type 2 diabetes. *Annals of the New York Academy of Sciences* 1212: E37-45, 2010.

4.   Alessi MC, Bastelica D, Morange P, Berthet B, Leduc I, Verdier M, Geel O, and Juhan-Vague I. Plasminogen activator inhibitor 1, transforming growth factor-beta1, and BMI are closely associated in human adipose tissue during morbid obesity. *Diabetes* 49: 1374-1380, 2000.

5.   Alvira CM, Guignabert C, Kim YM, Chen C, Wang L, Duong TT, Yeung RS, Li DY, and Rabinovitch M. Inhibition of transforming growth factor beta worsens elastin degradation in a murine model of Kawasaki disease. *Am J Pathol* 178: 1210-1220, 2011.

6.   Andrianantoandro E and Pollard TD. Mechanism of actin filament turnover by severing and nucleation at different concentrations of ADF/cofilin. *Mol Cell* 24: 13-23, 2006.

7.   Aneja A, El-Atat F, McFarlane SI, and Sowers JR. Hypertension and obesity. *Recent Prog Horm Res* 59: 169-205, 2004.

8.   Anfinogenova Y, Wang R, Li QF, Spinelli AM, and Tang DD. Abl silencing inhibits CAS-mediated process and constriction in resistance arteries. *Circ Res* 101: 420-428, 2007.

9.   Arribas SM, Briones AM, Bellingham C, Gonzalez MC, Salaices M, Liu K, Wang Y, and Hinek A. Heightened aberrant deposition of hard-wearing elastin in conduit arteries of prehypertensive SHR is associated with increased stiffness and inward remodeling. *Am J Physiol Heart Circ Physiol* 295: H2299-2307, 2008.

10.   Aston-Mourney K, Zraika S, Udayasankar J, Subramanian SL, Green PS, Kahn SE, and Hull RL. Matrix metalloproteinase-9 reduces islet amyloid formation by degrading islet amyloid polypeptide. *The Journal of biological chemistry* 288: 3553-3559, 2013.

11.   Bakker EN, Buus CL, Spaan JA, Perree J, Ganga A, Rolf TM, Sorop O, Bramsen LH, Mulvany MJ, and Vanbavel E. Small artery remodeling depends on tissue-type transglutaminase. *Circulation research* 96: 119-126, 2005.

12.   Bakker EN, Buus CL, VanBavel E, and Mulvany MJ. Activation of resistance arteries with endothelin-1: from vasoconstriction to functional adaptation and remodeling. *Journal of vascular research* 41: 174-182, 2004.

13.   Bakker EN, Pistea A, Spaan JA, Rolf T, de Vries CJ, van Rooijen N, Candi E, and VanBavel E. Flow-dependent remodeling of small arteries in mice deficient for tissue-type transglutaminase: possible compensation by macrophage-derived factor XIII. *Circ Res* 99: 86-92, 2006.

14.   Bakker EN, Pistea A, and VanBavel E. Transglutaminases in vascular biology: relevance for vascular remodeling and atherosclerosis. *J Vasc Res* 45: 271-278, 2008.

15.   Bakker EN, van Der Meulen ET, Spaan JA, and VanBavel E. Organoid culture of cannulated rat resistance arteries: effect of serum factors on vasoactivity and remodeling. *Am J Physiol Heart Circ Physiol* 278: H1233-1240., 2000.

16.   Bakker EN, van der Meulen ET, van den Berg BM, Everts V, Spaan JA, and VanBavel E. Inward remodeling follows chronic vasoconstriction in isolated resistance arteries. *Journal of vascular research* 39: 12-20, 2002.

17.   Baron AD. Insulin resistance and vascular function. *Journal of diabetes and its complications* 16: 92-102, 2002.

18.   Baumbach GL, Dobrin PB, Hart MN, and Heistad DD. Mechanics of cerebral arterioles in hypertensive rats. *Circulation research* 62: 56-64, 1988.

19.   Baumbach GL and Hajdu MA. Mechanics and composition of cerebral arterioles in renal and spontaneously hypertensive rats. *Hypertension* 21: 816-826, 1993.

125

20.   Baumbach GL, Walmsley JG, and Hart MN. Composition and mechanics of cerebral arterioles in hypertensive rats. *The American journal of pathology* 133: 464-471, 1988.

21.   Beazley KE, Banyard D, Lima F, Deasey SC, Nurminsky DI, Konoplyannikov M, and Nurminskaya MV. Transglutaminase inhibitors attenuate vascular calcification in a preclinical model. *Arterioscler Thromb Vasc Biol* 33: 43-51, 2013.

22.   Bendeck MP, Conte M, Zhang M, Nili N, Strauss BH, and Farwell SM. Doxycycline modulates smooth muscle cell growth, migration, and matrix remodeling after arterial injury. *American Journal of Pathology* 160: 1089-1095, 2002.

23.   Blystone SD. Integrating an integrin: a direct route to actin. *Biochim Biophys Acta* 1692: 47-54, 2004.

24.   Boak AM, Roy R, Berk J, Taylor L, Polgar P, Goldstein RH, and Kagan HM. Regulation of lysyl oxidase expression in lung fibroblasts by transforming growth factor-beta 1 and prostaglandin E2. *Am J Respir Cell Mol Biol* 11: 751-755, 1994.

25.   Boden G and Salehi S. Why does obesity increase the risk for cardiovascular disease? *Current pharmaceutical design* 19: 5678-5683, 2013.

26.   Bostick B, Habibi J, Ma L, Aroor A, Rehmer N, Hayden MR, and Sowers JR. Dipeptidyl peptidase inhibition prevents diastolic dysfunction and reduces myocardial fibrosis in a Mouse model of Western diet induced obesity. *Metabolism* 63: 1000-1011, 2014.

27.   Briones AM, Gonzalez JM, Somoza B, Giraldo J, Daly CJ, Vila E, Gonzalez MC, McGrath JC, and Arribas SM. Role of elastin in spontaneously hypertensive rat small mesenteric artery remodelling. *The Journal of physiology* 552: 185-195, 2003.

28.   Briones AM, Rodriguez-Criado N, Hernanz R, Garcia-Redondo AB, Rodrigues-Diez RR, Alonso MJ, Egido J, Ruiz-Ortega M, and Salaices M. Atorvastatin prevents angiotensin II-induced vascular remodeling and oxidative stress. *Hypertension* 54: 142-149, 2009.

29.   Butler B, Gao C, Mersich AT, and Blystone SD. Purified integrin adhesion complexes exhibit actin-polymerization activity. *Curr Biol* 16: 242-251, 2006.

30.   Campia U, Tesauro M, Di Daniele N, and Cardillo C. The vascular endothelin system in obesity and type 2 diabetes: Pathophysiology and therapeutic implications. *Life sciences*, 2014.

31.   Castagneto M and Mingrone G. The effect of gastrointestinal surgery on insulin resistance and insulin secretion. *Current atherosclerosis reports* 14: 624-630, 2012.

32.   Castorena-Gonzalez JA, Staiculescu MC, Foote C, and Martinez-Lemus LA. Mechanisms of the inward remodeling process in resistance vessels: is the actin cytoskeleton involved? *Microcirculation* 21: 219-229, 2014.

33.   Castorena-Gonzalez JA, Staiculescu MC, Foote CA, Polo-Parada L, and Martinez-Lemus LA. The obligatory role of the actin cytoskeleton on inward remodeling induced by dithiothreitol activation of endogenous transglutaminase in isolated arterioles. *American journal of physiology Heart and circulatory physiology* 306: H485-495, 2014.

34.   Castro MM, Rizzi E, Ceron CS, Guimaraes DA, Rodrigues GJ, Bendhack LM, Gerlach RF, and Tanus-Santos JE. Doxycycline ameliorates 2K-1C hypertension-induced vascular dysfunction in rats by attenuating oxidative stress and improving nitric oxide bioavailability. *Nitric Oxide* 26: 162-168, 2012.

35.   Castro MM, Rizzi E, Rodrigues GJ, Ceron CS, Bendhack LM, Gerlach RF, and Tanus-Santos JE. Antioxidant treatment reduces matrix metalloproteinase-2-induced vascular changes in renovascular hypertension. *Free radical biology & medicine* 46: 1298-1307, 2009.

36.   Chen NX, O'Neill K, Chen X, Kiattisunthorn K, Gattone VH, and Moe SM. Transglutaminase 2 accelerates vascular calcification in chronic kidney disease. *American journal of nephrology* 37: 191-198, 2013.

37.   Chillon JM and Baumbach GL. Effects of chronic nitric oxide synthase inhibition on cerebral arterioles in Wistar-Kyoto rats. *J Hypertens* 22: 529-534, 2004.

38.   Christensen KL and Mulvany MJ. Location of resistance arteries. *Journal of vascular research* 38: 1-12, 2001.

39.   Christensen KL and Mulvany MJ. Vasodilatation, not hypotension, improves resistance vessel design during treatment of essential hypertension: a literature survey. *J Hypertens* 19: 1001-1006, 2001.

40.   Clifford PS, Ella SR, Stupica AJ, Nourian Z, Li M, Martinez-Lemus LA, Dora KA, Yang Y, Davis MJ, Pohl U, Meininger GA, and Hill MA. Spatial distribution and mechanical function of elastin in resistance arteries: a role in bearing longitudinal stress. *Arteriosclerosis, thrombosis, and vascular biology* 31: 2889-2896, 2011.

41.   Clifford PS, Ella SR, Stupica AJ, Nourian Z, Li M, Martinez-Lemus LA, Dora KA, Yang Y, Davis MJ, Pohl U, Meininger GA, and Hill MA. Spatial distribution and mechanical function of elastin in resistance arteries: a role in bearing longitudinal stress. *Arterioscler Thromb Vasc Biol* 31: 2889-2896, 2011.

42.   Corteling RL, Brett SE, Yin H, Zheng X-L, Walsh MP, and Welsh DG. The functional consequence of RhoA knockdown by RNA interference in rat cerebral arteries. *American Journal of Physiology - Heart and Circulatory Physiology* 293: H440-H447, 2007.

43.   Coue M, Brenner SL, Spector I, and Korn ED. Inhibition of actin polymerization by latrunculin A. *FEBS letters* 213: 316-318, 1987.

44.   Davis EC. Elastic lamina growth in the developing mouse aorta. *J Histochem Cytochem* 43: 1115-1123, 1995.

45.   de Onis M BM, Borghi E. Global prevalence and trends of overweight and obesity among preschool children. *Am J Clin Nutr* 92: 1257-1264, 2010.

46.   del Campo L, Guvenc Tuna B, Ferrer M, van Bavel E, and Bakker EN. Testosterone and beta-oestradiol prevent inward remodelling of rat small mesenteric arteries: role of NO and transglutaminase. *Clin Sci (Lond)* 124: 719-728, 2013.

47.   Delano FA, Zhang H, Tran EE, Zhang C, and Schmid-Schonbein GW. A New Hypothesis for Insulin Resistance in Hypertension Due to Receptor Cleavage. *Expert review of endocrinology & metabolism* 5: 149-158, 2010.

48.   DeMali KA, Barlow CA, and Burridge K. Recruitment of the Arp2/3 complex to vinculin: coupling membrane protrusion to matrix adhesion. *J Cell Biol* 159: 881-891, 2002.

49.   Dirksen C, Jorgensen NB, Bojsen-Moller KN, Jacobsen SH, Hansen DL, Worm D, Holst JJ, and Madsbad S. Mechanisms of improved glycaemic control after Roux-en-Y gastric bypass. *Diabetologia* 55: 1890-1901, 2012.

50.   Dobrin PB. Mechanical properties of arteries. *Physiological Reviews* 58: 397-460, 1978.

51.   Dumont O, Loufrani L, and Henrion D. Key role of the NO-pathway and matrix metalloprotease-9 in high blood flow-induced remodeling of rat resistance arteries. *Arterioscler Thromb Vasc Biol* 27: 317-324, 2007.

52.   Duprez DA and Cohn JN. Arterial stiffness as a risk factor for coronary atherosclerosis. *Curr Atheroscler Rep* 9: 139-144, 2007.

53.   Eftekhari A, Rahman A, Schaebel LH, Chen H, Rasmussen CV, Aalkjaer C, Buus CL, and Mulvany MJ. Chronic cystamine treatment inhibits small artery remodelling in rats. *J Vasc Res* 44: 471-482, 2007.

54.   Emoto M, Nishizawa Y, Maekawa K, Hiura Y, Kanda H, Kawagishi T, Shoji T, Okuno Y, and Morii H. Homeostasis model assessment as a clinical index of insulin resistance in type 2 diabetic patients treated with sulfonylureas. *Diabetes Care* 22: 818-822, 1999.

55.   Eringa EC, Stehouwer CD, Merlijn T, Westerhof N, and Sipkema P. Physiological concentrations of insulin induce endothelin-mediated vasoconstriction during inhibition of NOS or PI3-kinase in skeletal muscle arterioles. *Cardiovascular research* 56: 464-471, 2002.

56.   Fain JN, Tichansky DS, and Madan AK. Transforming growth factor beta1 release by human adipose tissue is enhanced in obesity. *Metabolism* 54: 1546-1551, 2005.

57.   Fernandez-Patron C, Radomski MW, and Davidge ST. Vascular matrix metalloproteinase-2 cleaves big endothelin-1 yielding a novel vasoconstrictor. *Circ Res* 85: 906-911, 1999.

58.   Frankwich K, Tibble C, Torres-Gonzalez M, Bonner M, Lefkowitz R, Tyndall M, Schmid-Schonbein GW, Villarreal F, Heller M, and Herbst K. Proof of Concept: Matrix metalloproteinase inhibitor decreases inflammation and improves muscle insulin sensitivity in people with type 2 diabetes. *Journal of inflammation* 9: 35, 2012.

59.   Fujioka H, Horiike K, Takahashi M, Ishida T, Kinoshita M, and Nozaki M. Dithiothreitol-induced triphasic response of dog coronary arteries. *European journal of pharmacology* 166: 13-22, 1989.

60.   Fujioka H, Horiike K, Takahashi M, Ishida T, Kinoshita M, and Nozaki M. Triphasic vascular effects of thiol compounds and their oxidized forms on dog coronary arteries. *Experientia* 49: 47-50, 1993.

61.   Gaede V and Günter O. Multidimensional access methods. *ACM Computing Surveys* 30: 170-231, 1998.

62.   Griffin M, Casadio R, and Bergamini CM. Transglutaminases: nature's biological glues. *Biochem J* 368: 377-396, 2002.

63.   Guilherme A, Virbasius JV, Puri V, and Czech MP. Adipocyte dysfunctions linking obesity to insulin resistance and type 2 diabetes. *Nat Rev Mol Cell Biol* 9: 367-377, 2008.

64.   Gunst SJ and Zhang W. Actin cytoskeletal dynamics in smooth muscle: a new paradigm for the regulation of smooth muscle contraction. *American journal of physiology Cell physiology* 295: C576-587, 2008.

65.   Gurgenian SV, Vatinian S, and Zelveian PA. [Arterial hypertension in metabolic syndrome: pathophysiological aspects]. *Terapevticheskii arkhiv* 86: 128-132, 2014.

66.   Habibi J, Hayden MR, Ferrario CM, Sowers JR, and Whaley-Connell AT. Salt Loading Promotes Kidney Injury via Fibrosis in Young Female Ren2 Rats. *Cardiorenal medicine* 4: 43-52, 2014.

67.   Habibi J, Hayden MR, Sowers JR, Pulakat L, Tilmon RD, Manrique C, Lastra G, Demarco VG, and Whaley-Connell A. Nebivolol attenuates redox-sensitive glomerular and tubular mediated proteinuria in obese rats. *Endocrinology* 152: 659-668, 2011.

68.   Hall A. Rho GTPases and the Actin Cytoskeleton. *Science* 279: 509-514, 1998.

69.   Heagerty AM, Aalkjaer C, Bund SJ, Korsgaard N, and Mulvany MJ. Small artery structure in hypertension. Dual processes of remodeling and growth. *Hypertension* 21: 391-397, 1993.

70.   Heerkens EH, Izzard AS, and Heagerty AM. Integrins, vascular remodeling, and hypertension. *Hypertension* 49: 1-4, 2007.

71.   Heerkens EH, Shaw L, Ryding A, Brooker G, Mullins JJ, Austin C, Ohanian V, and Heagerty AM. alphaV integrins are necessary for eutrophic inward remodeling of small arteries in hypertension. *Hypertension* 47: 281-287, 2006.

72.   Heinemann L. Insulin assay standardization: leading to measures of insulin sensitivity and secretion for practical clinical care: response to Staten et al. *Diabetes Care* 33: e83; author reply e84, 2010.

73.   Henry KM, Pase L, Ramos-Lopez CF, Lieschke GJ, Renshaw SA, and Reyes-Aldasoro CC. PhagoSight: an open-source MATLAB(R) package for the analysis of fluorescent neutrophil and macrophage migration in a zebrafish model. *PLoS ONE* 8: e72636, 2013.

74.   Heron M. Deaths: leading causes for 2010. *National vital statistics reports : from the Centers for Disease Control and Prevention, National Center for Health Statistics, National Vital Statistics System* 62: 1-96, 2013.

75.   Hill MA and Ege EA. Active and passive mechanical properties of isolated arterioles from STZ-induced diabetic rats. Effect of aminoguanidine treatment. *Diabetes* 43: 1450-1456, 1994.

76.   Hoffler U, Hobbie K, Wilson R, Bai R, Rahman A, Malarkey D, Travlos G, and Ghanayem BI. Diet-induced obesity is associated with hyperleptinemia, hyperinsulinemia, hepatic steatosis, and glomerulopathy in C57Bl/6J mice. *Endocrine* 36: 311-325, 2009.

77.   Hofmann C, Lorenz K, Braithwaite SS, Colca JR, Palazuk BJ, Hotamisligil GS, and Spiegelman BM. Altered gene expression for tumor necrosis factor-alpha and its receptors during drug and dietary modulation of insulin resistance. *Endocrinology* 134: 264-270, 1994.

78.   Hong Z, Sun Z, Li Z, Mesquitta WT, Trzeciakowski JP, and Meininger GA. Coordination of fibronectin adhesion with contraction and relaxation in microvascular smooth muscle. *Cardiovasc Res* 96: 73-80, 2012.

79.   Hopps E and Caimi G. Matrix metalloproteinases in metabolic syndrome. *European journal of internal medicine* 23: 99-104, 2012.

80.   Horiguchi M, Inoue T, Ohbayashi T, Hirai M, Noda K, Marmorstein LY, Yabe D, Takagi K, Akama TO, Kita T, Kimura T, and Nakamura T. Fibulin-4 conducts proper elastogenesis via interaction with cross-linking enzyme lysyl oxidase. *Proc Natl Acad Sci U S A* 106: 19029-19034, 2009.

81.   Hotamisligil GS, Arner P, Caro JF, Atkinson RL, and Spiegelman BM. Increased adipose tissue expression of tumor necrosis factor-alpha in human obesity and insulin resistance. *J Clin Invest* 95: 2409-2415, 1995.

82.   Hotamisligil GS, Shargill NS, and Spiegelman BM. Adipose expression of tumor necrosis factor-alpha: direct role in obesity-linked insulin resistance. *Science* 259: 87-91, 1993.

83.   Huxley R, Barzi F, and Woodward M. Excess risk of fatal coronary heart disease associated with diabetes in men and women: meta-analysis of 37 prospective cohort studies. *BMJ* 332: 73-78, 2006.

84.   Iantorno M, Campia U, Di Daniele N, Nistico S, Forleo GB, Cardillo C, and Tesauro M. Obesity, inflammation and endothelial dysfunction. *Journal of biological regulators and homeostatic agents* 28: 169-176, 2014.

85.   Intengan HD, Deng LY, Li JS, and Schiffrin EL. Mechanics and composition of human subcutaneous resistance arteries in essential hypertension. *Hypertension* 33: 569-574, 1999.

86.   Intengan HD and Schiffrin EL. Structure and mechanical properties of resistance arteries in hypertension: role of adhesion molecules and extracellular matrix determinants. *Hypertension* 36: 312-318, 2000.

87.   Iwatani Y, Numa H, Atagi S, Takayama F, Mio M, and Kawasaki H. [Mechanisms underlying enhanced vasodilator responses to various vasodilator agents following endothelium removal in rat mesenteric resistance arteries]. *Yakugaku zasshi : Journal of the Pharmaceutical Society of Japan* 127: 729-733, 2007.

88.   Janiak A, Zemskov EA, and Belkin AM. Cell surface transglutaminase promotes RhoA activation via integrin clustering and suppression of the Src-p190RhoGAP signaling pathway. *Mol Biol Cell* 17: 1606-1619, 2006.

89.   Johnson JL, Dwivedi A, Somerville M, George SJ, and Newby AC. Matrix metalloproteinase (MMP)-3 activates MMP-9 mediated vascular smooth muscle cell migration and neointima formation in mice. *Arteriosclerosis, Thrombosis, and Vascular Biology* 31: e35-e44, 2011.

90.   Johnson KA, Polewski M, and Terkeltaub RA. Transglutaminase 2 is central to induction of the arterial calcification program by smooth muscle cells. *Circulation research* 102: 529-537, 2008.

91.   Johnson KB, Petersen-Jones H, Thompson JM, Hitomi K, Itoh M, Bakker EN, Johnson GV, Colak G, and Watts SW. Vena cava and aortic smooth muscle cells express transglutaminases 1 and 4 in addition to transglutaminase 2. *American journal of physiology Heart and circulatory physiology* 302: H1355-1366, 2012.

92.   Johnson KB, Thompson JM, and Watts SW. Modification of proteins by norepinephrine is important for vascular contraction. *Frontiers in physiology* 1: 131, 2010.

93.   Kaess BM, Rong J, Larson MG, Hamburg NM, Vita JA, Levy D, Benjamin EJ, Vasan RS, and Mitchell GF. Aortic stiffness, blood pressure progression, and incident hypertension. *Jama* 308: 875-881, 2012.

94.   Kaibuchi K, Kuroda S, and Amano M. Regulation of the Cytoskeleton and Cell Adhesion by the Rho Family GTPases in Mammalian Cells. *Annual Review of Biochemistry* 68: 459-486, 1999.

95.   Kamper AM, de Craen AJ, Westendorp RG, and Blauw GJ. Endothelium-dependent NO-mediated vasodilation in humans is attenuated by peripheral alpa1-adrenoceptor activation. *Vascular health and risk management* 1: 251-256, 2005.

96.   Kern PA, Saghizadeh M, Ong JM, Bosch RJ, Deem R, and Simsolo RB. The expression of tumor necrosis factor in human adipose tissue. Regulation by obesity, weight loss, and relationship to lipoprotein lipase. *J Clin Invest* 95: 2111-2119, 1995.

97.   Kielty CM. Elastic fibres in health and disease. *Expert reviews in molecular medicine* 8: 1-23, 2006.

98.   Kielty CM, Sherratt MJ, and Shuttleworth CA. Elastic fibres. *J Cell Sci* 115: 2817-2828, 2002.

99.   Kim HR, Appel S, Vetterkind S, Gangopadhyay SS, and Morgan KG. Smooth muscle signalling pathways in health and disease. *J Cell Mol Med* 12: 2165-2180, 2008.

100.   Kohli R, Stefater MA, and Inge TH. Molecular insights from bariatric surgery. *Reviews in endocrine & metabolic disorders* 12: 211-217, 2011.

101.   Kohno M, Ohmori K, Nozaki S, Mizushige K, Yasunari K, Kano H, Minami M, and Yoshikawa J. Effects of valsartan on angiotensin II-induced migration of human coronary artery smooth muscle cells. *Hypertension Research* 23: 677-681, 2000.

102.   Kozma R, Ahmed S, Best A, and Lim L. The Ras-related protein Cdc42Hs and bradykinin promote formation of peripheral actin microspikes and filopodia in Swiss 3T3 fibroblasts. *Mol Cell Biol* 15: 1942-1952., 1995.

103.   Kuang PP, Joyce-Brady M, Zhang XH, Jean JC, and Goldstein RH. Fibulin-5 gene expression in human lung fibroblasts is regulated by TGF-beta and phosphatidylinositol 3-kinase activity. *Am J Physiol Cell Physiol* 291: C1412-1421, 2006.

104.   Kucich U, Rosenbloom JC, Abrams WR, Bashir MM, and Rosenbloom J. Stabilization of elastin mRNA by TGF-beta: initial characterization of signaling pathway. *Am J Respir Cell Mol Biol* 17: 10-16, 1997.

105.   Kucich U, Rosenbloom JC, Abrams WR, and Rosenbloom J. Transforming growth factor-beta stabilizes elastin mRNA by a pathway requiring active Smads, protein kinase C-delta, and p38. *Am J Respir Cell Mol Biol* 26: 183-188, 2002.

106.   Kwon HM, Sangiorgi G, Spagnoli LG, Miyauchi K, Holmes DR, Jr., Schwartz RS, and Lerman A. Experimental hypercholesterolemia induces ultrastructural changes in the internal elastic lamina of porcine coronary arteries. *Atherosclerosis* 139: 283-289, 1998.

107.   Lagaud G, Gaudreault N, Moore EDW, Breemen Cv, and Laher I. Pressure-dependent myogenic constriction of cerebral arteries occurs independently of voltage-dependent activation. *American Journal of Physiology - Heart and Circulatory Physiology* 283: H2187-H2195, 2002.

108.   Ledoux J, Taylor MS, Bonev AD, Hannah RM, Solodushko V, Shui B, Tallini Y, Kotlikoff MI, and Nelson MT. Functional architecture of inositol 1,4,5-trisphosphate signaling in restricted spaces of myoendothelial projections. *Proc Natl Acad Sci U S A* 105: 9627-9632, 2008.

109.   Lewandowski KC, Banach E, Bienkiewicz M, and Lewinski A. Matrix metalloproteinases in type 2 diabetes and non-diabetic controls: effects of short-term and chronic hyperglycaemia. *Archives of medical science : AMS* 7: 294-303, 2011.

110.   Liu Y, Li H, Bubolz AH, Zhang DX, and Gutterman DD. Endothelial cytoskeletal elements are critical for flow-mediated dilation in human coronary arterioles. *Medical & biological engineering & computing* 46: 469-478, 2008.

111.   Livak KJ and Schmittgen TD. Analysis of relative gene expression data using real-time quantitative PCR and the 2(-Delta Delta C(T)) Method. *Methods* 25: 402-408, 2001.

112.   Loufrani L and Henrion D. Role of the cytoskeleton in flow (shear stress)-induced dilation and remodeling in resistance arteries. *Medical & biological engineering & computing* 46: 451-460, 2008.

113.   Majane OH, Vengethasamy L, du Toit EF, Makaula S, Woodiwiss AJ, and Norton GR. Dietary-induced obesity hastens the progression from concentric cardiac hypertrophy to pump dysfunction in spontaneously hypertensive rats. *Hypertension* 54: 1376-1383, 2009.

114.   Martinez-Lemus LA. The dynamic structure of arterioles. *Basic & clinical pharmacology & toxicology* 110: 5-11, 2012.

115.   Martinez-Lemus LA. Persistent agonist-induced vasoconstriction is not required for angiotensin II to mediate inward remodeling of isolated arterioles with myogenic tone. *Journal of vascular research* 45: 211-221, 2008.

116.   Martinez-Lemus LA, Hill MA, Bolz SS, Pohl U, and Meininger GA. Acute mechanoadaptation of vascular smooth muscle cells in response to continuous arteriolar vasoconstriction: implications for functional remodeling. *FASEB journal : official publication of the Federation of American Societies for Experimental Biology* 18: 708-710, 2004.

117.   Martinez-Lemus LA, Hill MA, and Meininger GA. The plastic nature of the vascular wall: a continuum of remodeling events contributing to control of arteriolar diameter and structure. *Physiology* 24: 45-57, 2009.

118.   Martinez-Lemus LA, Wu X, Wilson E, Hill MA, Davis GE, Davis MJ, and Meininger GA. Integrins as unique receptors for vascular control. *Journal of vascular research* 40: 211-233, 2003.

119.   Martinez-Lemus LA, Zhao G, Galinanes EL, and Boone M. Inward remodeling of resistance arteries requires reactive oxygen species-dependent activation of matrix metalloproteinases. *American journal of physiology Heart and circulatory physiology* 300: H2005-2015, 2011.

120.   Martinez-Lemus LA, Zhao G, Galinanes EL, and Boone M. Inward remodeling of resistance arteries requires reactive oxygen species-dependent activation of matrix metalloproteinases. *American journal of physiology Heart and circulatory physiology* 300: H2005-2015, 2011.

121.   Mathers CD and Loncar D. Projections of global mortality and burden of disease from 2002 to 2030. *PLoS medicine* 3: e442, 2006.

122.   Mathiassen ON, Buus NH, Larsen ML, Mulvany MJ, and Christensen KL. Small artery structure adapts to vasodilatation rather than to blood pressure during antihypertensive treatment. *J Hypertens* 25: 1027-1034, 2007.

123.   Mathiassen ON, Buus NH, Sihm I, Thybo NK, Morn B, Schroeder AP, Thygesen K, Aalkjaer C, Lederballe O, Mulvany MJ, and Christensen KL. Small artery structure is an independent predictor of cardiovascular events in essential hypertension. *J Hypertens* 25: 1021-1026, 2007.

124.   Matlung HL, Neele AE, Groen HC, van Gaalen K, Tuna BG, van Weert A, de Vos J, Wentzel JJ, Hoogenboezem M, van Buul JD, VanBavel E, and Bakker EN. Transglutaminase activity regulates atherosclerotic plaque composition at locations exposed to oscillatory shear stress. *Atherosclerosis* 224: 355-362, 2012.

125.   Matthews DR, Hosker JP, Rudenski AS, Naylor BA, Treacher DF, and Turner RC. Homeostasis model assessment: insulin resistance and beta-cell function from fasting plasma glucose and insulin concentrations in man. *Diabetologia* 28: 412-419, 1985.

126.   McGill HC, Jr., McMahan CA, Herderick EE, Zieske AW, Malcom GT, Tracy RE, and Strong JP. Obesity accelerates the progression of coronary atherosclerosis in young men. *Circulation* 105: 2712-2718, 2002.

127.   McGowan SE, Jackson SK, Olson PJ, Parekh T, and Gold LI. Exogenous and endogenous transforming growth factors-beta influence elastin gene expression in cultured lung fibroblasts. *Am J Respir Cell Mol Biol* 17: 25-35, 1997.

128.   Mehta D and Gunst SJ. Actin polymerization stimulated by contractile activation regulates force development in canine tracheal smooth muscle. *The Journal of physiology* 519 Pt 3: 829-840, 1999.

129.   Misurski DA, Wu SQ, McNeill JR, Wilson TW, and Gopalakrishnan V. Insulin-induced biphasic responses in rat mesenteric vascular bed: role of endothelin. *Hypertension* 37: 1298-1302, 2001.

130.   Moriyama K and Yahara I. Two activities of cofilin, severing and accelerating directional depolymerization of actin filaments, are affected differentially by mutations around the actin-binding helix. *Embo J* 18: 6752-6761, 1999.

131.   Muniyappa R and Sowers JR. Endothelial Insulin and IGF-1 Receptors: When Yes Means NO. *Diabetes* 61: 2225-2227, 2012.

132.   Nagareddy PR, Chow FL, Hao L, Wang X, Nishimura T, MacLeod KM, McNeill JH, and Fernandez-Patron C. Maintenance of adrenergic vascular tone by MMP transactivation of the EGFR requires PI3K and mitochondrial ATP synthesis. *Cardiovasc Res* 84: 368-377, 2009.

133.   Nagase H, Visse R, and Murphy G. Structure and function of matrix metalloproteinases and TIMPs. *Cardiovascular research* 69: 562-573, 2006.

134.   Nistala R, Habibi J, Lastra G, Manrique C, Aroor AR, Hayden MR, Garro M, Meuth A, Johnson M, Whaley-Connell A, and Sowers JR. Prevention of obesity induced renal injury in male mice by DPP4 inhibition. *Endocrinology*: en20131920, 2014.

135.   Nobes CD and Hall A. Rho GTPases Control Polarity, Protrusion, and Adhesion during Cell Movement. *The Journal of Cell Biology* 144: 1235-1244, 1999.

136.   Nobes CD and Hall A. Rho, Rac, and Cdc42 GTPases regulate the assembly of multimolecular focal complexes associated with actin stress fibers, lamellipodia, and filopodia. *Cell* 81: 53-62, 1995.

137.   Nurminskaya MV and Belkin AM. Cellular functions of tissue transglutaminase. *International review of cell and molecular biology* 294: 1-97, 2012.

138.   Obara K and Yabu H. Effect of cytochalasin B on intestinal smooth muscle cells. *Eur J Pharmacol* 255: 139-147, 1994.

139.   Ogden CL, Carroll MD, Kit BK, and Flegal KM. Prevalence of obesity among adults: United States, 2011-2012. *NCHS data brief*: 1-8, 2013.

140.   Ogden CL, Carroll MD, Kit BK, and Flegal KM. Prevalence of obesity in the United States, 2009-2010. *NCHS data brief*: 1-8, 2012.

141.   Ohanian V, Gatfield K, and Ohanian J. Role of the actin cytoskeleton in G-protein-coupled receptor activation of PYK2 and paxillin in vascular smooth muscle. *Hypertension* 46: 93-99, 2005.

142.	Ohashi K, Nagata K, Maekawa M, Ishizaki T, Narumiya S, and Mizuno K. Rho-associated kinase ROCK activates LIM-kinase 1 by phosphorylation at threonine 508 within the activation loop. *J Biol Chem* 275: 3577-3582, 2000.

143.	Otsu N. A threshold selection method from gray level histograms. *IEEE Trans Syst Man Cybern* 9: 62-66, 1979.

144.	Papazoglou D, Papatheodorou K, Papanas N, Papadopoulos T, Gioka T, Kabouromiti G, Kotsiou S, and Maltezos E. Matrix metalloproteinase-1 and tissue inhibitor of metalloproteinases-1 levels in severely obese patients: what is the effect of weight loss? *Experimental and clinical endocrinology & diabetes : official journal, German Society of Endocrinology [and] German Diabetes Association* 118: 730-734, 2010.

145.	Parikh NI, Pencina MJ, Wang TJ, Lanier KJ, Fox CS, D'Agostino RB, and Vasan RS. Increasing trends in incidence of overweight and obesity over 5 decades. *The American journal of medicine* 120: 242-250, 2007.

146.	Payne RA, Wilkinson IB, and Webb DJ. Arterial stiffness and hypertension: emerging concepts. *Hypertension* 55: 9-14, 2010.

147.	Perez-Vizcaino F, Cogolludo AL, Zaragoza-Arnaez F, Fajardo S, Ibarra M, Lopez-Lopez JG, and Tamargo J. Vasodilator effects of sodium nitroprusside, levcromakalim and their combination in isolated rat aorta. *British journal of pharmacology* 128: 1419-1426, 1999.

148.	Phillips SA, Sylvester FA, and Frisbee JC. Oxidant stress and constrictor reactivity impair cerebral artery dilation in obese Zucker rats. *Am J Physiol Regul Integr Comp Physiol* 288: R522-530, 2005.

149.	Qiu H, Zhu Y, Sun Z, Trzeciakowski JP, Gansner M, Depre C, Resuello RR, Natividad FF, Hunter WC, Genin GM, Elson EL, Vatner DE, Meininger GA, and Vatner SF. Short communication: vascular smooth muscle cell stiffness as a mechanism for increased aortic stiffness with aging. *Circ Res* 107: 615-619, 2010.

150.	Rao RS, Yanagisawa R, and Kini S. Insulin resistance and bariatric surgery. *Obesity reviews : an official journal of the International Association for the Study of Obesity* 13: 316-328, 2012.

151.   Rembold CM, Tejani AD, Ripley ML, and Han S. Paxillin phosphorylation, actin polymerization, noise temperature, and the sustained phase of swine carotid artery contraction. *Am J Physiol Cell Physiol* 293: C993-1002, 2007.

152.   Rhodin JAG. Architecture of the Vessel Wall. In: *Compr Physiol 2011, Supplement 7: Handbook of Physiology, The Cardiovascular System, Vascular Smooth Muscle: 1-31.First published in print 1980. doi:* : 10.1002/cphy.cp020201.

153.   Rhodin JAG. The ultrastructure of mammalian arterioles and precapillary sphincters. *Journal of Ultrasructure Research* 18: 181-223, 1967.

154.   Ridley AJ. Rho family proteins and regulation of the actin cytoskeleton. *Progress in molecular and subcellular biology* 22: 1-22, 1999.

155.   Ridley AJ and Hall A. The small GTP-binding protein rho regulates the assembly of focal adhesions and actin stress fibers in response to growth factors. *Cell* 70: 389-399, 1992.

156.   Rizzoni D, Porteri E, Boari GE, De Ciuceis C, Sleiman I, Muiesan ML, Castellano M, Miclini M, and Agabiti-Rosei E. Prognostic significance of small-artery structure in hypertension. *Circulation* 108: 2230-2235, 2003.

157.   Rizzoni D, Porteri E, Guelfi D, Muiesan ML, Valentini U, Cimino A, Girelli A, Rodella L, Bianchi R, Sleiman I, and Rosei EA. Structural alterations in subcutaneous small arteries of normotensive and hypertensive patients with non-insulin-dependent diabetes mellitus. *Circulation* 103: 1238-1244, 2001.

158.   Rodilla E, Costa JA, Martin J, Gonzalez C, Pascual JM, and Redon J. Impact of abdominal obesity and ambulatory blood pressure in the diagnosis of left ventricular hypertrophy in never treated hypertensives. *Medicina clinica* 142: 235-242, 2014.

159.   Rubino F, Shukla A, Pomp A, Moreira M, Ahn SM, and Dakin G. Bariatric, metabolic, and diabetes surgery: what's in a name? *Annals of surgery* 259: 117-122, 2014.

160. Saito S, Watabe S, Ozaki H, Fusetani N, and Karaki H. Mycalolide B, a novel actin depolymerizing agent. *The Journal of biological chemistry* 269: 29710-29714, 1994.

161. Saito SY, Hori M, Ozaki H, and Karaki H. Cytochalasin D inhibits smooth muscle contraction by directly inhibiting contractile apparatus. *Journal of smooth muscle research = Nihon Heikatsukin Gakkai kikanshi* 32: 51-60, 1996.

162. Samad F, Uysal KT, Wiesbrock SM, Pandey M, Hotamisligil GS, and Loskutoff DJ. Tumor necrosis factor alpha is a key component in the obesity-linked elevation of plasminogen activator inhibitor 1. *Proc Natl Acad Sci U S A* 96: 6902-6907, 1999.

163. Samad F, Yamamoto K, Pandey M, and Loskutoff DJ. Elevated expression of transforming growth factor-beta in adipose tissue from obese mice. *Mol Med* 3: 37-48, 1997.

164. Sandow SL, Tare M, Coleman HA, Hill CE, and Parkington HC. Involvement of myoendothelial gap junctions in the actions of endothelium-derived hyperpolarizing factor. *Circulation research* 90: 1108-1113, 2002.

165. Sane DC, Kontos JL, and Greenberg CS. Roles of transglutaminases in cardiac and vascular diseases. *Front Biosci* 12: 2530-2545, 2007.

166. Santhanam L, Tuday EC, Webb AK, Dowzicky P, Kim JH, Oh YJ, Sikka G, Kuo M, Halushka MK, Macgregor AM, Dunn J, Gutbrod S, Yin D, Shoukas A, Nyhan D, Flavahan NA, Belkin AM, and Berkowitz DE. Decreased S-nitrosylation of tissue transglutaminase contributes to age-related increases in vascular stiffness. *Circ Res* 107: 117-125, 2010.

167. Sauzeau V, Sevilla MA, Montero MJ, and Bustelo XR. The Rho/Rac exchange factor Vav2 controls nitric oxide-dependent responses in mouse vascular smooth muscle cells. *J Clin Invest* 120: 315-330, 2010.

168. Schiffrin EL. Remodeling of resistance arteries in essential hypertension and effects of antihypertensive treatment. *American journal of hypertension* 17: 1192-1200, 2004.

169.   Schmid-Schonbein GW. An emerging role of degrading proteinases in hypertension and the metabolic syndrome: autodigestion and receptor cleavage. *Current hypertension reports* 14: 88-96, 2012.

170.   Schnittler HJ, Schneider SW, Raifer H, Luo F, Dieterich P, Just I, and Aktories K. Role of actin filaments in endothelial cell-cell adhesion and membrane stability under fluid shear stress. *Pflugers Archiv : European journal of physiology* 442: 675-687, 2001.

171.   Schubert R, Kalentchuk VU, and Krien U. Rho kinase inhibition partly weakens myogenic reactivity in rat small arteries by changing calcium sensitivity. *American Journal of Physiology - Heart and Circulatory Physiology* 283: H2288-H2295, 2002.

172.   Schubert R, Krien U, Wulfsen I, Schiemann D, Lehmann G, Ulfig N, Veh RW, Schwarz JR, and Gago H. Nitric oxide donor sodium nitroprusside dilates rat small arteries by activation of inward rectifier potassium channels. *Hypertension* 43: 891-896, 2004.

173.   Sehgel NL, Zhu Y, Sun Z, Trzeciakowski JP, Hong Z, Hunter WC, Vatner DE, Meininger GA, and Vatner SF. Increased Vascular Smooth Muscle Cell Stiffness; a Novel Mechanism for Aortic Stiffness in Hypertension. *Am J Physiol Heart Circ Physiol*, 2013.

174.   Sehgel NL, Zhu Y, Sun Z, Trzeciakowski JP, Hong Z, Hunter WC, Vatner DE, Meininger GA, and Vatner SF. Increased vascular smooth muscle cell stiffness: a novel mechanism for aortic stiffness in hypertension. *Am J Physiol Heart Circ Physiol* 305: H1281-1287, 2013.

175.   Sept D and McCammon JA. Thermodynamics and kinetics of actin filament nucleation. *Biophys J* 81: 667-674, 2001.

176.   Shi J, Wang A, Sen S, Wang Y, Kim HJ, Mitts TF, and Hinek A. Insulin induces production of new elastin in cultures of human aortic smooth muscle cells. *Am J Pathol* 180: 715-726, 2012.

177.   Somlyo AP and Somlyo AV. Ca2+ Sensitivity of Smooth Muscle and Nonmuscle Myosin II: Modulated by G Proteins, Kinases, and Myosin Phosphatase. *Physiological Reviews* 83: 1325-1358, 2003.

178.	Souza-Smith FM, Katz PS, Trask AJ, Stewart JA, Jr., Lord KC, Varner KJ, Vassallo DV, and Lucchesi PA. Mesenteric resistance arteries in type 2 diabetic db/db mice undergo outward remodeling. *PLoS ONE* 6: e23337, 2011.

179.	Staiculescu MC, Galinanes EL, Zhao G, Ulloa U, Jin M, Beig MI, Meininger GA, and Martinez-Lemus LA. Prolonged vasoconstriction of resistance arteries involves vascular smooth muscle actin polymerization leading to inward remodelling. *Cardiovascular research* 98: 428-436, 2013.

180.	Stehouwer CD, Henry RM, and Ferreira I. Arterial stiffness in diabetes and the metabolic syndrome: a pathway to cardiovascular disease. *Diabetologia* 51: 527-539, 2008.

181.	Straub AC, Lohman AW, Billaud M, Johnstone SR, Dwyer ST, Lee MY, Bortz PS, Best AK, Columbus L, Gaston B, and Isakson BE. Endothelial cell expression of haemoglobin alpha regulates nitric oxide signalling. *Nature* 491: 473-477, 2012.

182.	Su Y, Edwards-Bennett S, Bubb MR, and Block ER. Regulation of endothelial nitric oxide synthase by the actin cytoskeleton. *American journal of physiology Cell physiology* 284: C1542-1549, 2003.

183.	Su Y, Zharikov SI, and Block ER. Microtubule-active agents modify nitric oxide production in pulmonary artery endothelial cells. *American journal of physiology Lung cellular and molecular physiology* 282: L1183-1189, 2002.

184.	Sutton-Tyrrell K, Newman A, Simonsick EM, Havlik R, Pahor M, Lakatta E, Spurgeon H, and Vaitkevicius P. Aortic stiffness is associated with visceral adiposity in older adults enrolled in the study of health, aging, and body composition. *Hypertension* 38: 429-433, 2001.

185.	Tack CJ, Ong MK, Lutterman JA, and Smits P. Insulin-induced vasodilatation and endothelial function in obesity/insulin resistance. Effects of troglitazone. *Diabetologia* 41: 569-576, 1998.

186.	Toto-Moukouo JJ, Achimastos A, Asmar RG, Hugues CJ, and Safar ME. Pulse wave velocity in patients with obesity and hypertension. *Am Heart J* 112: 136-140, 1986.

187.   Tounian P, Aggoun Y, Dubern B, Varille V, Guy-Grand B, Sidi D, Girardet JP, and Bonnet D. Presence of increased stiffness of the common carotid artery and endothelial dysfunction in severely obese children: a prospective study. *Lancet* 358: 1400-1404, 2001.

188.   Tseng S, Kim R, Kim T, Morgan KG, and Hai CM. F-actin disruption attenuates agonist-induced [Ca2+], myosin phosphorylation, and force in smooth muscle. *Am J Physiol* 272: C1960-1967, 1997.

189.   Tsioufis C, Bafakis I, Kasiakogias A, and Stefanadis C. The role of matrix metalloproteinases in diabetes mellitus. *Current topics in medicinal chemistry* 12: 1159-1165, 2012.

190.   Ueki Y, Uda Y, Sakamoto N, and Sato M. Measurements of strain on single stress fibers in living endothelial cells induced by fluid shear stress. *Biochemical and biophysical research communications* 395: 441-446, 2010.

191.   Unterberger MJ, Schmoller KM, Bausch AR, and Holzapfel GA. A new approach to model cross-linked actin networks: multi-scale continuum formulation and computational analysis. *Journal of the mechanical behavior of biomedical materials* 22: 95-114, 2013.

192.   van den Akker J, Schoorl MJ, Bakker EN, and Vanbavel E. Small Artery Remodeling: Current Concepts and Questions. *J Vasc Res* 47: 183-202, 2009.

193.   Van Den Akker J, Schoorl MJC, Bakker ENTP, and Vanbavel E. Small artery remodeling: Current concepts and questions. *Journal of Vascular Research* 47: 183-202, 2010.

194.   van den Akker J, VanBavel E, van Geel R, Matlung HL, Guvenc Tuna B, Janssen GM, van Veelen PA, Boelens WC, De Mey JG, and Bakker EN. The redox state of transglutaminase 2 controls arterial remodeling. *PloS one* 6: e23067, 2011.

195.   van Popele NM, Grobbee DE, Bots ML, Asmar R, Topouchian J, Reneman RS, Hoeks AP, van der Kuip DA, Hofman A, and Witteman JC. Association between arterial stiffness and atherosclerosis: the Rotterdam Study. *Stroke* 32: 454-460, 2001.

196.   VanBavel E, van der Meulen E, and Spaan J. Role of Rho-associated protein kinase in tone and calcium sensitivity of cannulated rat mesenteric small arteries. *Experimental Physiology* 86: 585-592, 2001.

197.   Wagenseil JE and Mecham RP. Elastin in large artery stiffness and hypertension. *J Cardiovasc Transl Res* 5: 264-273, 2012.

198.   Wang X, Chow FL, Oka T, Hao L, Lopez-Campistrous A, Kelly S, Cooper S, Odenbach J, Finegan BA, Schulz R, Kassiri Z, Lopaschuk GD, and Fernandez-Patron C. Matrix metalloproteinase-7 and ADAM-12 (a disintegrin and metalloproteinase-12) define a signaling axis in agonist-induced hypertension and cardiac hypertrophy. *Circulation* 119: 2480-2489, 2009.

199.   Watts SW, Priestley JR, and Thompson JM. Serotonylation of vascular proteins important to contraction. *PLoS ONE* 4: e5682, 2009.

200.   Weisbrod RM, Shiang T, Al Sayah L, Fry JL, Bajpai S, Reinhart-King CA, Lob HE, Santhanam L, Mitchell G, Cohen RA, and Seta F. Arterial stiffening precedes systolic hypertension in diet-induced obesity. *Hypertension* 62: 1105-1110, 2013.

201.   Whaley-Connell AT, Chowdhury NA, Hayden MR, Stump CS, Habibi J, Wiedmeyer CE, Gallagher PE, Tallant EA, Cooper SA, Link CD, Ferrario C, and Sowers JR. Oxidative stress and glomerular filtration barrier injury: role of the renin-angiotensin system in the Ren2 transgenic rat. *American journal of physiology Renal physiology* 291: F1308-1314, 2006.

202.   Whaley-Connell AT, Habibi J, Aroor A, Ma L, Hayden MR, Ferrario CM, Demarco VG, and Sowers JR. Salt loading exacerbates diastolic dysfunction and cardiac remodeling in young female Ren2 rats. *Metabolism: clinical and experimental* 62: 1761-1771, 2013.

203.   Wildman RP, Mackey RH, Bostom A, Thompson T, and Sutton-Tyrrell K. Measures of obesity are associated with vascular stiffness in young and older adults. *Hypertension* 42: 468-473, 2003.

204.   Yamin R and Morgan KG. Deciphering actin cytoskeletal function in the contractile vascular smooth muscle cell. *The Journal of physiology* 590: 4145-4154, 2012.

205.   Yang N, Higuchi O, Ohashi K, Nagata K, Wada A, Kangawa K, Nishida E, and Mizuno K. Cofilin phosphorylation by LIM-kinase 1 and its role in Rac-mediated actin reorganization. *Nature* 393: 809-812, 1998.

206.   Yu G, Zou H, Prewitt RL, and Hill MA. Impaired arteriolar mechanotransduction in experimental diabetes mellitus. *J Diabetes Complications* 13: 235-242, 1999.

207.   Zayani Y, Allal-Elasmi M, Jacob MP, Zidi W, Ftouhi B, Feki M, Slimane H, and Kaabachi N. Abnormal circulating levels of matrix metalloproteinases and their inhibitors in diabetes mellitus. *Clinical laboratory* 58: 779-785, 2012.

208.   Zhang G, Matsumura Y, Matsumoto S, Hayashi Y, and Mori T. Effects of Ca2+ and sulfhydryl reductant on the polymerization of soybean glycinin catalyzed by mammalian and microbial transglutaminases. *J Agric Food Chem* 51: 236-243, 2003.

209.   Zhou MS, Jaimes EA, and Raij L. Vascular but not cardiac remodeling is associated with superoxide production in angiotensin II hypertension. *J Hypertens* 23: 1737-1743, 2005.

210.   Zhou X, Ma L, Habibi J, Whaley-Connell A, Hayden MR, Tilmon RD, Brown AN, Kim JA, Demarco VG, and Sowers JR. Nebivolol improves diastolic dysfunction and myocardial remodeling through reductions in oxidative stress in the Zucker obese rat. *Hypertension* 55: 880-888, 2010.

211.   Zhu Y, Qiu H, Trzeciakowski JP, Sun Z, Li Z, Hong Z, Hill MA, Hunter WC, Vatner DE, Vatner SF, and Meininger GA. Temporal analysis of vascular smooth muscle cell elasticity and adhesion reveals oscillation waveforms that differ with aging. *Aging cell* 11: 741-750, 2012.

VITA

Jorge A. Castorena-Gonzalez was born in León, Guanajuato, México in September 19th, 1984. He graduated from the high school program of the *Universidad de León* in 2002. In the same year, Jorge was accepted at the *Universidad de Guanajuato*, where he joined the Physics Department and obtained in 2007 his Bachelor's degree in Physics. His thesis research received *Cum Laude* honors and was titled: "Λ^0 and anti-Λ^0 polarization in pp$\rightarrow$p$_f$p$_s\Lambda^0$anti-Λ^0 at 800-GeV/c". While in college, Jorge was awarded a scholarship to participate in an international student research program. As a result of this achievement, he spent five months at CERN (European Organization for Nuclear Research) in 2006. During this time, Jorge had the opportunity to work for the CERN - Accelerator and Beams Department under the supervision of Jens Spangaard. In 2007, Jorge joined the Master's program at the same university. It was during this time when Jorge was invited to be part of an international collaboration with the neutrino experiment MINERvA at Fermi National Accelerator Laboratory (Fermilab) in Batavia, IL, USA. He graduated with a Master's degree in Physics in 2009. His thesis research summarized the work he performed while at Fermilab, and it was titled: "FNAL E938: MINERvA – Assembling, Commissioning, Calibration and First Results of the Tracking Prototype System". In 2010, Dr. Luis Polo-Parada invited Jorge to join his laboratory at Dalton Cardiovascular Research Center and the Ph.D. program at the Biological Engineering Department of the University of Missouri - Columbia. In 2012, Jorge joined Dr. Luis A. Martinez-Lemus laboratory at Dalton Cardiovascular Research Center and started his work focusing in vascular remodeling, hypertension, obesity and diabetes.

147